

Diplomarbeit

Dynamic analysis of MEMS structures

Ausgeführt am Institut für Sensor und Aktuatorssysteme
der Technischen Universität Wien

unter der Anleitung von

Ao.Univ.Prof. Dipl.-Ing. Dr.techn.

Franz Keplinger

und

Univ.Lektor Mag.rer.nat. Mag.rer.nat. Dr.techn.

Michael Stifter

durch

Nikolaus Berlakovich

Gutshof 1, 7304 Nebersdorf

Matr.-Nr. 0929001

Wien, am 18. Oktober 2016

Unterschrift Student

To my family

Contents

Abstract	ix
Kurzfassung	xi
Nomenclature	xiii
0.1 List of Abbreviations	xiii
0.2 List of Constants	xiii
0.3 List of Variables	xiv
0.4 General Notation	xix
1 Introduction	1
1.1 Bimetallic thermometer	1
1.2 Thermistor	2
1.3 Thermocouple	3
1.4 Fiber Bragg grating sensor	4
1.5 Pyrometer	5
2 Theory	7
3 Comsol Verification	11
3.1 Cantilever with normal force	11
3.2 Cantilever with shear load	16
3.3 Eigenfrequencies of a clamped beam including thermal expansion	21
4 Investigation of a double-U structure	27
4.1 Investigation	28
4.2 1. ss-mode	36
4.3 1. as-mode	43
4.4 1. sa-mode	45
4.5 1. aa-mode	48
4.6 2. ss-mode	50
4.7 2. as-mode	55
4.8 Summary of the results	57
4.8.1 Modes symmetric about the S2-axis	57
4.8.2 Modes asymmetric about the S2-axis	59
5 Experimental verification of the simulation	61
5.1 Fabrication of the structure	64
5.2 Results and discussion	66

6	Temperature sensor application	69
6.1	Vanadium oxide resonant thermal sensor	73
6.2	Quartz crystals	74
6.3	String-based temperature sensors	74
6.4	Temperature sensor based on electrical spring softening	75
6.5	Resonant MEMS temperature sensor	76
7	Structure with temperature independent resonance	79
8	Conclusion and Outlook	83
	Bibliography	85

Abstract

In many modern electronic devices MEMS systems are utilized as sensing elements. MEMS technology doesn't tap its full potential and research as well as development are still demanded. Especially resonating structures such as cantilevers or bridges have attracted the attention over the last two decades. One of the most outstanding feature of them is the high quality factor of the mechanical resonance that can exceed 10 000. However, the structures are vulnerable to mechanical stress which is also influenced by the temperature. It is in the scope of this thesis to investigate its influence on the resonant frequency and how the consequences can be compensated. Therefore, the thesis deals with the design of the resonant frequencies and their dependence on the temperature. In particular, H-shaped structures are investigated and the corresponding mode shapes are examined. Furthermore, an analysis of the change of the resonant frequencies caused by parameter alteration of the beam structures is performed. This was done to reveal effects which can be utilized to construct beam structures featuring special desired resonant frequency dependencies with the temperature. Within the investigations we present two different structures. One structure where the resonant frequency strongly varies with the temperature and another where the resonant frequency is almost independent of the temperature.

Kurzfassung

In vielen modernen elektronischen Geräten werden MEMS-Systeme als Messelemente eingesetzt. Das Potential der MEMS-Technologie ist jedoch noch lange nicht ausgeschöpft und Forschung sowie Entwicklung sind nach wie vor gefragt. Besonders Resonanzstrukturen wie Biegebalken oder Brücken haben in den letzten zwei Jahrzehnten die Aufmerksamkeit auf sich gezogen. Ihre herausragende Eigenschaft zeichnet sich durch einen hohen Qualitätsfaktor der mechanischen Resonanz aus, welcher über 10 000 hinausgehen kann. Die Strukturen sind jedoch sehr anfällig auf mechanische Spannungen, die unter anderem durch Temperaturänderungen hervorgerufen werden. Im Rahmen dieser Diplomarbeit wird untersucht welchen Einfluss die Temperatur auf Resonanzfrequenzen hat und wie man diesen kompensieren könnte. Die Arbeit beschäftigt sich daher mit dem Strukturdesign, der Einstellung der Resonanzfrequenzen und ihrer Temperaturabhängigkeit. Im Speziellen werden H-förmige Strukturen untersucht und die Gestalt der dazugehörigen Schwingungsmoden betrachtet. Des Weiteren wird die Änderung der Resonanzfrequenzen aufgrund von Parameter-Modifikation analysiert. Diese Analyse wird durchgeführt um Effekte aufzudecken, die verwendet werden können, um Balkenstrukturen mit speziellen, gewünschten Resonanzfrequenzen in Abhängigkeit der Temperatur zu konstruieren. Im Zuge der Untersuchungen präsentieren wir zwei verschiedene Strukturen. Eine Struktur, deren Resonanzfrequenz stark mit der Temperatur variiert und eine andere, die eine nahezu temperaturunabhängige Resonanz aufweist.

Nomenclature

0.1 List of Abbreviations

Abbreviation	Description
FEM	finite element method
MEMS	microelectromechanical systems
MSA	micros system analyser
NTC	negative temperature coefficient
PTC	positive temperature coefficient

0.2 List of Constants

Symbol	Description	Value
e	Euler's number	2.7182
i	imaginary unit	$\sqrt{-1}$
σ	Stefan Boltzmann constant	$5.6703 \cdot 10^{-8} \text{ kg/s}^3\text{K}^4$
π		3.1415

0.3 List of Variables

Symbol	Description	Unit
A_s	beams cross-section	m^2
A	width of gold load	m
Bl	geometrical parameter of double-U, barbell and narrow-double-U structure	m
Bw	geometrical parameter of double-U, barbell and narrow-double-U structure	m
\mathbf{b}	body force vector	N
b	width of beam	m
d	gap spacing between resonator beam and electrode	m
\mathbf{E}	Green strain tensor	
E	Young's modulus	Pa
\mathbf{E}_{el}	elastic strain tensor	
\mathbf{E}_{th}	thermal strain tensor	
ET	relative error between COMSOL- and analytical solution for tensor element \mathbf{T}_{11}	
\mathbf{E}_{tot}	total strain tensor	
Eu	relative error between COMSOL- and analytical solution for displacement u_x	
F	force	N
\mathbf{F}	force vector	N
F_c	critical buckling force	N
\mathbf{F}_s	internal force vector of a beams's cross section	N
f	constant defined in (3.21)	$1/m^2$
G	shear modulus	Pa
\mathbf{H}	displacement gradient	

Symbol	Description	Unit
H	geometrical parameter of double-U and narrow-double-U structure	m
h	height of beam	m
H_b	geometrical parameter of barbell structure	m
H_c	geometrical parameter of barbell structure	m
H_l	height of Au-lead	m
\mathbf{H}_{el}	elastic displacement gradient	
\mathbf{H}_{th}	thermal displacement gradient	
\mathbf{H}_{tot}	total displacement gradient	
I	second moment of area	m^4
I_z	is the second moment of area concerning the z-coordinate	m^4
j	emissive power (total energy radiated per unit surface area of a black body across all wavelengths per unit time)	J/sm^2
k	defined in (3.21)	kg/Nm^3
k_e	electrical spring stiffness	N/m^2
k_ν	average slope of frequency over temperature interval	$1/Ks$
$k_{\nu nar}$	average slope of frequency over temperature interval of the narrow-double-U structure	$1/Ks$
$k_{\nu bas}$	average slope of frequency over temperature interval of the basic double-U structure	$1/Ks$
Δk_ν	average slope of frequency over temperature interval caused by geometrical parameter modification	$1/Ks$
L	defined in (3.23)	$1/m$
ll	geometrical parameter of double-U and narrow-double-U structure	m

Symbol	Description	Unit
Lw	geometrical parameter of double-U and narrow-double-U structure	m
L'	defined in (3.23)	1/m
l	length of beam	m
M_s	internal moment vector of a beams's cross section	Nm
M_T	internal moment of a beams's cross section causing torsion	Nm
M_2	internal moment of a beams's cross section about the y -axis	Nm
M_3	internal moment of a beams's cross section about the z -axis	Nm
N	internal force orthogonal to a beam's cross section	N
n	refractive index	
p	shear load of beam	N/m ²
P_{in}	power of incoming light	J/s
P_{ref}	power of reflected light	J/s
P_{trans}	power of transmitted light	J/s
Q_1	internal force of a beams's cross section into y -direction	N
Q_2	internal force of a beams's cross section into z -direction	N
R	electrical resistivity	Ω
\mathbf{r}	position vector	m
\mathbf{r}_{cb}	center of the surface of a beam	m
\mathbf{r}_{cs}	cross section-center of beam	m
\mathbf{S}	stiffness matrix	N/m ²
\mathbf{T}	Cauchy stress tensor	N/m ²
T	temperature	K
T_c	critical buckling temperature	K

Symbol	Description	Unit
t	time	s
T_0	reference temperature	K
T_M	measured temperature	K
T_{st}	temperature of structure	K
T_{fr}	temperature of frame	K
U	voltage	V
Ul	geometrical parameter of double-U, barbell and narrow-double-U structure	m
Uw	geometrical parameter of double-U, barbell and narrow-double-U structure	m
\mathbf{u}	displacement vector	m
\mathbf{u}_{el}	elastic displacement vector	m
\mathbf{u}_{th}	thermal displacement vector	m
\mathbf{u}_{tot}	total displacement vector	m
u_x	displacement into the x -direction	m
u_y	displacement into the y -direction	m
V_P	dc voltage	V
v_i	ac voltage	V
x, y, z	Cartesian coordinates	m
Z	geometrical parameter of gold trace on double-U structure	m
α	linear coefficient of thermal expansion	1/K
β	buckling coefficient	
ϵ	relative deviation	
ϵ	emissivity	
η	ratio between slope of narrow-double-U and basic double-U	

Symbol	Description	Unit
λ	wavelength	m
λ_B	Bragg wavelength	m
ν	frequency	1/s
ν	Poisson's ratio	
ν_{223K}	frequency at $T = 223$ K	1/s
$\Delta\nu_{223K}$	change of frequency caused by geometrical parameter modification at $T = 223$ K	1/s
ρ	volumetric mass density	kg/m ³
ρ_{eff}	effective volumetric mass density	kg/m ³
σ	stress tensor element \mathbf{T}_{11}	N/m ²
σ_c	critical buckling stress	N/m ²
ω	angular frequency	1/s

Symbol	Description	Unit
--------	-------------	------

0.4 General Notation

Notation	Description
$\mathbf{a} \cdot \mathbf{b}$	scalar product
\mathbf{ab}	dyadic product
$f(\bullet)$	function
\mathbf{H}^T	transpose of tensor \mathbf{H}
$Tr\mathbf{H}$	trace of tensor \mathbf{H}
H_{ij}	tensor element ij of tensor \mathbf{H}
∇	nabla operator
Δ	laplace operator
$\mathbb{1}$	identity matrix

Chapter 1

Introduction

Temperature is one of the most important physical quantities and plays a major role in many parts of science, technique and even in our daily life. Thus, the necessity of devices that sense this physical quantity such as temperature sensors is doubtless great. Many kinds of temperature sensors relying on different physical principles have been developed. But as we need these devices in a huge range of scientific and technical applications with their very specific specifications and requirements there is still a lot of space for future development. The common temperature sensors utilize physical principles like thermal expansion, thermoelectric effect (Seebeck effect), electrical resistivity, thermal radiation etc. [10]. In the following we want to present a few typically used thermal sensors in order to provide the reader a short overview of the current state of temperature sensors and their principles.

1.1 Bimetallic thermometer

Actually a sensor is an element that produces an electrical signal. The bimetal is only a transducer. It utilizes the thermal expansion. The setup of a bimetal is shown in Fig. 1.1.

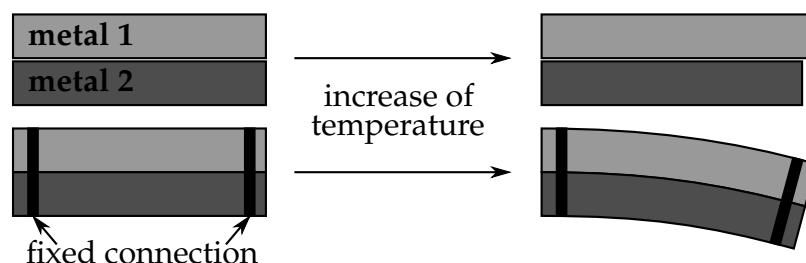


Figure 1.1: Setup and principle of a bimetal [12].

The bimetal consists of two metals (metal 1 and metal 2) where the thermal expansion coefficients of the two metals are different. If the expansion coefficient of metal 1 is larger than the one of metal 2 metal 1 will exhibit a stronger

expansion with an increase of the temperature than metal 2 shown in Fig. 1.1. If the two metals are fixed together the different expansion entails internal forces which lead to bending of the two metals, i. e. of the bimetal. Hence, the deflection of the bimetal depends on the temperature and the difference of the expansion coefficients. The thermal deflection can be readout via a capacitor [11].

1.2 Thermistor

The thermistor exploits the temperature dependence of the electrical resistivity. Basically one distinguishes between PTC (positive temperature coefficient) and NTC (negative temperature coefficient) sensors depending on whether the resistivity increases (PTC) or decreases (NTC) with higher temperature. The characteristics are shown in Fig. 1.2 by means of a PT1000 (PTC) and a NTC1.8K (NTC) developed by the company Inocal [19].

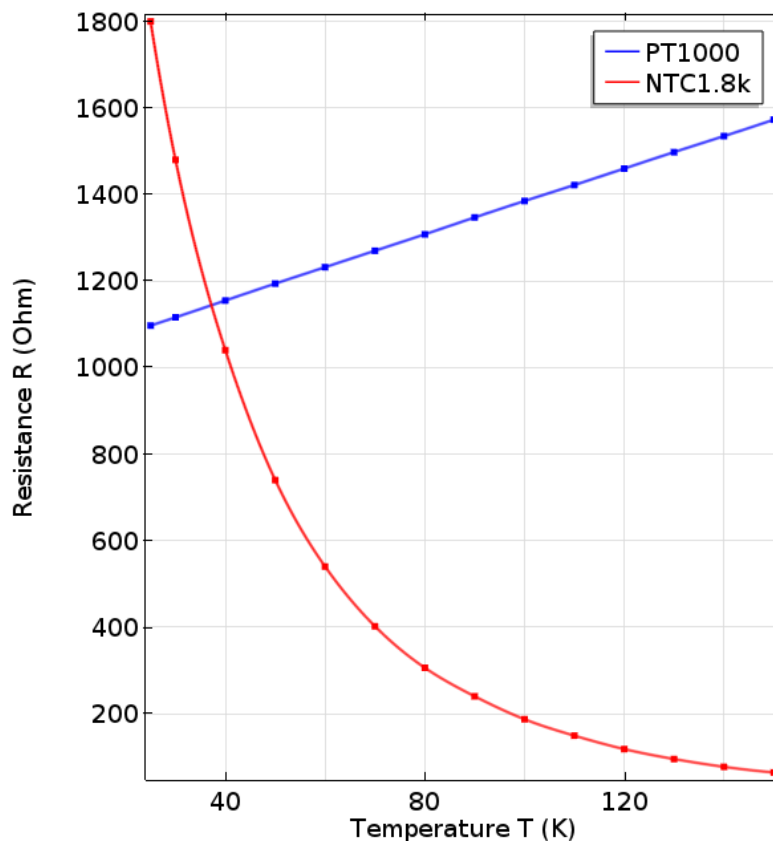


Figure 1.2: Typical electrical resistance R (in Ω) vs. the temperature T (in K) for a PTC and NTC sensor by means of a PT1000 and a NTC1.8K [19].

If one knows the PTC or NTC characteristics one can determine the temperature by measuring the electrical resistivity. Commonly used materials for PTCs

are platinum, nickel or special ceramics (for example doped barium titanate). Although barium titanate is a semiconductor they are primarily used as NTC materials [13] (mostly a compound of metal oxides). As an example for a thermistor and its construction, Figure 1.3 depicts a germanium thermistor with metal strips exhibiting a Ti-Au-Cr sandwich [20].

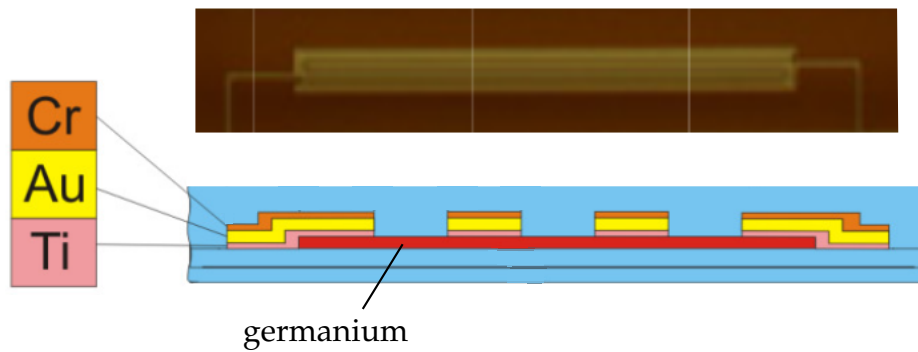


Figure 1.3: Thermistor consisting of germanium film contacted by four metal strips. Horizontal section (top) and cross section (bottom) [20] [21].

1.3 Thermocouple

This kind of temperature sensor utilizes the Seebeck effect which is a thermoelectric effect. The setup of a thermocouple is shown in Fig. 1.4. A wire made of material A is at each end connected with another wire made of material B. Furthermore, the two wires of material B are connected to a voltmeter in order to measure a generated voltage. Both materials exhibit a different Seebeck coefficient.

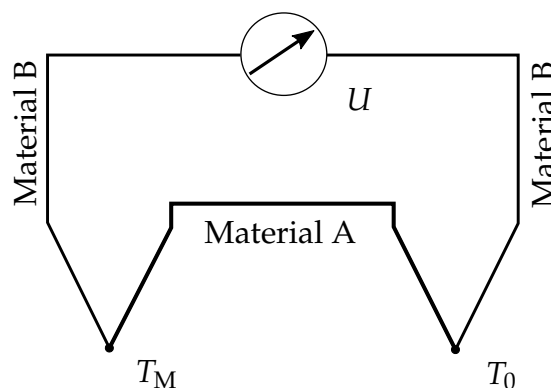


Figure 1.4: Setup of a thermocouple.

If we have different temperatures at both sites where the wires are connected (T_0 and T_M in Fig. 1.4) we measure a voltage U at the voltmeter. That is pro-

portional to the difference between the two temperatures $\Delta T = T_0 - T_M$. Thus, if one knows the reference temperature T_0 one is able to determine T_M via the measured voltage U [14].

1.4 Fiber Bragg grating sensor

This type of sensors is based on optical effects of a fiber Bragg grating sensor (Fig. 1.5). The optical fiber exhibits a core with a periodically changing refractive index (variation between n_2 and n_3).

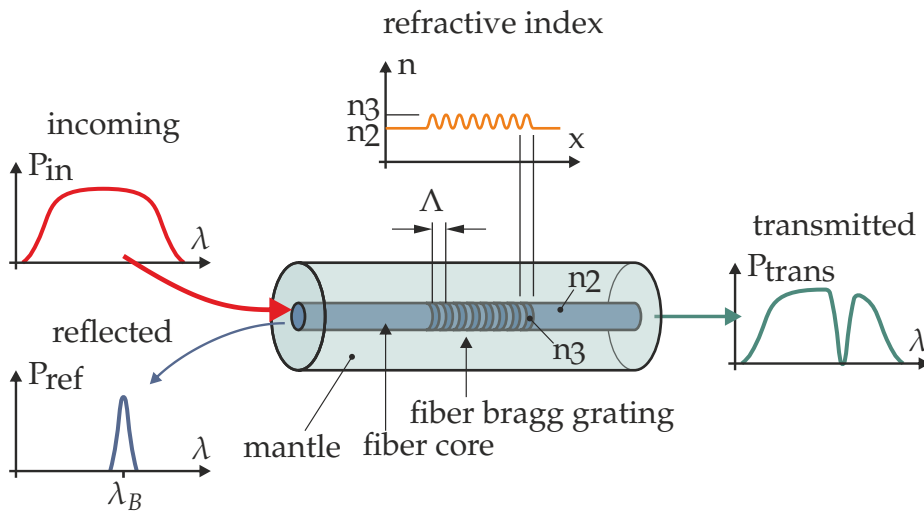


Figure 1.5: Setup and feature of a fiber Bragg grating sensor [15].

This yields the fiber to act as a wavelength specific reflector or filter. If a ray of light with a broad frequency distribution is sent into the fiber the fiber will reflect light with a specific wavelength (λ_B called the Bragg wavelength) where the rest of the incoming light will be transmitted. Temperature changes cause among others two effects, namely thermal expansion of the fiber (if the fiber is fixed on a material the fibers expansion is equal to the one of the material) and a change of the refractive index of the fiber. Both effects lead to a remarkable change of the Bragg wavelength λ_B . Thus, the wavelength of the reflected light is temperature dependent and if one knows the relation $\lambda_B(T)$ one is able to determine the temperature via the wavelength of the reflected light [15].

1.5 Pyrometer

The pyrometer uses thermal radiation emitted by an object in order to get information about its temperature. The Stefan-Boltzmann law implies that the power of thermal radiation emitted by a body is proportional to the fourth power of the body's temperature. The relation is given by:

$$j = \epsilon\sigma T^4 \quad (1.1)$$

where j is the emissive power, σ is the Boltzmann constant and ϵ is the emissivity of the body.



Figure 1.6: Typical commercial pyrometer, that shows the temperature of a specific surface pointed with a laser [17].

With a pyrometer (device shown in Fig. 1.6) the emissive power j of an object is recorded and the temperature of the object is computed via Stefan-Boltzmann's law [16]. One disadvantage is that the pyrometer needs to know the emissivity ϵ of the considered object for the temperature evaluation. Thus if one has no information about the object's ϵ a pyrometer is useless. Furthermore, the measurement can be defective due to reflection and transmission (glas) of the thermal radiation. As a consequence of these disadvantageous reasons the pyrometer is useful for a quick temperature estimation but certainly not suitable for precise measurements.

With the devices shown in the last sections we have a summary of the conventional temperature sensors. But the demand on sensors with new or better features is still far away from being over. Especially size and costs of sensors play an important role in technical and scientific applications. Thus the attractiveness of MEMS (microelectromechanical systems) as sensors at the microscale grew remarkably in the last decades. Owing to technical progress one is able to construct smaller (down to the nanoscale) structures acting as sensors which exhibit a sensitivity that can compete with conventional (larger) sensors shown above. MEMS show clear benefits compared with conventional systems. They are very small, allow integration with other devices and lead to low manufacturing costs.

The standard material used for MEMS is silicon, which is widely used in microelectronics, offering a huge variety of well implemented technological processes. Due to that, there are several design tools, developed in the last fifty years, available. Furthermore, silicon offers controllable and well understood electrical characteristics and desirable mechanical properties [18].

Due to the advantages of MEMS, their need is great and still development and research are demanded. In the course of dynamical investigations of a beam structure made of silicon we were able to create a beam structure with a strong temperature dependent resonant frequency (presented in chapter 6) which could be the basis of high sensitive resonant temperature sensors. Additionally, owing to the dynamical investigations we were also able to construct beam structures which are nearly independent of the temperature (chapter 7).

In the following section we want to provide the reader a theoretical introduction for the essential mechanical basis.

Chapter 2

Theory

The aim of this thesis is to determine the eigenfrequencies in terms of the temperature of metallic beam-structures and to analyze how the eigenfrequencies are influenced by geometrical parameter changes. To get the eigenfrequencies we start with equations of Continuum Mechanics describing the dynamics of our structures. The first one is the well-known Cauchy equation of motion

$$\nabla \cdot \mathbf{T}(\mathbf{r}, t) + \rho(\mathbf{r}, t)\mathbf{b}(\mathbf{r}, t) = \rho(\mathbf{r}, t)\ddot{\mathbf{u}}(\mathbf{r}, t), \quad (2.1)$$

where \mathbf{T} denotes the Cauchy stress tensor, \mathbf{b} the body force vector, ρ the volumetric mass density and \mathbf{u} the displacement vector. With Eq. (2.1) the acceleration of an infinitesimal volume element at the position \mathbf{r} is determined at any time t .

The second equation we need to determine the dynamics of the continuum gives the relation between the Cauchy stress tensor \mathbf{T} and the Green strain tensor \mathbf{E} :

$$\mathbf{T} = f(\mathbf{E}) \quad (2.2)$$

f denotes a function. \mathbf{E} is given by:

$$\mathbf{E} = \frac{1}{2}(\mathbf{H} + \mathbf{H}^T + \mathbf{H}^T\mathbf{H}) \quad \text{with} \quad \mathbf{H} = \nabla\mathbf{u} \quad (2.3)$$

\mathbf{H} is called the displacement gradient. Now we can write Eq. (2.2) as a Taylor series and restrict ourselves to the term which is linear in \mathbf{E} . If we calculate the Taylor expansion around $\mathbf{E} = 0$ the zeroth order term (the term which is independent of \mathbf{E}) need to be 0 as there can't be stress without strain. All the other higher-order terms can be neglected. Thus, we simplified Eq. (2.2) to:

$$\mathbf{T}_\alpha = \mathbf{S}_{\alpha\beta}\mathbf{E}_\beta \quad (2.4)$$

\mathbf{S} is called the stiffness matrix. Equation (2.4) fully written-out gives:

$$\begin{pmatrix} T_{11} \\ T_{22} \\ T_{33} \\ T_{23} \\ T_{31} \\ T_{12} \end{pmatrix} = \begin{pmatrix} S_{11} & S_{12} & S_{13} & S_{14} & S_{15} & S_{16} \\ S_{21} & S_{22} & S_{23} & S_{24} & S_{25} & S_{26} \\ S_{31} & S_{32} & S_{33} & S_{34} & S_{35} & S_{36} \\ S_{41} & S_{42} & S_{43} & S_{44} & S_{45} & S_{46} \\ S_{51} & S_{52} & S_{53} & S_{54} & S_{55} & S_{56} \\ S_{61} & S_{62} & S_{63} & S_{64} & S_{65} & S_{66} \end{pmatrix} \begin{pmatrix} E_{11} \\ E_{22} \\ E_{33} \\ E_{23} \\ E_{31} \\ E_{12} \end{pmatrix}$$

Additionally, we assume that the material of our beam-structures is isotropic. Hence, we get for our stiffness matrix:

$$\mathbf{S} = \frac{G}{1-2\nu} \begin{pmatrix} 2(1-\nu) & 2\nu & 2\nu & 0 & 0 & 0 \\ 2\nu & 2(1-\nu) & 2\nu & 0 & 0 & 0 \\ 2\nu & 2\nu & 2(1-\nu) & 0 & 0 & 0 \\ 0 & 0 & 0 & 1-2\nu & 0 & 0 \\ 0 & 0 & 0 & 0 & 1-2\nu & 0 \\ 0 & 0 & 0 & 0 & 0 & 1-2\nu \end{pmatrix} \quad (2.5)$$

$$\text{with } G = \frac{E}{2(1+\nu)}$$

E denotes the well-known Young's modulus and ν the Poisson's ratio. G is called shear modulus.

Equation (2.1) and Eq. (2.4) with boundary and initial conditions determine the dynamics of our beam-structures if there is no thermal strain. As we want to obtain the eigenfrequencies of beam-structures in terms of the temperature T we also need to take thermal effects in the beam-material into account. We know from daily life that temperature causes thermal strain in materials. To describe this effect continuum mechanics provide us the following equation:

$$\mathbf{E}_{\text{th}} = \alpha(T - T_0)\mathbb{1} \quad (2.6)$$

\mathbf{E}_{th} denotes the thermal strain tensor, α is called the linear coefficient of thermal expansion and T_0 is the reference temperature at which we observe no thermal strain.

Hence, the total strain is given by:

$$\mathbf{E}_{\text{tot}} = \mathbf{E}_{\text{el}} + \mathbf{E}_{\text{th}} = \frac{1}{2}(\mathbf{H}_{\text{el}} + \mathbf{H}_{\text{el}}^T + \mathbf{H}_{\text{el}}^T \mathbf{H}_{\text{el}}) + \frac{1}{2}(\mathbf{H}_{\text{th}} + \mathbf{H}_{\text{th}}^T + \mathbf{H}_{\text{th}}^T \mathbf{H}_{\text{th}}) \quad (2.7)$$

\mathbf{E}_{el} denotes the elastic strain corresponding to the stress (see Eq. (2.4)).

With Eq. (2.1), Eq. (2.4) and Eq. (2.6) we are now able to determine the dynamics of our beam-structures at a special temperature T .

You probably ask yourself why we don't assume an isotropic, linear elastic material, i. e. the well-known Hookean material. The answer is that in this case the eigenfrequencies of our system don't change with the temperature or in other words: We have the same eigenfrequencies for any temperature. We want to show this fact in the following proof.

Let us assume a Hookean material for our beam-structures. Then the Green strain tensor \mathbf{E} would be linearized:

$$\mathbf{E} = \frac{1}{2}(\mathbf{H} + \mathbf{H}^T) \quad \text{with} \quad \mathbf{H} = \nabla \mathbf{u} \quad (2.8)$$

The stiffness matrix would be the same as in Eq. (2.5). The total strain tensor is now given by:

$$\mathbf{E}_{\text{tot}} = \mathbf{E}_{\text{el}} + \mathbf{E}_{\text{th}} = \frac{1}{2}(\mathbf{H}_{\text{el}} + \mathbf{H}_{\text{el}}^T) + \frac{1}{2}(\mathbf{H}_{\text{th}} + \mathbf{H}_{\text{th}}^T) \quad (2.9)$$

Owing to the linear form of \mathbf{E} we can rearrange Eq. (2.9) and find an expression for the total displacement gradient \mathbf{H}_{tot} or in further consequence an expression for the total displacement vector \mathbf{u}_{tot} :

$$\begin{aligned} \mathbf{E}_{\text{tot}} &= \frac{1}{2}(\mathbf{H}_{\text{el}} + \mathbf{H}_{\text{el}}^T) + \frac{1}{2}(\mathbf{H}_{\text{th}} + \mathbf{H}_{\text{th}}^T) = \\ &= \frac{1}{2}((\mathbf{H}_{\text{el}} + \mathbf{H}_{\text{th}}) + (\mathbf{H}_{\text{el}} + \mathbf{H}_{\text{th}})^T) = \\ &= \frac{1}{2}((\nabla \mathbf{u}_{\text{el}} + \nabla \mathbf{u}_{\text{th}}) + (\nabla \mathbf{u}_{\text{el}} + \nabla \mathbf{u}_{\text{th}})^T) \\ &= \frac{1}{2}((\nabla(\mathbf{u}_{\text{el}} + \mathbf{u}_{\text{th}})) + (\nabla(\mathbf{u}_{\text{el}} + \mathbf{u}_{\text{th}}))^T) = \\ &= \frac{1}{2}((\nabla \mathbf{u}_{\text{tot}}) + (\nabla \mathbf{u}_{\text{tot}})^T) = \\ &= \frac{1}{2}(\mathbf{H}_{\text{tot}} + \mathbf{H}_{\text{tot}}^T) \end{aligned} \quad (2.10)$$

The Cauchy equation of motion without body forces is given by (see Eq. (2.1)):

$$\nabla \cdot \mathbf{T}(\mathbf{r}, t) = \rho(\mathbf{r}, t) \ddot{\mathbf{u}}_{\text{tot}}(\mathbf{r}, t) \quad (2.11)$$

Inserting the stress-strain relation (see Eq. (2.4)) for a Hookean model gives:

$$2G \nabla \cdot \left[\mathbf{E}_{\text{el}}(\mathbf{r}, t) + \frac{\nu}{1-2\nu} (\text{Tr} \mathbf{E}_{\text{el}}(\mathbf{r}, t)) \mathbb{1} \right] = \rho(\mathbf{r}, t) \ddot{\mathbf{u}}_{\text{tot}}(\mathbf{r}, t) \quad (2.12)$$

With $\mathbf{H}_{\text{el}} = \nabla \mathbf{u}_{\text{el}}$ one can rearrange Eq. (2.12) to (see [1]):

$$G \left[\Delta \mathbf{u}_{\text{el}}(\mathbf{r}, t) + \frac{1}{1-2\nu} \nabla (\nabla \cdot \mathbf{u}_{\text{el}}(\mathbf{r}, t)) \right] = \rho(\mathbf{r}, t) \ddot{\mathbf{u}}_{\text{tot}}(\mathbf{r}, t) \quad (2.13)$$

Looking at derivation Eq. (2.10) we see that $\mathbf{u}_{\text{tot}} = \mathbf{u}_{\text{el}} + \mathbf{u}_{\text{th}}$. The temperature T should not change with time t as we want to calculate the eigenfrequencies of the system at one special temperature. Thus, the thermal displacement is independent of time $\mathbf{u}_{\text{th}} = \mathbf{u}_{\text{th}}(\mathbf{r})$. If we insert $\mathbf{u}_{\text{tot}}(\mathbf{r}, t) = \mathbf{u}_{\text{el}}(\mathbf{r}, t) + \mathbf{u}_{\text{th}}(\mathbf{r})$ into Eq. (2.13) the second derivative with respect to time cancels $\mathbf{u}_{\text{th}}(\mathbf{r})$ because it is independent of time:

$$\begin{aligned} G \left[\Delta \mathbf{u}_{\text{el}}(\mathbf{r}, t) + \frac{1}{1-2\nu} \nabla(\nabla \cdot \mathbf{u}_{\text{el}}(\mathbf{r}, t)) \right] &= \rho(\mathbf{r}, t) \frac{d^2}{dt^2} (\mathbf{u}_{\text{el}}(\mathbf{r}, t) + \mathbf{u}_{\text{th}}(\mathbf{r})) \\ &= G \left[\Delta \mathbf{u}_{\text{el}}(\mathbf{r}, t) + \frac{1}{1-2\nu} \nabla(\nabla \cdot \mathbf{u}_{\text{el}}(\mathbf{r}, t)) \right] = \rho(\mathbf{r}, t) \frac{d^2}{dt^2} \mathbf{u}_{\text{el}}(\mathbf{r}, t) \end{aligned} \quad (2.14)$$

Looking at derivation Eq. (2.14) we conclude that the final equation that determines the dynamics of our structures is independent of the thermal displacement $\mathbf{u}_{\text{th}}(\mathbf{r})$ and thus, independent of the temperature T . Hence, we need the assumption of a nonlinear material, which prevents a rearrangement like in derivation Eq. (2.10) and leads to a more complicated relation between \mathbf{u}_{el} , \mathbf{u}_{th} and $\mathbf{u}_{\text{tot}} = f(\mathbf{u}_{\text{el}}, \mathbf{u}_{\text{th}})$.

Chapter 3

Comsol Verification

In chapter 2 we prepared the equations for motion, stiffness and thermal expansion, i. e. Eq. (2.1), Eq. (2.4) and Eq. (2.6), that are necessary to calculate the eigenfrequencies of our beam-structures in terms of the temperature. To solve these equations we use the software COMSOL Multiphysics, which uses the finite element method for computations. Before we start with our main simulations we first want to verify the reliability of this software. We do this by considering mechanical problems that can be solved analytically and compare this analytical solution with the results of the FEM software. In the following sections we deal with three mechanical problems to verify the software.

3.1 Cantilever with normal force

For our first verification we consider a beam, which is fixed at one end (=cantilever) and loaded at the other with a force F . The force is acting perpendicular onto the center of the surface of the beam ($= r_{cb}$). Our purpose is to determine the displacement of the beam into the x -direction caused by the force F . The beam's length $l = 20$ mm, its height $h = 2$ mm and its width $b = 3$ mm. The beam's material is isotropic and linear elastic (=Hookean) with a Young's modulus of $E = 2$ Pa. We neglect the gravitation and set $F = 3 \cdot 10^{-6}$ N

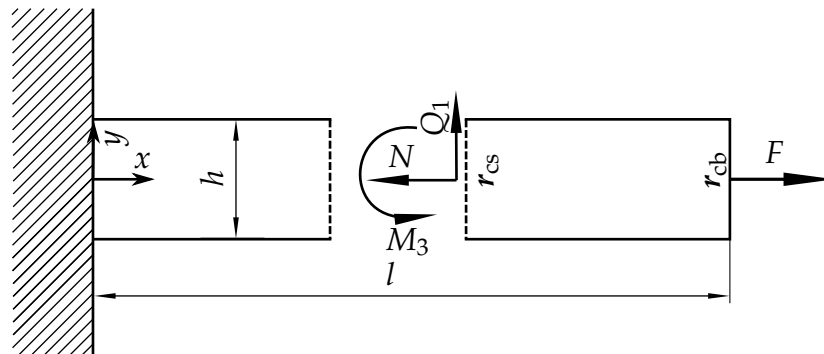


Figure 3.1: Cantilever with normal force F . Cross-section to z -coordinate.

Analytic calculation: At first we determine the internal forces F_s and moments M_s (the moments are about the section-center \mathbf{r}_{cs}) of a cross section at the position x . Force equilibrium and moment equilibrium result in:

$$\mathbf{F}_s(x) + \mathbf{F} = \begin{pmatrix} -N(x) \\ Q_1(x) \\ Q_2(x) \end{pmatrix} + \begin{pmatrix} F \\ 0 \\ 0 \end{pmatrix} = 0$$

$$\Rightarrow N(x) = N = F, \quad Q_1(x) = 0, \quad Q_2(x) = 0 \quad (3.1)$$

$$\mathbf{M}_s(x) + \mathbf{F} \times (\mathbf{r}_{cs} - \mathbf{r}_{cb}) = \begin{pmatrix} M_T(x) \\ M_2(x) \\ M_3(x) \end{pmatrix} + \left(\begin{pmatrix} l \\ 0 \\ 0 \end{pmatrix} - \begin{pmatrix} x \\ 0 \\ 0 \end{pmatrix} \right) \times \begin{pmatrix} F \\ 0 \\ 0 \end{pmatrix} =$$

$$\begin{pmatrix} M_T(x) \\ M_2(x) \\ M_3(x) \end{pmatrix} + 0 = 0$$

$$\Rightarrow M_T(x) = 0, \quad M_2(x) = 0, \quad M_3(x) = 0 \quad (3.2)$$

All internal forces and moments are 0 except of $N = F$. One can show that in this case the following approximation for the stress tensor \mathbf{T} is reliable for beams with a small cross-section (see [2]).

$$\mathbf{T} = \begin{pmatrix} \sigma & 0 & 0 \\ 0 & 0 & 0 \\ 0 & 0 & 0 \end{pmatrix} \quad \text{with} \quad \sigma = \frac{N}{hb} = \frac{N}{A_s} = \frac{F}{A_s} \quad (3.3)$$

The beam's material should be a Hookean material, thus the connection between the stress tensor \mathbf{T} and strain tensor \mathbf{E} (see Eq. (2.8)) is described by Eq. (2.4) with stiffness \mathbf{S} given by Eq. (2.5). One can rearrange Eq. (2.4) with Eq. (2.5) to the following expression (see [3]):

$$\mathbf{E} = \frac{1}{2}(\nabla \mathbf{u} + (\nabla \mathbf{u})^T) = \frac{1}{2G} \left[\mathbf{T} - \frac{\nu}{1+\nu} (\text{Tr} \mathbf{T}) \mathbf{1} \right] \quad (3.4)$$

As mentioned above we are interested in the displacement of the beam into the x -direction, i. e. u_x . With Eq. (3.4) and Eq. (3.3) we find that the off-diagonal elements of \mathbf{E} are 0 and thus, we get only one differential equation including u_x namely:

$$\mathbf{E}_{11} = \frac{\partial u_x}{\partial x} = \frac{F}{EA_s} \quad (3.5)$$

Integration leads us to:

$$u_x = \int_0^x \frac{F}{EA_s} d\tilde{x} = \frac{F}{EA_s} \tilde{x} \Big|_0^x = \frac{Fx}{EA_s} \quad (3.6)$$

With $F = 3 \cdot 10^{-6}$ N, $A_s = hb = 6 \cdot 10^{-6}$ m² and $E = 2$ Pa = 2 N/m² we get the following solution for u_x :

$$u_x = \frac{Fx}{EA_s} = \frac{3 \cdot 10^{-6} x}{2 \cdot 6 \cdot 10^{-6}} = \frac{x}{4} \text{ mm} \quad (3.7)$$

FEM solution: We let COMSOL Multiphysics simulate the same mechanical problem. As mentioned above the software bases on the finite element method which is a powerful method to solve differential equations. Before the simulation starts, we need to define a mesh comprising the finite elements. On the one hand the numerical error becomes smaller if the mesh consists of more elements but on the other hand an increasing number of elements also entails a longer simulation time. Hence, one needs to check which upper bound of the numerical error is sufficient and how much time for the simulation is available. The mesh we chose for our simulation consists of 29474 tetrahedral elements shown in Fig. 3.2 yielding 128262 degrees of freedom.

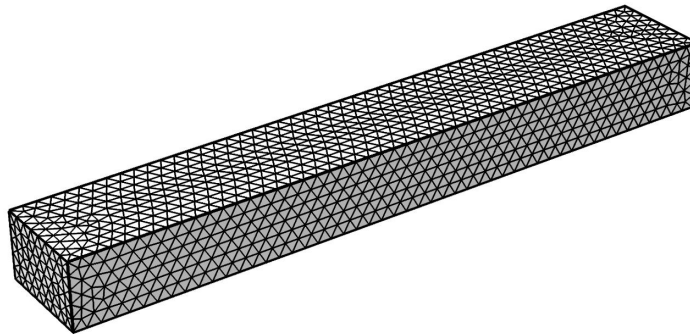


Figure 3.2: Mesh of the beam consisting of 29474 tetrahedral elements with 128262 degrees of freedom.

The simulation took a time of 92s and in Fig. 3.3 and Fig. 3.4 we show its results for the stress tensor element $\mathbf{T}_{11} = \sigma$ and the displacement into the x -direction u_x . Additionally, we plotted in both Figures the analytical solutions for σ (Eq. (3.3) which leads with $F = 3 \cdot 10^{-6} \text{ N}$, $A_s = 6 \cdot 10^{-6} \text{ m}^2$ to $\sigma = 0.5 \text{ N/m}^2$) and u_x (Eq. (3.7)). We Furthermore, show in each Figure the relative error of the COMSOL- and the analytical solution to simplify comparison of the two results.

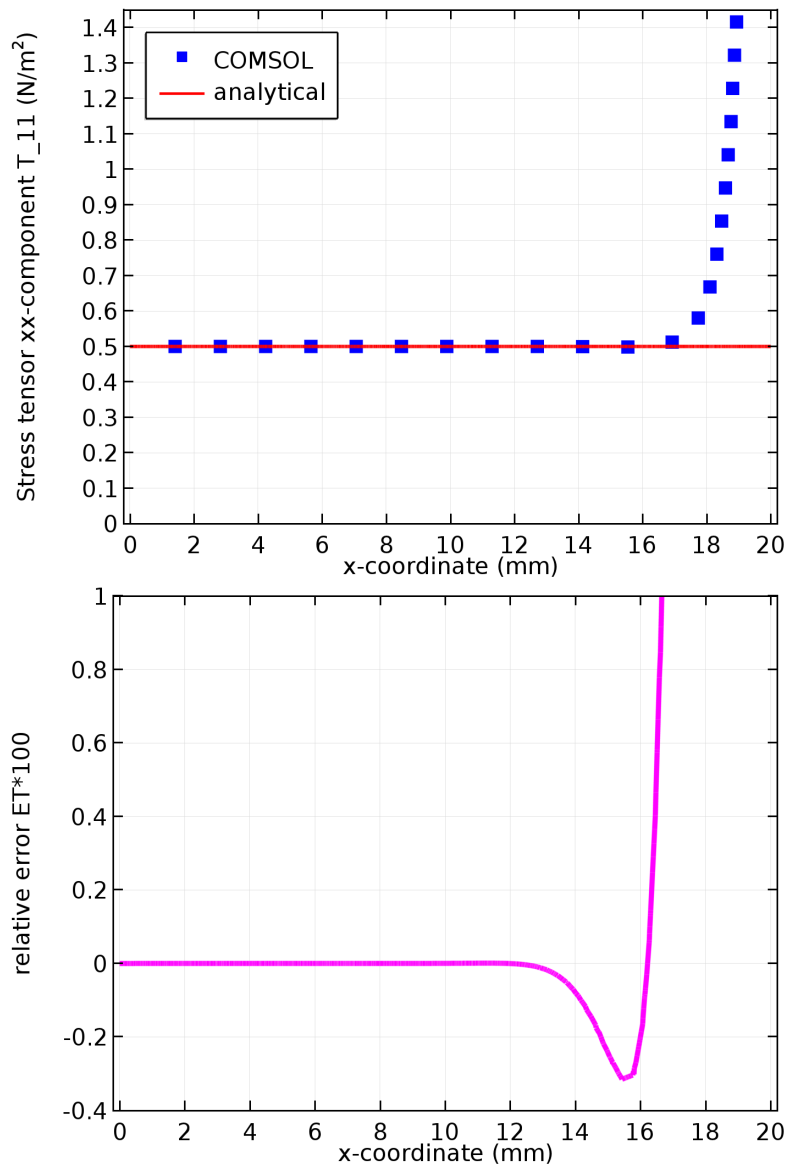


Figure 3.3: Top: COMSOL-solution (points) and analytical solution (line) for the stress tensor element \mathbf{T}_{11} (in N/m^2) versus x -coordinate (in mm).

Bottom: The relative error $ET = (\mathbf{T}_{11\text{comsol}} - \mathbf{T}_{11\text{analytic}}) / \mathbf{T}_{11\text{analytic}}$ of \mathbf{T}_{11} between COMSOL- and analytical solution multiplied by a factor of 100.

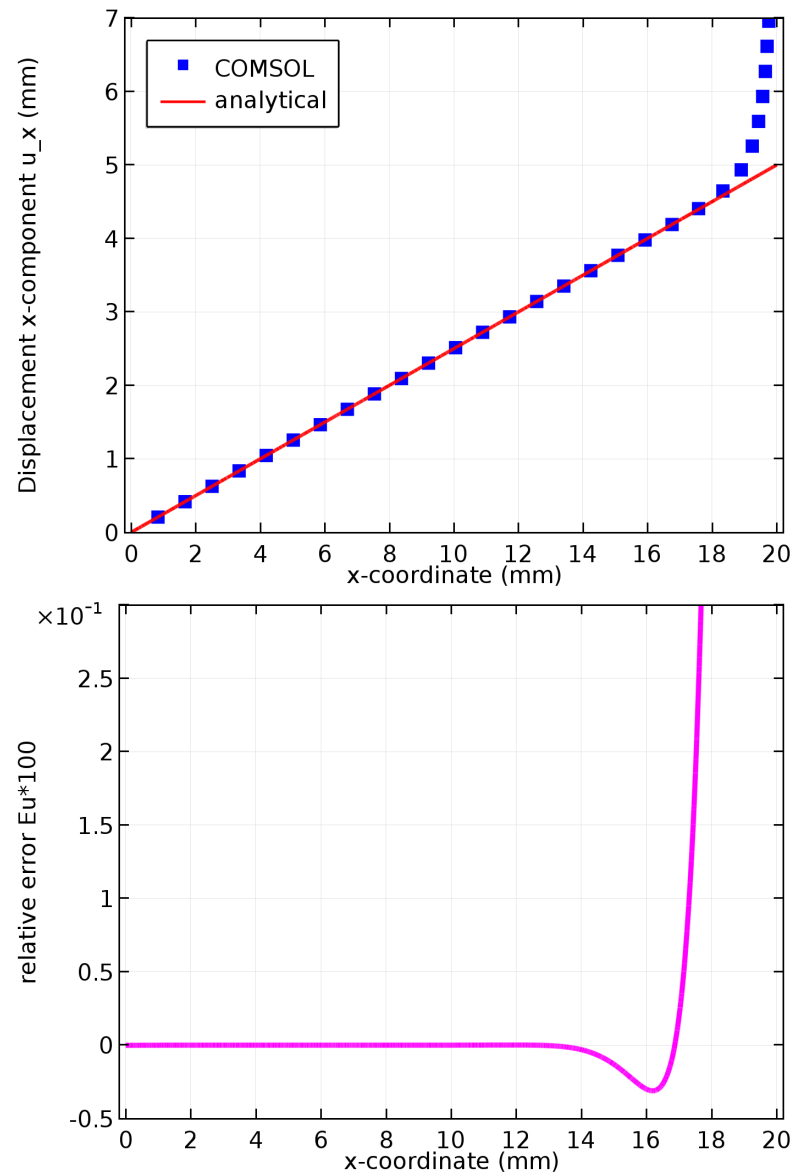


Figure 3.4: Top: COMSOL-solution (points) and analytical solution (line) for the displacement component u_x (in mm) versus x -coordinate (in mm). Bottom: The relative error $Eu = (u_{x\text{comsol}} - u_{x\text{analytic}})/u_{x\text{analytic}}$ of u_x between COMSOL- and analytical solution multiplied by a factor of 100.

Looking at the software-solution of \mathbf{T}_{11} (Fig. 3.3) we see that it is in principal constant at a value of 0.5 N/m^2 for $x = 0 \rightarrow 16 \text{ mm}$ and starts increasing from $x = 16 \text{ mm} \rightarrow 20 \text{ mm}$. We observe the same characteristic for the FEM solution of u_x . For $x = 0 \rightarrow 17 \text{ mm}$ $u_x = \frac{x}{4}$ and for $x = 17 \rightarrow 20 \text{ mm}$ u_x rises. Comparing the software-solutions with our analytical results we conclude that both almost

coincide for $x = 0 \rightarrow 16 - 17$ mm and start to differ significantly with $x > 16 - 17$ mm where the deviation increases with greater x . The reason for this is not a numerical error by the simulation with COMSOL but in our analytical calculation. In Eq. (3.3) we made an approximation for the stress tensor that becomes better if the ratio between the beam's length and its cross-section (i. e. l/A_s) gets larger. The approximation would be exact if the ratio $l/A_s \rightarrow \infty$ or if the force F does not act on only one point but on all surface-points equally, i. e. like a pressure. In reality at the end of the beam, points of the cross-section the closer they are to the point where the force acts the stronger they will be pulled into the x -direction. This is exactly the property that our FEM result for u_x exhibits. Due to this fact we conclude that COMSOL has simulated our mechanical issue well.

3.2 Cantilever with shear load

In the second verification-problem we again consider a cantilever but now the upper surface is exposed to a shear load p . The shear load is applied uniformly and not to a single point like in the previous section 3.1. Thus, p is defined as a force per unit area $p = 2 \text{ N/m}^2 = 2 \cdot 10^{-6} \text{ N/mm}^2$. The gravity is again neglected. The cantilever has the same geometry like the one in section 3.1. We assume a Hookean material for our beam with a Young's modulus of $E = 10^4 \text{ Pa}$. This time we are interested in the beam's displacement regarding the y -direction, i. e. u_y .

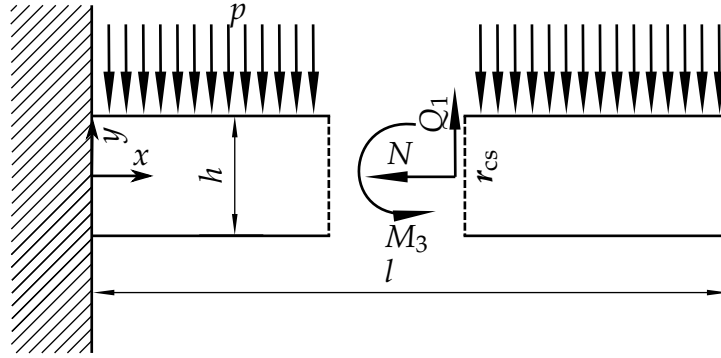


Figure 3.5: Cantilever with shear load p . Cross-section to z -coordinate.

Analytic calculation: We get with force and moment equilibrium of the internal forces F_s and moments M_s (the moments are about the section-center r_{cs}) of a cross section at the position x :

$$\mathbf{F}_s(x) + \mathbf{Q}(x) = \begin{pmatrix} -N(x) \\ Q_1(x) \\ Q_2(x) \end{pmatrix} + \begin{pmatrix} 0 \\ \int_x^l \int_{-b/2}^{b/2} -pd\tilde{x}d\tilde{z} \\ 0 \end{pmatrix} = 0$$

$$\Rightarrow N(x) = 0, \quad Q_1(x) = (l-x)pb = (20-x)6 \cdot 10^{-6} \text{ N}, \quad Q_2(x) = 0 \quad (3.8)$$

$$\begin{aligned} \mathbf{M}_s(x) + \int_x^l \int_{-b/2}^{b/2} (\mathbf{r}_p - \mathbf{r}_{cs}) \times \mathbf{p} d\tilde{x}d\tilde{z} &= \\ \begin{pmatrix} M_T(x) \\ M_2(x) \\ M_3(x) \end{pmatrix} + \int_x^l \int_{-b/2}^{b/2} \left(\begin{pmatrix} \tilde{x} \\ h/2 \\ \tilde{z} \end{pmatrix} - \begin{pmatrix} x \\ 0 \\ 0 \end{pmatrix} \right) \times \begin{pmatrix} 0 \\ -p \\ 0 \end{pmatrix} d\tilde{x}d\tilde{z} &= \\ \begin{pmatrix} M_T(x) \\ M_2(x) \\ M_3(x) \end{pmatrix} + \int_x^l \int_{-b/2}^{b/2} \begin{pmatrix} \tilde{z}p \\ 0 \\ (x-\tilde{x})p \end{pmatrix} d\tilde{x}d\tilde{z} &= \\ \begin{pmatrix} M_T(x) \\ M_2(x) \\ M_3(x) \end{pmatrix} + \frac{1}{2} \begin{pmatrix} 0 \\ 0 \\ -(l^2 - 2xl + x^2)pb \end{pmatrix} &= 0 \end{aligned}$$

$$\Rightarrow M_T(x) = 0, \quad M_2(x) = 0, \quad M_3(x) = \frac{1}{2}(l^2 - 2xl + x^2)pb \quad (3.9)$$

We are allowed to approximate the stress tensor \mathbf{T} with the following expression [4]:

$$\mathbf{T} = \begin{pmatrix} \sigma_y & 0 & 0 \\ 0 & 0 & 0 \\ 0 & 0 & 0 \end{pmatrix} \quad \text{with} \quad \sigma_y = \frac{yM_3(x)}{I_z} = \frac{12yM_3(x)}{bh^3} \quad (3.10)$$

I_z is the second moment of area and defined by $I_z \equiv \int_{-b/2}^{b/2} \int_{-h/2}^{h/2} y^2 d\tilde{y}d\tilde{z}$.

To determine u_y we take the relation between stress and strain for a Hookean material given by Eq. (3.4), insert Eq. (3.10) for \mathbf{T} and prepare with Eq. (3.4) the following differential equation for u_y [4]:

$$\frac{\partial^2 u_y}{\partial x^2} = \frac{-M_3(x)}{EI_z} = \frac{-12M_3(x)}{Ebh^3} \quad (3.11)$$

Two times integration yields:

$$u_y = \int \int \frac{-12M_3(x)}{Ebh^3} = \frac{-6p}{Eh^3} \left(\frac{l^2 x^2}{2} - \frac{lx^3}{3} + \frac{x^4}{12} \right) + u'_y(0) + u_y(0) \quad (3.12)$$

The beam is fixed at $x = 0$ thus, $u'_y(0) = 0$ and $u_y(0) = 0$. With $p = 2 \cdot 10^{-6} \text{ N/mm}^2$, $E = 10^5 \text{ Pa} = 10^{-2} \text{ N/mm}^2$, $l = 20 \text{ mm}$ and $h = 2 \text{ mm}$ we get our final analytical solution for $u_y(x)$:

$$u_y(x) = (-30x^2 + x^3 - \frac{1}{80}x^4) \cdot 10^{-3} \text{ mm} \quad (3.13)$$

FEM solution: The same problem is solved with COMSOL Multiphysics. The mesh we used for the numerical computation comprises 29467 tetrahedral elements with 129705 degrees of freedom. The simulation lasted 64 s. Figure 3.6 and Fig. 3.7 depict the yielded stress tensor element \mathbf{T}_{11} and the displacement into the y -direction u_y respectively. We also plotted the analytical solutions namely Eq. (3.10) for \mathbf{T}_{11} and Eq. (3.13) for u_y . For easy comparison of the software solutions and the analytical ones we additionally show in both Figures the relative errors between them. \mathbf{T}_{11} depends on both the x - and y -direction.

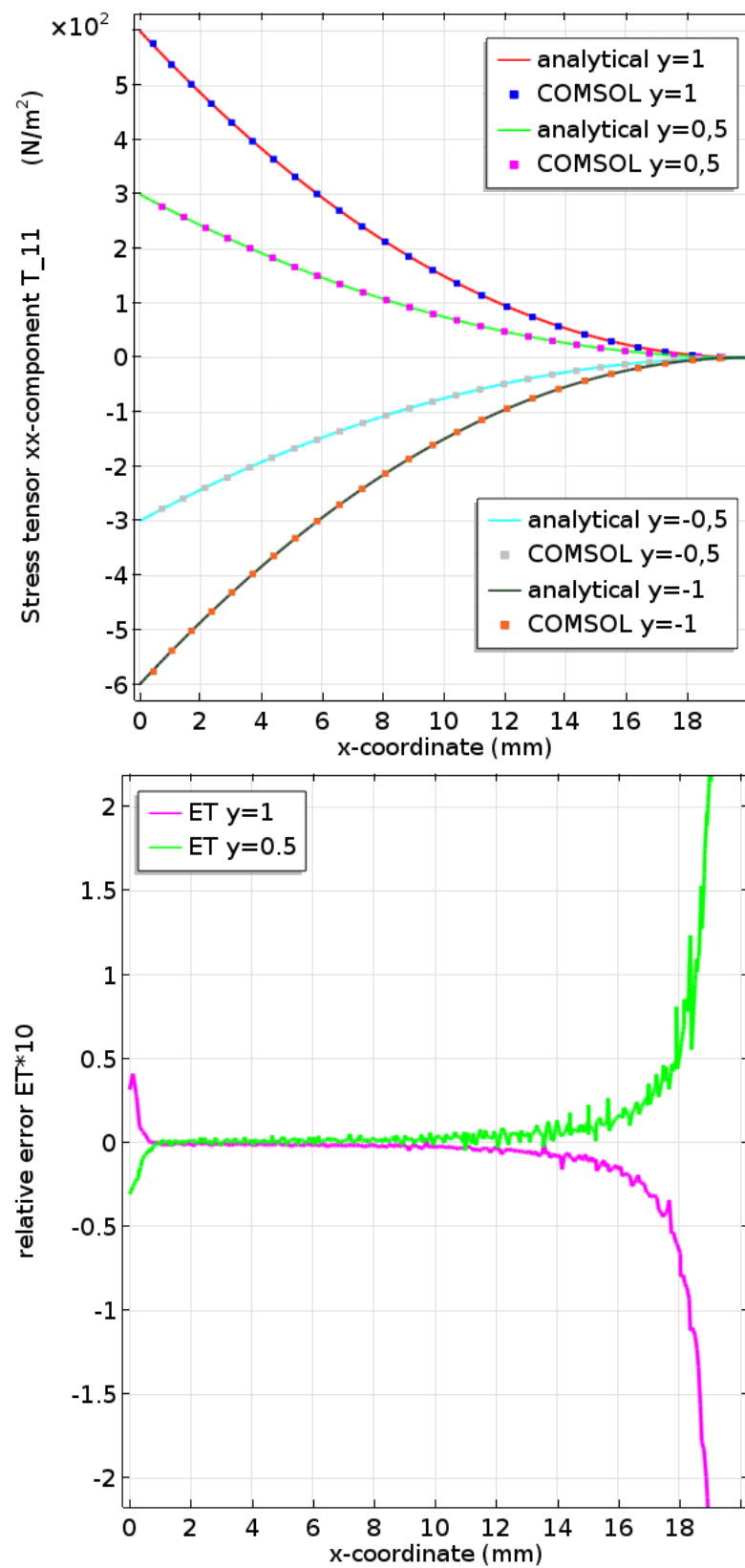


Figure 3.6: Top: FEM solution (points) and analytical solution (line) for the stress tensor element T_{11} (in N/m^2) at $y = 1, 0.5, -0.5$ and -1 mm versus x -coordinate (in mm). Bottom: The relative error $ET = (\mathbf{T}_{11\text{comsol}} - \mathbf{T}_{11\text{analytic}}) / \mathbf{T}_{11\text{analytic}}$ of T_{11} between COMSOL- and analytical solution at $y = 1$ and 0.5 mm multiplied by a factor of 10.

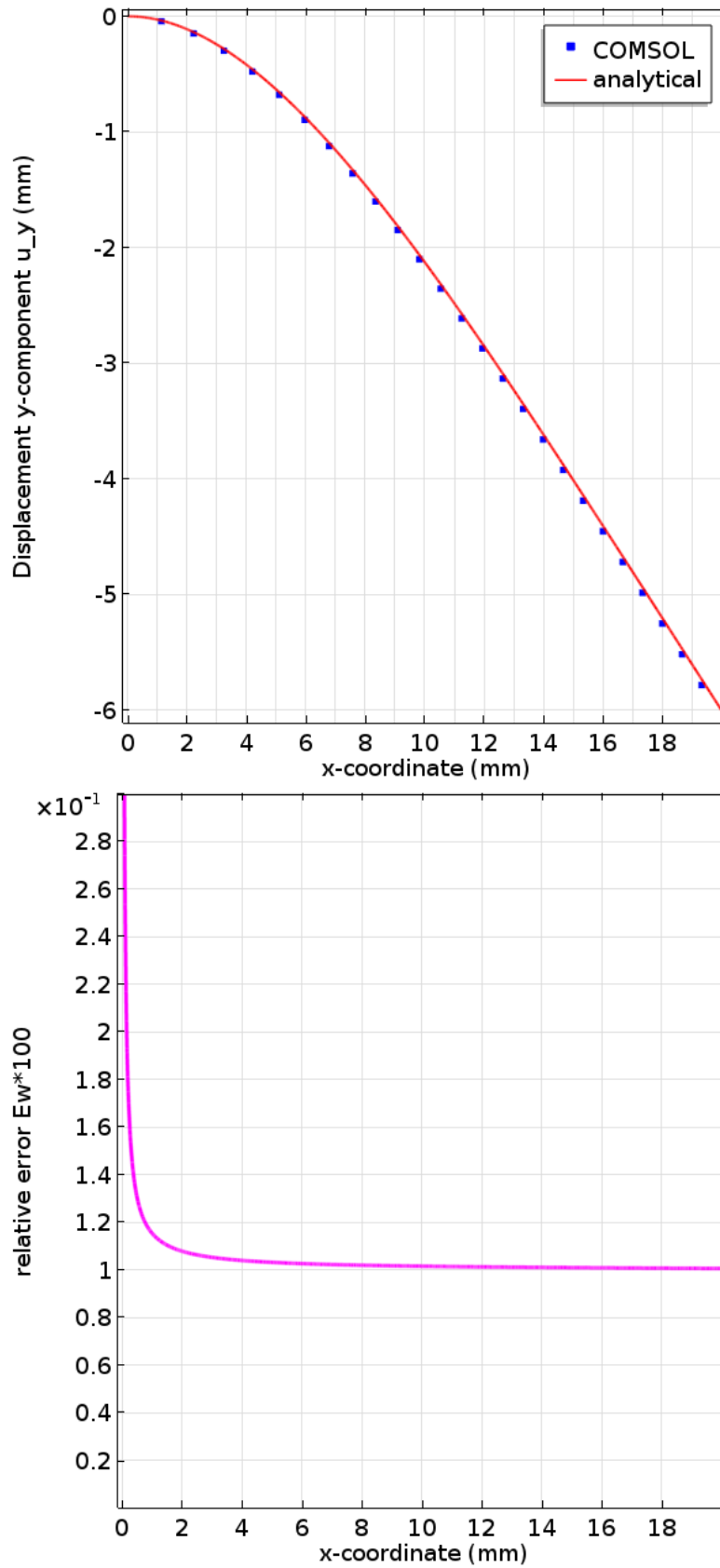


Figure 3.7: Top: FEM solution (points) and analytical solution (line) for the displacement component u_y (in mm) at $y = 0$ mm versus x -coordinate (in mm) for a cantilever with uniformly distributed load. Bottom: The relative error $E_w = (u_{y\text{comsol}} - u_{y\text{analytic}}) / u_{y\text{analytic}}$ of u_y between COMSOL- and analytical solution multiplied by a factor of 100.

Fig. 3.6 stresses the quality of the COMSOL-solution for T_{11} (at least for such single geometries). The same is true for the u_y results in Fig. 3.7. Nevertheless we observe, that both relative errors ET and Ew grow at the end of the beam where it is clamped. The increased errors at $x = 0$ mm is due to the fact, that we didn't take the entire boundary condition for u at $x = 0$ mm into account. In our analytical computation we only considered $u'_y(0) = 0$ and $u_y(0) = 0$ and ignored the other displacement components $u_x(0) = 0$ and $u_z(0) = 0$. This clearly leads to a mistake (especially around $x = 0$ mm) in the analytical solution and as a consequence the relative error for T_{11} and u_y rises. Furthermore, the relative error ET increases at the end of the beam ($x = 20$ mm) too. The reason for this might be that due to the deflection of the beam the angle between the surface and the shear load differs from 90° , i. e. the angle gets acute and this more at the end of the beam as there the deflection u_y is the largest. In the analytical calculation we didn't take this fact into account yielding a mistake for T_{11} at the end of the beam. Whether this effect has a strong influence on u_y or not is difficult to say and would need a more detailed examination. All in all one concludes that the relative errors are basically a consequence of mistakes in the analytical calculation. Hence, one can state that the numerical solution of the FEM software and the analytical solution coincide over a huge range of the mechanical deflection.

3.3 Eigenfrequencies of a clamped beam including thermal expansion

In our last verification we consider a beam fixed on both sides. There is no external force like in the last setups. The beam is clamped at the temperature $T = 298$ K (=room temperature) and then cooled down to $T = 283$ K. Our goal is to determine the beam's eigenfrequencies of modes regarding the y -direction, i. e. flexural modes. Additionally, the thermal expansion caused by the cooling should be taken into account. Beam geometry: length $l = 100$ mm, height $h = 1$ mm and width $b = 2$ mm. Beam material: silicon with a density of $\rho = 2329$ kg/m³ and a Young's modulus of $E = 170 \cdot 10^9$ Pa. The linear coefficient of thermal expansion of silicon $\alpha = 2.6 \cdot 10^{-6}$ 1/K.

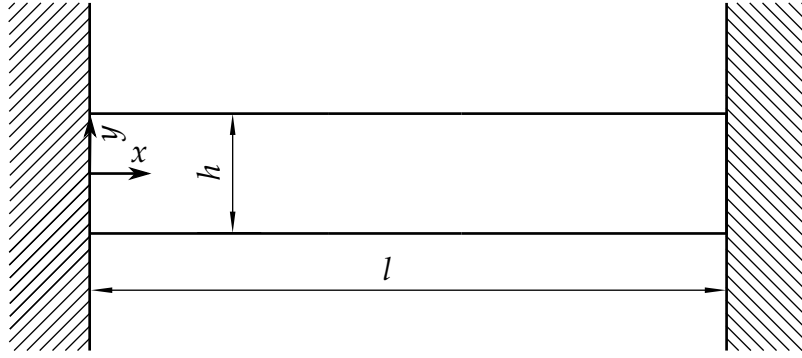


Figure 3.8: Clamped beam. Cross-section to z -coordinate.

Analytic calculation: Due to cooling down to $T = 283$ K the material gets a thermal strain \mathbf{E}_{th} described by Eq. (2.6). If the beam would not be clamped it would contract. The suspension is considered to be rigid. This is fulfilled for the most MEMS since the supporting structure is typically much thicker than the moving one. Thus thermal strain into the x -direction \mathbf{E}_{th11} needs to be compensated by an elastic strain regarding the same direction \mathbf{E}_{el11} . Hence, we get for \mathbf{E}_{el11} :

$$\mathbf{E}_{th11} = \alpha(T - T_0) = -\mathbf{E}_{el11} \quad (3.14)$$

Furthermore, force equilibrium and moment equilibrium together with an approximation for the stress tensor \mathbf{T} result in [2], [4]:

$$\mathbf{T} = \begin{pmatrix} \sigma & 0 & 0 \\ 0 & 0 & 0 \\ 0 & 0 & 0 \end{pmatrix} \quad \text{where } \sigma \text{ is indefinite} \quad (3.15)$$

\mathbf{E}_{el} is linked to the stress tensor \mathbf{T} by Eq. (2.4) with a stiffness given by Eq. (2.5). Thus, we get together with Eq. (3.15):

$$\mathbf{E}_{el} = \frac{1}{2G} \left[\mathbf{T} - \frac{\nu}{1+\nu} (\text{Tr}\mathbf{T})\mathbf{1} \right] \quad (3.16)$$

$$\Rightarrow \mathbf{E}_{el} = \frac{1}{E} \begin{pmatrix} \sigma & 0 & 0 \\ 0 & -\nu\sigma & 0 \\ 0 & 0 & -\nu\sigma \end{pmatrix} \quad (3.17)$$

With Eq. (3.14) we know the strain tensor element \mathbf{E}_{el11} and thus, we are able to determine σ :

$$E_{el11} = \alpha(T_0 - T) = \frac{\sigma}{E} \Rightarrow \sigma = \alpha E(T_0 - T) = 6.63 \cdot 10^6 \text{ N/m}^2. \quad (3.18)$$

Cooling down the beam from $T = 298\text{ K}$ to $T = 283\text{ K}$ causes an internal force N in the beam perpendicular to the $y - z$ -plane given by:

$$N = \int_{-h/2}^{h/2} \int_{-b/2}^{b/2} \sigma d\tilde{y}d\tilde{z} = hb\sigma = A_s\sigma \quad (3.19)$$

To determine the eigenfrequencies of the clamped beam. We need first the equations which describe the dynamics of the system (chapter 2, Eq. (2.1), Eq. (2.4) and Eq. (2.6)). However these equations cannot be solved analytically. Hence, we need an approximation for them and one can show that the dynamics of a clamped beam with an internal normal force N are well described by the well-known Euler-Bernoulli equation extended with a term including N :

$$\frac{\partial^4 u_y}{\partial x^4} - \frac{N}{EI_z} \frac{\partial^2 u_y}{\partial x^2} + \frac{\rho A_s}{EI_z} \frac{\partial^2 u_y}{\partial t^2} = 0 \quad (3.20)$$

The second moment of area I_z is for the beam cross section $I_z = \frac{bh^3}{12}$. It is sufficient to consider only the dynamics regarding u_y as we are solely interested in the eigenfrequencies of modes concerning displacements into the y -direction. From Eq. (3.20) we want to derive the eigenfrequencies. Thus, we solve the system with a separation ansatz $u_y(x, t) = U(x)e^{i\omega t}$, insert it into Eq. (3.20) and get after canceling the exponents:

$$\begin{aligned} \frac{\partial^4 U(x)}{\partial x^4} - f \frac{\partial^2 U(x)}{\partial x^2} - k\omega^2 U(x) &= 0 \\ \text{with } f = \frac{N}{EI_z} = \frac{12\sigma}{Eh^2} \text{ and } k = \frac{\rho A_s}{EI_z} = \frac{12\rho}{Eh^2} \end{aligned} \quad (3.21)$$

The ansatz $U(x) = Ce^{\lambda x}$ yields after canceling the exponents and constant C :

$$\lambda^4 - f\lambda^2 - k\omega^2 = 0. \quad (3.22)$$

This equation has four solutions for λ :

$$\begin{aligned} \lambda_{1,2} &= \pm \sqrt{\frac{f}{2} + \sqrt{\frac{f^2}{4} + k\omega^2}} = \pm L \\ \lambda_{3,4} &= \pm i \sqrt{-\frac{f}{2} + \sqrt{\frac{f^2}{4} + k\omega^2}} = \pm iL' \end{aligned} \quad (3.23)$$

The fundamental solution for $U(x)$ is hence:

$$U(x) = C_1 e^{xL} + C_2 e^{-xL} + C_3 e^{ixL'} + C_4 e^{-ixL'} \quad (3.24)$$

The beam is clamped at $x = 0$ and $x = l$ thus, we have the following boundary conditions:

$$U(0) = 0 \quad U'(0) = 0 \quad U(l) = 0 \quad U'(l) = 0 \quad (3.25)$$

Inserting the fundamental solution for $U(x)$ (Eq. (3.24)) into the boundary conditions (Eq. (3.25)) leads to a linear system of equations for $C_{1,2,3,4}$ consisting of four equations. The linear equation system can be written as a matrix equation:

$$\mathbf{M}_{4 \times 4} \mathbf{C} = 0 \quad \text{with} \quad \mathbf{C}^T = (C_1, C_2, C_3, C_4) \quad (3.26)$$

Equation (3.26) has only a non trivial solution if $\det(M) = 0$. After some calculation we find that this condition is only fulfilled if:

$$2 + \left(\frac{L}{L'} - \frac{L'}{L} \right) \sin(1L') \sinh(1L) - 2\cos(1L) \cos(1L') = 0 \quad (3.27)$$

Equation (3.27) is only for a set of ω_n fulfilled which represent the desired eigenfrequencies. To solve Eq. (3.27) we use the software Mathematica. We calculated the first four flexural modes and get with $\omega_n = 2\pi\nu_n$:

$$\nu_1 = 927\text{Hz} \quad \nu_2 = 2488\text{Hz} \quad \nu_3 = 4820\text{Hz} \quad \nu_4 = 7923\text{Hz} \quad (3.28)$$

FEM solution: Again, we solved our example with COMSOL and plotted in Fig. 3.9 the simulated stress tensor element $\mathbf{T}_{11} = \sigma$ together with the analytical results and the relative error ET between them. The geometry was meshed with 4713 tetrahedral elements yielding 54500 degrees of freedom and the simulation lasted 27s.

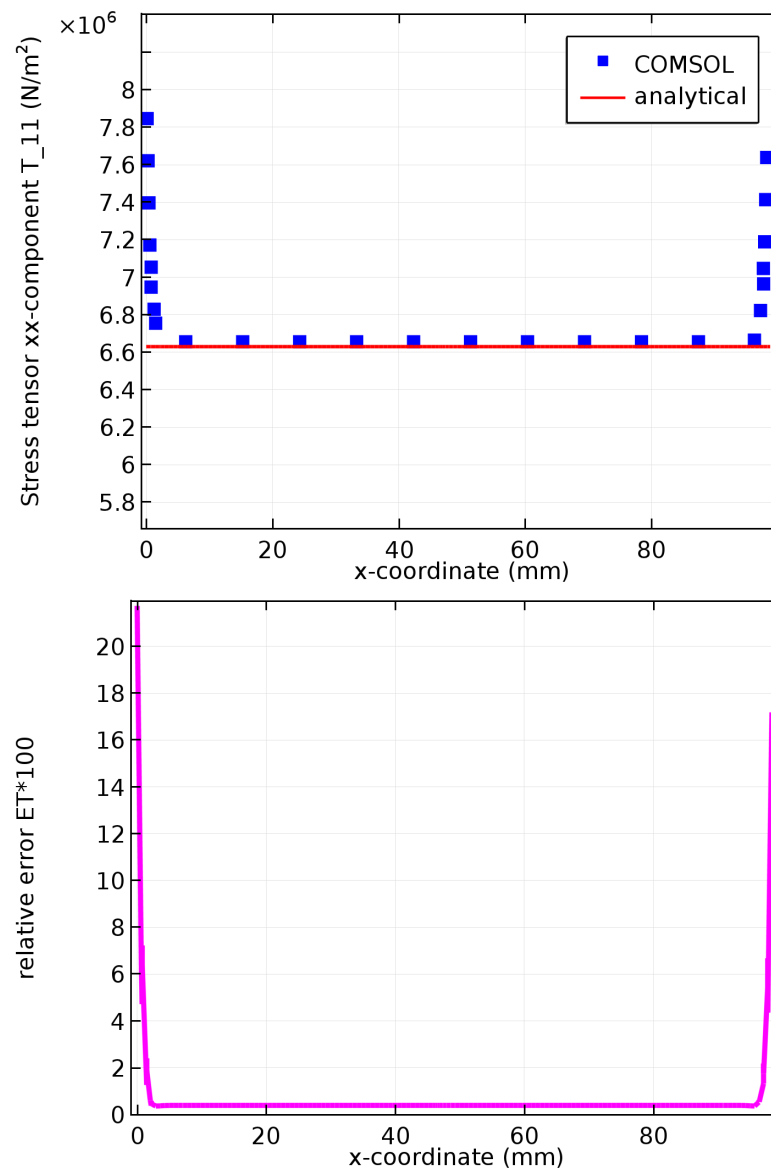


Figure 3.9: Top: COMSOL-solution (points) and analytical solution (line) for the stress tensor element \mathbf{T}_{11} (in N/m^2) versus x -coordinate (in mm). Bottom: The relative error $ET = (\mathbf{T}_{11\text{comsol}} - \mathbf{T}_{11\text{analytic}})/\mathbf{T}_{11\text{analytic}}$ of \mathbf{T}_{11} between COMSOL- and analytical solution multiplied by a factor of 100.

Looking at Fig. 3.9 and comparing the software solution for σ with the analytical one (Eq. (3.18)) we observe that both are in principle the same along the beam. Only at the ends of the beam the FEM solution deviates from the analytical σ . Again, this is not caused by the software but by our analytical calculation. The beam's ends are fixed thus, we have actually the following conditions for the displacement: $\mathbf{u}(x = 0) = 0$ and $\mathbf{u}(x = l) = 0$. Our analytical conditions for strain and stress given by Eq. (3.15) and Eq. (3.14) lead us to the followong

expression for the elastic strain:

$$\mathbf{E}_{\text{el}} = \begin{pmatrix} \alpha(T - T_0) & 0 & 0 \\ 0 & -\nu\alpha(T - T_0) & 0 \\ 0 & 0 & -\nu\alpha(T - T_0) \end{pmatrix}. \quad (3.29)$$

Hence, the total strain at $x = 0$ and $x = l$ becomes

$$\mathbf{E}_{\text{tot}}(0) = \mathbf{E}_{\text{el}}(0) + \mathbf{E}_{\text{th}}(0) = \mathbf{E}_{\text{tot}}(l) = \mathbf{E}_{\text{el}}(l) + \mathbf{E}_{\text{th}}(l) = \begin{pmatrix} 0 & 0 & 0 \\ 0 & \alpha(T - T_0)(1 + \nu) & 0 \\ 0 & 0 & \alpha(T - T_0)(1 + \nu) \end{pmatrix}. \quad (3.30)$$

Due to the fact that the diagonal-elements of $\mathbf{E}_{\text{tot}}(0)$ and $\mathbf{E}_{\text{tot}}(l)$ are not 0, the displacement components $u_{y,z}(0) \neq 0$ and $u_{y,z}(l) \neq 0$. Thus, the boundary conditions for \mathbf{u} , i. e. $\mathbf{u}(x = 0) = 0$ and $\mathbf{u}(x = l) = 0$, are not entirely satisfied in the analytical calculation. The boundary conditions for \mathbf{u} lead to nontrivial deviations of σ at the ends of the beam. We observe these deviations at the COMSOL-results and conclude that the software has taken the entire boundary conditions for \mathbf{u} into account.

The software solution for the eigenfrequencies are:

$$\nu_1 = 928\text{Hz} \quad \nu_2 = 2489\text{Hz} \quad \nu_3 = 4817\text{Hz} \quad \nu_4 = 7907\text{Hz} \quad (3.31)$$

Comparing these eigenfrequencies with the analytical ones we get a relative deviation of maximal $2 \cdot 10^{-3}$.

With our COMSOL-verifications performed in the sections 3.1, 3.2 and 3.3 we state that COMSOL Multiphysics is a reliable software for our purpose namely to determine the eigenfrequencies of a beam structure (more complicated than the structure consisting of only one beam like in 3.3) in terms of the temperature.

Chapter 4

Investigation of a double-U structure

In this chapter we consider a clamped beam structure shown in Fig. 4.1 which we want to call a double-U structure. The structure is as we see in Fig. 4.1 fixed at its four legs. The structure is mirror symmetric about the S_1 - and S_2 -axis. The structure's width is given by $Ul = 2000 \mu\text{m}$. Its legs have a length of $Ll = 319 \mu\text{m}$ and a width of $Lw = 177 \mu\text{m}$. At each side of the structure there are two legs coupled by a beam (with a width of $Uw = 200 \mu\text{m}$) respectively forming a "U".

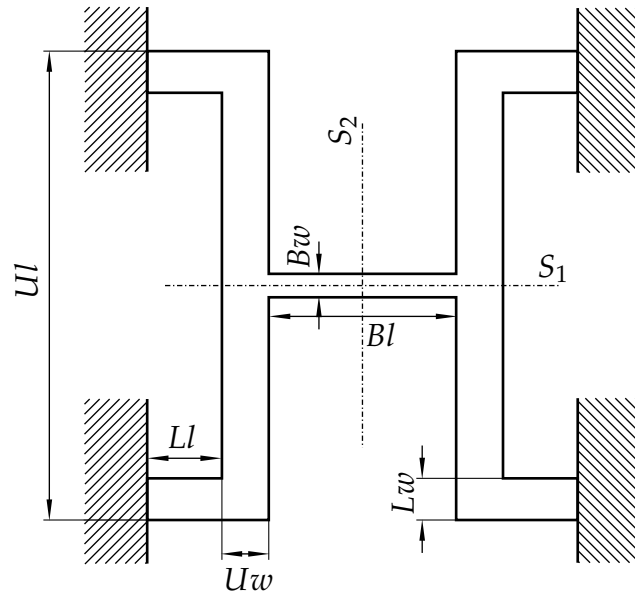


Figure 4.1: Clamped double-U beam structure with $Ll = 319 \mu\text{m}$, $Lw = 177 \mu\text{m}$, $Ul = 2000 \mu\text{m}$, $Uw = 200 \mu\text{m}$, $Bl = 800 \mu\text{m}$ and $Bw = 100 \mu\text{m}$. Horizontal section.

The two Us are connected by a small beam (like a bridge) with a length of $Bl = 800 \mu\text{m}$ and a width of $Bw = 100 \mu\text{m}$. The beam structure's height $H = 20 \mu\text{m}$ is uniform over the whole structure.

Our structure is made of silicon with a mass density of 2329 kg/m^3 . The silicon is assumed to be nonlinear isotropic and its Young's modulus and Poisson's ratio are given by $E = 170 \cdot 10^9 \text{ Pa}$ and $\nu = 0.17$, respectively. Its thermal

expansion coefficient is $\alpha = 2.6 \cdot 10^{-6} \text{ 1/K}$.

4.1 Investigation

For the investigation of the eigenfrequencies and their dependence on geometrical parameters and on the temperature we only consider the first six modes because high modes are much more difficult to excite and have normally relatively small amplitudes, so that they are not so interesting for an application. For the temperature dependence we consider a range of $T = [223 \text{ to } 393] \text{ K}$ with the reference temperature $T_0 = 298 \text{ K}$.

To simplify explanations we divide the double-U structure into three parts namely legs, U-bottoms and bridge (Fig. 4.2). Furthermore, one can classify the modes into four groups depending on the symmetry of the mode's shape about the S1- and S2-axis (delineated in Fig. 4.2):

ss → mode shape symmetric about the S2- and S1-axis

sa → mode shape symmetric about the S2-axis
and asymmetric about the S1-axis

as → mode shape asymmetric about the S2-axis
and symmetric about the S1-axis

aa → mode shape asymmetric about the S2-axis
and asymmetric about the S1-axis

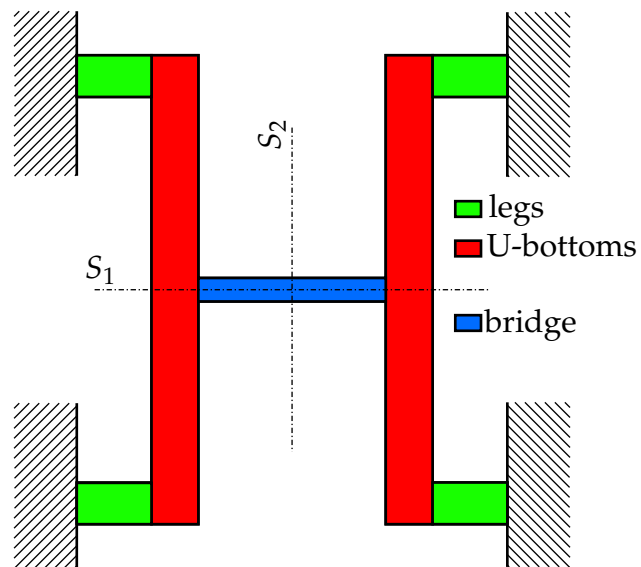


Figure 4.2: Double-U structure divided into three parts: legs, U-bottoms and bridge.

As a starting point for the design variation we determine the eigenfrequencies of the basic double-U beam structure (Fig. 4.1 with parameters listed) which serves as our initial structure for parameter variations.

The simulation delivered the results depicted in Fig. 4.3. As one can see, the 2. ss- and 2. as-modes are quite close to each other thus, they are plotted in a separate diagram (Fig. 4.4) with a better resolution.

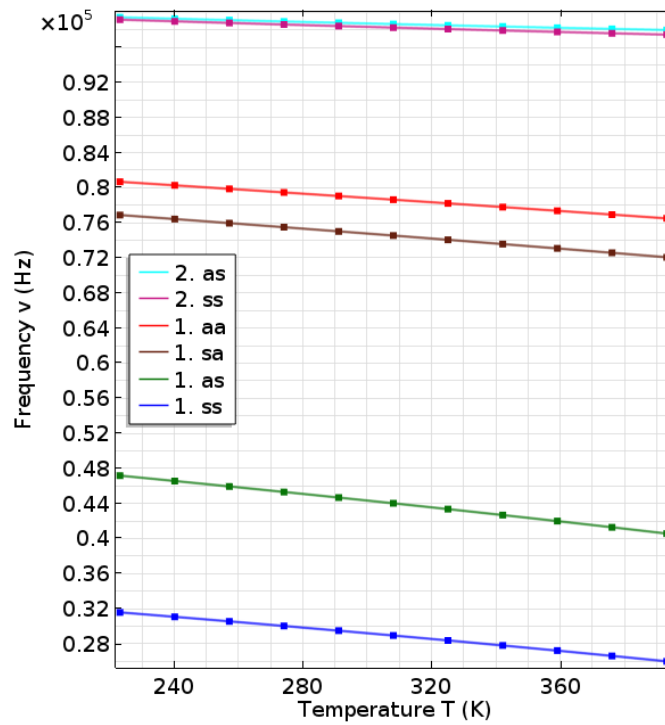


Figure 4.3: Frequency ν (in Hz) of the first 6 eigenmodes versus temperature T (in K) of the basic double-U structure.

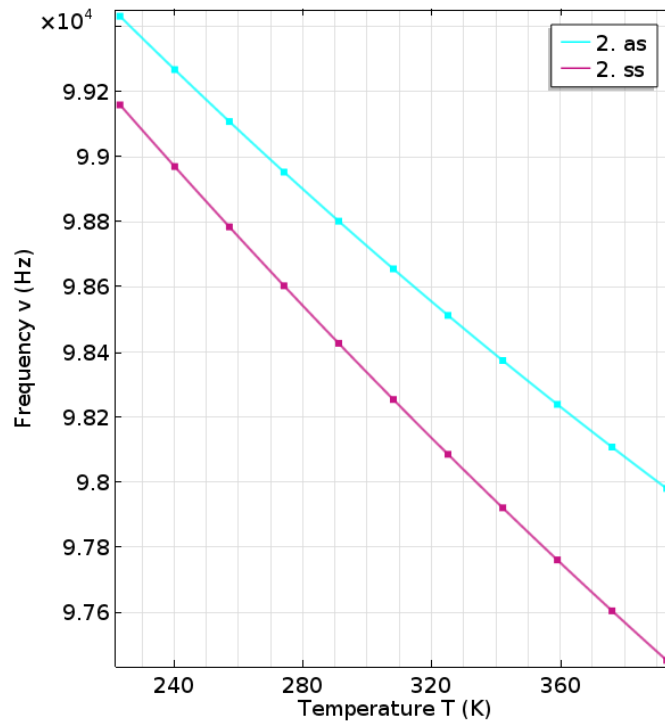


Figure 4.4: Frequency of the 2. ss- and 2. as-eigenmodes versus temperature of the basic double-U structure.

To make evaluation easier we show in Tab. 4.1 the eigenfrequency of each

mode at $T = 223$ K and the average value of the eigenfrequency's slope k_ν over the interval $T = [223 \text{ to } 393]$ K respectively. Knowing the average value of the slope is sufficient as it doesn't change much over the considered temperature interval.

Table 4.1: $\nu_{223\text{K}}$ the eigenfrequency at $T = 223$ K and k_ν the slope average of eigenfrequencies over the interval $T = [223 \text{ to } 393]$ K for each mode of the basic double-U structure.

	1. ss	1. as	1. sa	1. aa	2. ss	2. as
$\nu_{223\text{K}}(\text{kHz})$	31.6	47.2	76.9	80.7	99.2	99.5
$k_\nu(\text{Hz/K})$	-32.9	-38.8	-28.2	-24.7	-10	-8.8

As mentioned above we are interested in the eigenfrequencies' dependence on parameter changes over the interval $T = [223 \text{ to } 393]$ K. We perform this investigation by computing the eigenfrequencies in terms of the temperature for all (Ll, Lw, Ul, Uw, Bl, Bw) parameter combinations of the following set:

$$\begin{aligned}
 Ll &= 319; 638 \mu\text{m} & Lw &= 177; 355 \mu\text{m} \\
 Ul &= 2\,000 \mu\text{m} & Uw &= 200; 400 \mu\text{m} \\
 Bl &= 800; 1\,200 \mu\text{m} & Bw &= 100; 200 \mu\text{m}
 \end{aligned} \tag{4.1}$$

and then comparing them with those of our basic double-U structure (Fig. 4.1). All together we have 32 (Ll, Lw, Ul, Uw, Bl, Bw) combinations where one of them is equal to the one of our basic double-U structure. Instead of showing the eigenmode results for all parameter combinations we already compared them to the reference structure and listed the outcome in Tab. 4.2. In particular we show the difference between the reference frequency at $T = 223$ K ($= \nu_{223\text{K}}$, see Tab. 4.1) and the frequency at the same temperature of the respective double-U structure with an (Ll, Lw, Ul, Uw, Bl, Bw) -combination of Eq. (4.1) ($= \nu_{223\text{K}}(Ll, Lw, Ul, Uw, Bl, Bw)$), i. e. $\nu_{223\text{K}}(Ll, Lw, Ul, Uw, Bl, Bw) - \nu_{223\text{K}} = \Delta\nu_{223\text{K}}(Ll, Lw, Ul, Uw, Bl, Bw)$. Additionally, we listed the difference between the average values of the eigenfrequencies' slopes k_ν for our reference structure and the considered (Ll, Lw, Ul, Uw, Bl, Bw) -combination structure, i. e. $k_\nu(Ll, Lw, Ul, Uw, Bl, Bw) - k_\nu = \Delta k_\nu(Ll, Lw, Ul, Uw, Bl, Bw)$. In case of a non-approximately constant slope over the temperature we split the $[223 \text{ to } 393]$ K interval into sub intervals where $\Delta k_\nu(Ll, Lw, Ul, Uw, Bl, Bw)$ is sufficiently constant.

Again, $\Delta\nu_{223\text{K}}(Ll, Lw, Ul, Uw, Bl, Bw)$ and $\Delta k_\nu(Ll, Lw, Ul, Uw, Bl, Bw)$ are evaluated for all six eigenmodes. To save paperwork we indicate the respective parameter combination not by its values but by the parameter-letter if the corresponding parameter was changed concerning the basic structure and a minus if not. Let us demonstrate this indication by means of an example.

The basic double-U structure is given by the parameter set (Fig. 4.1)

$$(Ll_0, Lw_0, Ul_0, Uw_0, Bl_0, Bw_0) = \\ (319, 177, 2000, 200, 800, 100) \mu\text{m}$$

Thus, the following set of parameters can be notated as

$$(Ll, Lw, Ul, Uw, Bl, Bw) = \\ (319, 355, 2000, 200, 1200, 100) \mu\text{m} = \\ (-, Lw, -, -, Bl, -)$$

This notation is suitable as each parameter can only vary between two different values except of Ul , which doesn't change. Additionally, we neglect the combination-indication for $\Delta k_\nu(Ll, Lw, Ul, Uw, Bl, Bw) \rightarrow \Delta k_\nu$ as it is equal to the combination of $\Delta\nu_{223\text{K}}(Ll, Lw, Ul, Uw, Bl, Bw)$ which is always written above of Δk_ν in Tab. 4.2.

Table 4.2: $\Delta\nu_{223\text{K}}$ the eigenfrequency-alteration at $T = 223\text{ K}$ and Δk_ν the slope average-alteration of eigenfrequencies over the interval $T = [223 \text{ to } 393]\text{ K}$ caused by the parameter change from basic double-U structure ($Ll = 319\ \mu\text{m}$; $Lw = 177\ \mu\text{m}$; $Ul = 2000\ \mu\text{m}$; $Uw = 200\ \mu\text{m}$; $Bl = 800\ \mu\text{m}$; $Bw = 100\ \mu\text{m}$) to the new double-U structure (with (Ll, Lw, Ul, Uw, Bl, Bw) -combination from Eq. (4.1)).

(Ll, Lw, Ul, Uw, Bl, Bw)	1. ss	1. as	1. sa	1. aa	2. ss	2. as
$\Delta\nu_{223\text{K}}(\text{kHz})$ $(-, -, -, -, Bl, -)$	-2.5	-6	0	-1	2.3	0
$\Delta k_\nu(\text{Hz/K})$	-2.9	-5.8	-2.3	-2.3	0	0
$\Delta\nu_{223\text{K}}(\text{kHz})$ $(-, -, -, -, -, Bw)$	-2	1.3	0	3.5	2.8	2.3
$\Delta k_\nu(\text{Hz/K})$	2.9	4	-2.3	0	0	0
$\Delta\nu_{223\text{K}}(\text{kHz})$ $(-, -, -, -, Bl, Bw)$	-5.6	-5.9	0	1.7	3.4	2.45
$\Delta k_\nu(\text{Hz/K})$	2.35	0	-3.82	0	0	0

(Ll,Lw,Ul,Uw,Bl,Bw)	1. ss	1. as	1. sa	1. aa	2. ss	2. as
$\Delta\nu_{223\text{K}}(\text{kHz})$ (-, -, -,Uw, -, -)	-8.2	-9.6	-24	-25	-33.8	-33.2
$\Delta k_{\nu}(\text{Hz/K})$	-15	-14.7	0	0	8	11.1
$\Delta\nu_{223\text{K}}(\text{kHz})$ (-, -, -,Uw,Bl, -)	-9.4	-14.8	-24	-25.9	-34.3	-33.5
$\Delta k_{\nu}(\text{Hz/K})$	-26	-24.7	0	0	-1.1 (T=223-300K) -19.4 (T=300-393K)	7
$\Delta\nu_{223\text{K}}(\text{kHz})$ (-, -, -,Uw, -,Bw)	-8.5	-7.1	-23.6	-23	-32	-32
$\Delta k_{\nu}(\text{Hz/K})$	-14.7	-8	0	0	10	11.7
$\Delta\nu_{223\text{K}}(\text{kHz})$ (-, -, -,Uw,Bl,Bw)	-10.2	-13	-23.5	-24.2	-34	-32.5
$\Delta k_{\nu}(\text{Hz/K})$	-25.2	-17	0	0	-2.9 (T=223-300K) -17.6 (T=300-393K)	14.7
$\Delta\nu_{223\text{K}}(\text{kHz})$ (-,Lw, -, -, -, -)	14.7	18.3	21	20.7	21.2	20.6
$\Delta k_{\nu}(\text{Hz/K})$	-21.7	-25.8	-10	-10	-21.1	-22.3
$\Delta\nu_{223\text{K}}(\text{kHz})$ (-,Lw, -, -,Bl, -)	9.5	10.5	21.4	19.8	21	20.7
$\Delta k_{\nu}(\text{Hz/K})$	-24.7	-32.3	-12.9	-12.3	-18.2	-21.7
$\Delta\nu_{223\text{K}}(\text{kHz})$ (-,Lw, -, -, -,Bw)	11.1	20.3	21.4	23.8	22.4	21.8
$\Delta k_{\nu}(\text{Hz/K})$	-18.2	-22.3	-15.2	0	-17.9	-20
$\Delta\nu_{223\text{K}}(\text{kHz})$ (-,Lw, -,Uw, -, -)	1.1	1.1	-14	-15.9	17.2	-17.5
$\Delta k_{\nu}(\text{Hz/K})$	-40	-45.2	0	0	-8.8	-12.9
$\Delta\nu_{223\text{K}}(\text{kHz})$ (-,Lw, -, -,Bl,Bw)	4.4	10.7	21.2	22.2	22.3	21.9
$\Delta k_{\nu}(\text{Hz/K})$	-17.6	-27.6	-17	-12.9	-17.64	-18.8

(Ll,Lw,Ul,Uw,Bl,Bw)	1. ss	1. as	1. sa	1. aa	2. ss	2. as
$\Delta v_{223K}(\text{kHz})$ (-,Lw,-,Uw,Bl,-)	-0.8	-4.8	-14	-16.5	-17.3	-17.4
$\Delta k_v(\text{Hz/K})$	-35.3 (T=223-325K) -82.3 (T=325-393K)	-39.2 (T=223-325K) -83.8 (T=325-393K)	2.3	0	-8.2	-12.3
$\Delta v_{223K}(\text{kHz})$ (-,Lw,-,Uw,-,Bw)	0.7	4.9	-13.6	-13	-16.8	-17.3
$\Delta k_v(\text{Hz/K})$	-45.2	-41.7	-10.5	-7	-5.8	-9.4
$\Delta v_{223K}(\text{kHz})$ (-,Lw,-,Uw,Bl,Bw)	-2.2	-1.9	-13.5	-14.5	-17.3	-17.2
$\Delta k_v(\text{Hz/K})$	-42.2 (T=223-325K) -82.7 (T=325-393K)	-45 (T=223-325K) -77.9 (T=325-393K)	-11.7	-10	0	-7.6
$\Delta v_{223K}(\text{kHz})$ (Ll,-,-,-,-,-)	-12	-13.4	-37.6	-38.5	-36	-36
$\Delta k_v(\text{Hz/K})$	15.8	20	16.4	14.7	6.5	4.4
$\Delta v_{223K}(\text{kHz})$ (Ll,-,-,-,-,Bl,-)	-13.9	-19	-37.5	-39.3	-37.6	-37.1
$\Delta k_v(\text{Hz/K})$	13.5	15.8	15.8	13.5	4.7	4.7
$\Delta v_{223K}(\text{kHz})$ (Ll,-,-,-,-,Bw)	-13.1	-11.4	-37.5	-36.1	-37	-36.9
$\Delta k_v(\text{Hz/K})$	17.6	21.7	15.2	15.3	5.3	4.7
$\Delta v_{223K}(\text{kHz})$ (Ll,-,-,-Uw,-,-)	-17.4	-20.6	-46.1	-48	-45.8	-46.4
$\Delta k_v(\text{Hz/K})$	-4.7	4.1	8.8	7.1	20.5	18.8
$\Delta v_{223K}(\text{kHz})$ (Ll,Lw,-,-,-,-)	-5.4	-6.4	-30.9	-32.3	-26.5	-23.3
$\Delta k_v(\text{Hz/K})$	4.1	7.1	7.6	7.1	2.3	-19.4
$\Delta v_{223K}(\text{kHz})$ (Ll,-,-,-,-,Bl,Bw)	-15	-17.6	-37.4	-37.3	-38.7	-37.2
$\Delta k_v(\text{Hz/K})$	15.9	18.8	14.7	13.5	2.4	4.7

(Ll,Lw,Ul,Uw,Bl,Bw)	1. ss	1. as	1. sa	1. aa	2. ss	2. as
$\Delta\nu_{223\text{K}}(\text{kHz})$ (Ll, -, -,Uw,Bl, -)	-18	-24.9	-46	-48.4	-46	-46.4
$\Delta k_{\nu}(\text{Hz/K})$	-14.1	-7	7.6	5.3	21 (T=223-342K) -11.7 (T=342-393K)	18.8
$\Delta\nu_{223\text{K}}(\text{kHz})$ (Ll, -, -,Uw, -,Bw)	-17.2	-18.5	-45.9	-46	-45.3	-46.2
$\Delta k_{\nu}(\text{Hz/K})$	0	8.3	5.8	5.8	20.1 (T=223-308K) 15 (T=308-359K) 10 (T=359-393K)	19.4
$\Delta\nu_{223\text{K}}(\text{kHz})$ (Ll,Lw, -, -,Bl, -)	-7	-11.8	-30.9	-32.9	-29.5	-25
$\Delta k_{\nu}(\text{Hz/K})$	0	0	7.6	5.8	-17.6	-16.4
$\Delta\nu_{223\text{K}}(\text{kHz})$ (Ll,Lw, -, -, -,Bw)	-6.2	-3.7	-30.9	-30	-28.2	-23.7
$\Delta k_{\nu}(\text{Hz/K})$	4.1	8.8	6.5	7.6	-8.2	-17
$\Delta\nu_{223\text{K}}(\text{kHz})$ (Ll,Lw, -,Uw, -, -)	-13	-15.2	-41.2	-43.2	-36.1	-34.7
$\Delta k_{\nu}(\text{Hz/K})$	-8.8 (T=223-325K) -48.5 (T=325-393K)	-16 (T=223-325K) -38.2 (T=325-393K)	2.9	0	0	-10
$\Delta\nu_{223\text{K}}(\text{kHz})$ (Ll, -, -,Uw,Bl,Bw)	-18.1	-23	-45.8	-46.7	-45.7	-46.1
$\Delta k_{\nu}(\text{Hz/K})$	-10	0	4.1	2.4	21.4 (T=223-257K) -38.8 (T=359-393K)	18.8
$\Delta\nu_{223\text{K}}(\text{kHz})$ (Ll,Lw, -,Uw,Bl, -)	-13	-19.4	-41.2	-43.7	-37	-35.4
$\Delta k_{\nu}(\text{Hz/K})$	-26.4 (T=223-359K) -120.5 (T=359-393K)	-32.3 (T=223-359K) -88.2 (T=359-393K)	3.5	0	-8.5 (T=223-325K) -44.7 (T=325-359K) -113.5 (T=359-393K)	-8.2

(Ll,Lw,Ul,Uw,Bl,Bw)	1. ss	1. as	1. sa	1. aa	2. ss	2. as
$\Delta\nu_{223\text{K}}(\text{kHz})$ (Ll,Lw, -,Uw, -,Bw)	-12	12.5	-40.7	-41.2	-36.8	-34.7
$\Delta k_\nu(\text{Hz/K})$	-21 (T=223-342K) -56.8 (T=342-393K)	-19.7	-3.5	0	-4.7	-8.2
$\Delta\nu_{223\text{K}}(\text{kHz})$ (Ll,Lw, -, -,Bl,Bw)	-8.8	-10	-30.9	-30.1	-32.2	-25.9
$\Delta k_\nu(\text{Hz/K})$	0	0	4.7	5.3	-14.2	-24.11
$\Delta\nu_{223\text{K}}(\text{kHz})$ (Ll,Lw, -,Uw,Bl,Bw)	-13	17.2	-40.7	-42	-38.6	-35.6
$\Delta k_\nu(\text{Hz/K})$	-32.3 (T=223-359K) -138 (T=359-393K)	-29.4 (T=223-359K) -67.6 (T=359-393K)	-4.1	-2.9	-28 (T=223-325K) -61 (T=325-393K)	-8.2

In the following subsections we want to investigate our results shown in Tab. 4.2 more detailed. In particular we show the shape of each eigenmode (1. ss to 2. as) and want to deal with some parameter combinations, especially where $\Delta\nu_{223\text{K}}$ and Δk_ν are maximal or minimal, respectively.

4.2 1. ss-mode

The first ss-mode of our double-U structure has a shape shown in Fig. 4.5, computed by the FEM software. The mode is plotted with the basic double-U structure (see Fig. 4.1) at $T = 223\text{ K}$ but its shape is approximately the same for all the other parameter combinations and temperatures.

Furthermore, we extracted the parameter combinations from Tab. 4.2 which exhibit maximal or minimal $\Delta\nu_{223\text{K}}$ and Δk_ν concerning the first ss-eigenmode and listed the extremal values in Eq. (4.2). Additionally, we plotted in Fig. 4.6 the 1. ss-eigenmode's frequency of these parameter combinations together with the one of the reference parameter combination.

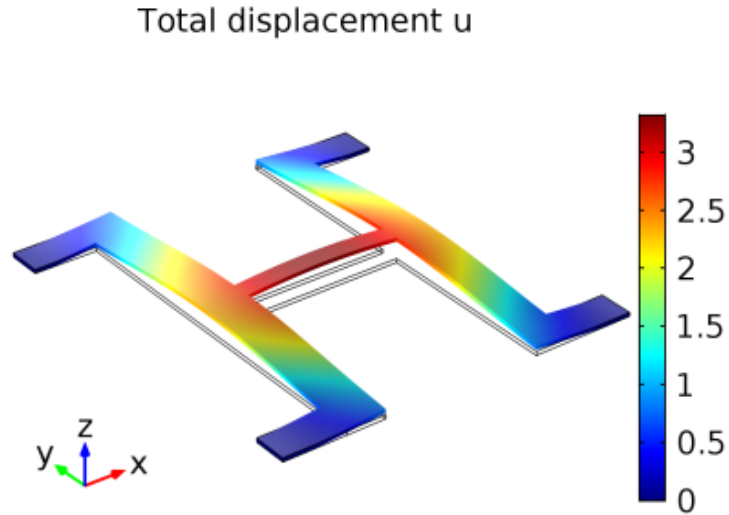


Figure 4.5: Displacements of the 1. ss-eigenmode of the basic double-U structure at $T = 223$ K. Scale is in arbitrary units.

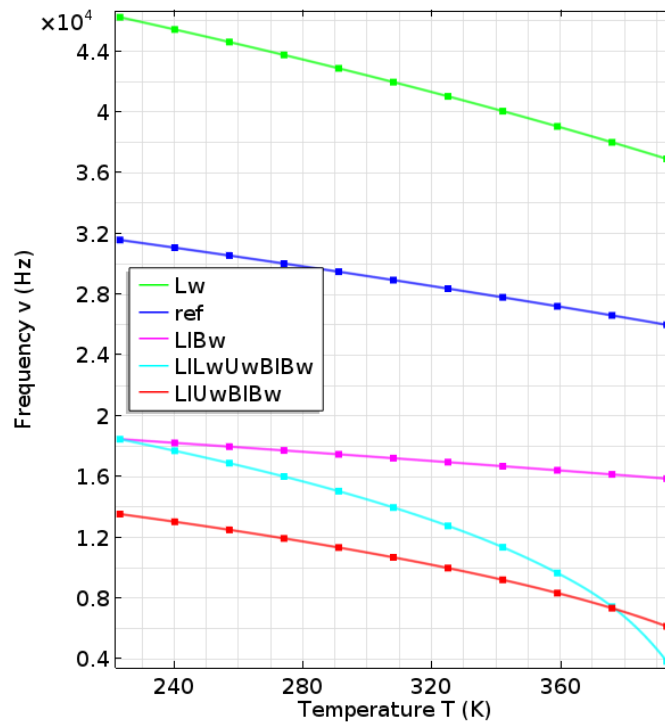


Figure 4.6: Frequency of 1. ss-eigenmode versus temperature for reference and extremal combinations: **1.** $Lw = (-, Lw, -, -, -, -) \rightarrow \max.\Delta v_{223K}$, **2.** $ref = (-, -, -, -, -, -)$, **3.** $LIBw = (Ll, -, -, -, -, Bw) \rightarrow \max.\Delta k_v$, **4.** $LILwUwBIBw = (Ll, Lw, -, Uw, Bl, Bw) \rightarrow \min.\Delta k_v$, **5.** $LIUwBIBw = (Ll, -, -, Uw, Bl, Bw) \rightarrow \min.\Delta v_{223K}$.

Again, we use the suitable notation to indicate the parameter combination like in Tab. 4.2 where a letter denotes a parameter change with respect to the reference structure and a minus denotes no change.

$$\begin{aligned}
& (Ll, Lw, Ul, Uw, Bl, Bw) \\
& (Ll, -, -, Uw, Bl, Bw) \rightarrow \min. \Delta\nu_{223K} = -18.1 \text{ kHz} \\
& (Lw, -, -, -, -, -) \rightarrow \max. \Delta\nu_{223K} = 14.7 \text{ kHz} \tag{4.2} \\
& (Ll, Lw, -, Uw, Bl, Bw) \rightarrow \min. \Delta k_\nu = -138.2 \text{ Hz/K for } T = 359 - 393K \\
& (Ll, -, -, -, -, Bw) \rightarrow \max. \Delta k_\nu = 17.64 \text{ Hz/K}
\end{aligned}$$

We now want to give an empiric justification or at least motivation for the extremal results shown in Eq. (4.2) and Fig. 4.6. For this we first want to discuss the effects of each single parameter change (all combinations where only one parameter was changed) on $\Delta\nu_{223K}$ and Δk_ν concerning the first ss-eigenmode. Additionally, we listed $\Delta\nu_{223K}$ and Δk_ν of the first ss-mode for each single parameter change in Tab. 4.3. After that we look whether the combinations for extremal $\Delta\nu_{223K}$ and Δk_ν are derivable with the results for combinations with single parameter modification or not.

Table 4.3: $\Delta\nu_{223K}$ and Δk_ν of the first ss-eigenmode for all combinations where only one parameter was changed.

	Ll	Lw	Uw	Bl	Bw
$\Delta\nu_{223K}(\text{kHz})$	-12	14.7	-8.2	-2.5	-2
$\Delta k_\nu(\text{Hz/K})$	15.8	-21.7	-15	-2.9	2.9

Discussion min. max. $\Delta\nu_{223K}$: The first ss-eigenmode's shape is similar to the shape of the first eigenmode described by the Euler-Bernoulli equation thus, we can follow this equation for our discussion. Considering the combination $(-, -, -, -, -, Bw)$ it is quite interesting that the frequency of the first ss-eigenmode even changes with Bw as the eigenfrequencies of the Euler-Bernoulli equation are independent of the beam's width (see Eq. (3.21)). The reason for this is that Bw (the width of the bridge) has an effect on the internal stress σ along the bridge, see Eq. (3.19). With thermal expansion of the bridge the U-bottoms bend and hence, act (actio-reactio) with a force N onto the bridge. Looking at Eq. (3.19) we deduce that the internal stress of the bridge $\sigma = N/A$. A is the bridges cross-section and thus proportional to the width Bw . Due to this relation, we conclude that with bigger Bw (=larger cross-section) the magnitude of the internal stress $|\sigma|$ of the bridge gets smaller. $\Delta\nu_{223K}$ is considered

at $T = 223 \text{ K}$ which is smaller than the reference temperature $T_0 = 298 \text{ K}$ thus, the bridge contracts and the bended U-bottoms generate a positive N (pull) ($\rightarrow \sigma$ is positive). Considering again the Euler-Bernoulli beam we see that its eigenfrequencies depend on σ (see Eq. (3.21)) and one can show that the eigenfrequencies decrease with lower σ .

Looking at Tab. 4.3 we find that the combination where Bl was changed $(-, -, -, -, Bl, -)$ has a negative effects on $\Delta\nu_{223\text{K}} = -2.5 \text{ kHz}$. In case of the Bl modification the bridge gets longer. Thus, the frequency of the mode gets lower and the first *ss-mode* enlongates. One can derive the same effect with the length considering an Euler-Bernoulli beam. With a longer bridge additionally the internal stress σ varies stronger with the temperature. This is because the absolute length change, due to thermal expansion, is bigger and hence, the U-bottoms are bended stronger which also means that they are acting with a stronger force N onto the bridge. Since the cross-section A of the bridge stays constant with a modification of Bl , the relation $\sigma = N/A$ Eq. (3.19) leads to a higher internal stress magnitude $|\sigma|$. As mentioned above, the bridge contracts due to $T = 223 \text{ K} < T_0 = 298 \text{ K}$ and the bended U-bottoms generate a positive N (pull). One can show with the Euler-Bernoulli equation that an increase of σ leads to an increase of the frequency. Altogether we have two effects one causing a decrease (longer bridge) and one an increase (stronger pull) of the frequency whereby the decreasing effect is stronger, leading to a negative $\Delta\nu_{223\text{K}}$. The $\Delta\nu_{223\text{K}} = -8.2 \text{ kHz}$ caused by the parameter change $(-, -, -, Uw, -, -)$ can also be explained with an Euler-Bernoulli beam. If we want to reduce the bridge with the U-bottoms at its both ends to an Euler-Bernoulli beam the U-bottoms can be described by an increased density ρ over a range with a length equal Uw at both ends of the Euler-Bernoulli beam. Again, we look at Eq. (3.21) and find that the Euler-Bernoulli equation depends on the density ρ and one can show that with a longer range (larger Uw) consisting of a higher density the frequencies of an Euler-Bernoulli beam decrease. Furthermore, the structure gets longer with larger Uw which implies the same effect already discussed for a modification of Bl causing a lower frequency. Additionally, the larger width of the U-bottoms leads them to act with a stronger force N onto the bridge if they get bended by the thermal contracted (or expanded) bridge. We get therefore, a larger $|\sigma|$ with the temperature and in case of ($T = 223 \text{ K}$) a contracted bridge σ is positive (pull) which together leads to an increase of the frequency. So we have three effects, two leading to a frequency-decrease (longer structure and more mass) and one leading to a frequency-increase (stronger pull) where

the decreasing effects are stronger together yielding a negative $\Delta v_{223\text{K}}$.

The min. $\Delta v_{223\text{K}} = -12 \text{ kHz}$ with the combination $(Ll, -, -, -, -, -)$ is firstly due to the fact that with the parameter Ll the whole structure gets longer which causes a lower frequency (same effect caused by change of Bl or Uw). If we again reduce the structure to an Euler-Bernoulli beam the U-bottoms can be described by a higher mass density in the Euler-Bernoulli beam like explained in the previous discussion for a change of Uw . With longer legs (larger Ll) of the structure the ratio between the distance d_{M-Ub} (= distance from the middle of the beam structure to one U-bottom) and the distance d_{Ub-E} , i. e. the distance from one U-bottom to the closer end of structure, gets smaller. Hence, also for our reduction to an Euler-Bernoulli beam the ratio between the distance $d_{M-\rho(Ub)}$ (= distance from the middle of the Euler-Bernoulli beam to a higher density region describing one U-bottom) and the distance $d_{\rho(Ub)-E}$, i. e. the distance from a higher density region describing one U-bottom to the closer end of the structure, gets smaller. Since one can show by means of the Euler-Bernoulli equation that the eigenfrequency of the first mode gets lower if the ratio $d_{M-\rho(Ub)}/d_{\rho(Ub)-E}$ gets smaller, we found an additional effect caused by larger Ll yielding a decrease of the frequency. Finally, we have a third effect concerning the internal stress over the bridge. When the bridge contracts or expands, due to thermal expansion, the U-bottoms get bent and with them also the legs. So actually the force N with which the U-bottoms act onto the bridge is a consequence of both U-bottoms and legs bendings. So if the legs are longer they get more flexible and hence, in case of thermal expansion of the bridge the legs can bend in an easier way which leads to a smaller force N as a reactio. Therefore, the magnitude of the stress $|\sigma|$ caused by thermal expansions gets smaller with larger Ll . In case of $T = 223 \text{ K}$ this means that σ (pull) decreases. As mentioned above one can show with the Euler-Bernoulli equation that this leads to a decrease of the eigenfrequency. Together we found three effects where all of them decrease the eigenfrequency which is the reason for the strongest frequency decrease caused by larger Ll .

Our max. $\Delta v_{223\text{K}} = 14.7 \text{ kHz}$ with Lw can be explained by the fact that with larger Lw the legs and U-bottoms get less flexible which means that in case of bending (caused by thermal expansion of the bridge) the force N as the reactio of the bending system onto the bridge gets stronger. Thus with larger Lw the internal stress σ varies stronger with thermal expansions of the bridge. In the case of a positive σ this yields a larger σ with bigger Lw and we finally get a higher frequency (derivable by the Euler-Bernoulli equation). Additionally, the smaller

flexibility of the legs and U-bottoms constrains the 1. ss-mode to the bridge. We depict this effect in Fig. 4.7 where the first ss-mode's shape is displayed of both the basic double-U (no parameter changed) structure and the structure where only the parameter Lw is changed, i. e. $(-, Lw, -, -, -, -)$.

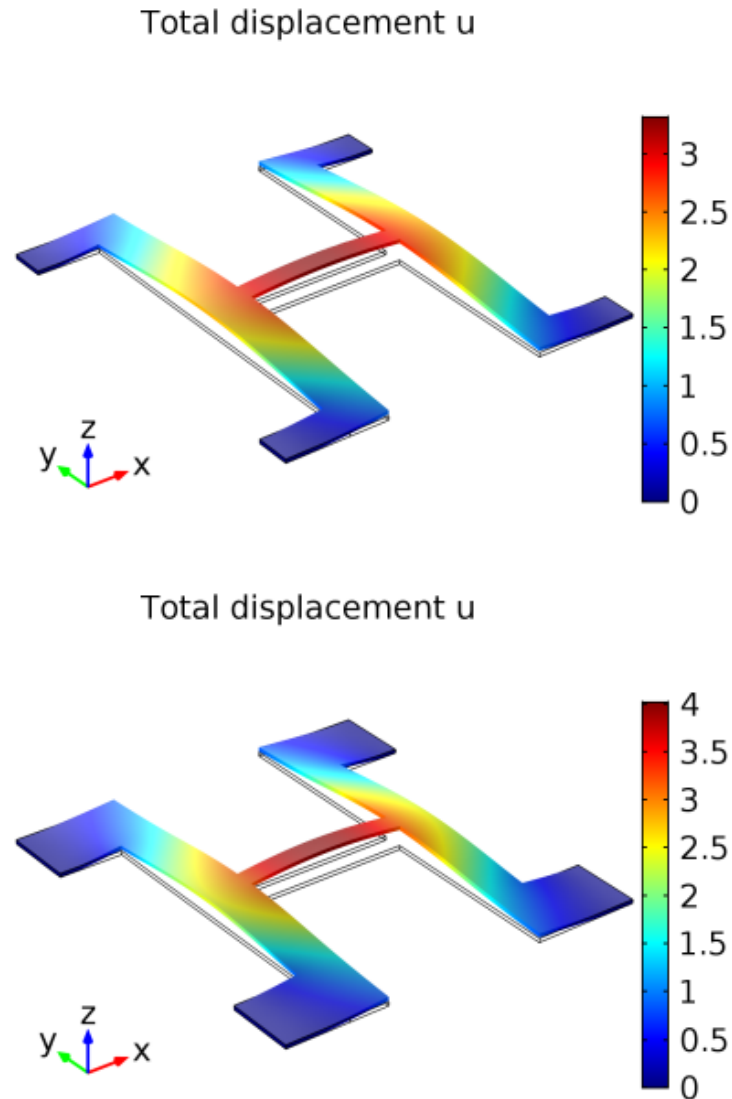


Figure 4.7: Displacements of the 1. ss-eigenmode of the reference structure $(-, -, -, -, -, -)$ (top) and the structure with increased Lw $(-, Lw, -, -, -, -)$ (bottom). Scale is in arbitrary units. The mode gets more restricted to the bridge with larger Lw .

This restriction entails on the one hand a shorter length for the mode yielding a higher frequency and on the other hand the U-bottoms get more to the border of the mode leading to higher frequency as less mass is moved. This is the same but opposite effect already explained in the discussion for a

modification of Ll namely that the high density regions (=U-bottoms in Euler-Bernoulli beam) get shifted outside (instead of inside like in the discussion concerning Ll). Thus, there are three effects yielding a higher frequency of the first ss-mode which leads to the maximal $\Delta\nu_{223K}$ with an enlargement of Lw .

Following the $\Delta\nu_{223K}$ -discussion for single parameter changes one might deduce that an alteration from the basic parameter combination $(-, -, -, -, -, -)$ to the combination $(Ll, -, -, Uw, Bl, Bw)$ should yield a minimal $\Delta\nu_{223K}$ and to the combination $(-, Lw, -, -, -, -)$ should lead to a maximal $\Delta\nu_{223K}$. This conclusion is correct and can be verified by looking at Eq. (4.2), leading to a minimal $\Delta\nu_{223K} = -18.1 \text{ kHz}$ with $(Ll, -, -, Uw, Bl, Bw)$ and a maximal $\Delta\nu_{223K} = 14.7 \text{ kHz}$ with $(-, Lw, -, -, -, -)$.

Discussion min. max. Δk_ν : To find the reason for the positive Δk_ν with a single change of $Bw \rightarrow (-, -, -, -, -, Bw)$ we just need to have a look at the $\Delta\nu_{223K}$ -discussion for the same parameter. There we find that the magnitude of the internal stress $|\sigma|$ over the bridge caused by thermal expansion of the bridge gets smaller with Bw . That means that σ and thereby the frequency varies less with the temperature or in other words the magnitude of the frequency's slope $|k_\nu|$ gets smaller. Hence, this effect leads to a positive Δk_ν as the first ss-mode's average slope of reference structure is negative $k_\nu = -32.9 \text{ Hz/K}$.

Considering a modification of the parameter $Bl \rightarrow (-, -, -, -, Bl, -)$ we have already discussed above ($\Delta\nu_{223K}$ -discussion) that with Bl σ of the bridge varies stronger with the temperature. This leads to a larger magnitude of the frequency's slope $|k_\nu|$ over the temperature. As already mentioned k_ν of the reference structure's first ss-mode is negative thus, Δk_ν is negative.

The modification of $Uw \rightarrow (-, -, -, Uw, -, -)$ yields a negative Δk_ν . This is also a consequence of a stronger temperature dependence of the internal stress of the bridge already discussed above in the $\Delta\nu_{223K}$ -discussion concerning Uw . The maximal positive Δk_ν with a change of $Ll \rightarrow (Ll, -, -, -, -, -)$ is due to the fact that with longer legs the internal stress of the bridge varies less with thermal expansions (discussed above). Again, as a consequence the average value of the frequency's slope $|k_\nu|$ gets smaller and hence, Δk_ν is positive because of a negative k_ν of the reference structure.

A change of the parameter $Lw \rightarrow (-, Lw, -, -, -, -)$ causes a maximal negative Δk_ν which is also justified by a stronger temperature dependence of the bridges internal stress explained above in the $\Delta\nu_{223K}$ -discussion.

With the results for single parameter changes we assume that with the combinations $(-, Lw, -, Uw, Bl, -)$ and $(Ll, -, -, -, -, Bw)$ we get a minimal and maximal Δk_v . Checking with Eq. (4.2) our assumption we find that it is correct for $(Ll, -, -, -, -, Bw)$ but not for $(-, Lw, -, Uw, Bl, -)$. Indeed Δk_v is quite negative over the whole temperature interval for $(-, Lw, -, Uw, Bl, -)$ but we find that the combination $(Ll, Lw, -, Uw, Bl, Bw)$ leads to a smaller $\Delta k_v = -138.2 \text{ Hz/K}$ over the temperature interval $359 - 393 \text{ K}$. The reason for this is that the 1. ss-mode gets the strongest constraint to the bridge with the temperature concerning the $(Ll, Lw, -, Uw, Bl, Bw)$ -combination. Thus, the effects caused by $(-, Lw, -, Uw, Bl, -)$ (the same effects are in $(Ll, Lw, -, Uw, Bl, Bw)$) which are actually effects only concerning the bridge and not the rest of the double-U structure get more influence than effects of the rest of the structure.

4.3 1. as-mode

In Fig. 4.8 the shape of the 1. as-mode is plotted, again for the basic double-U structure (see Fig. 4.1) at $T = 223 \text{ K}$. The shape stays in principle the same for all other parameter combinations and temperatures. The extremal $\Delta v_{223\text{K}}$ and Δk_v of the first as-mode are shown in Eq. (4.3) and the mode's frequency of the respective parameter combinations and the reference structure are plotted in Fig. 4.9 over the temperature.

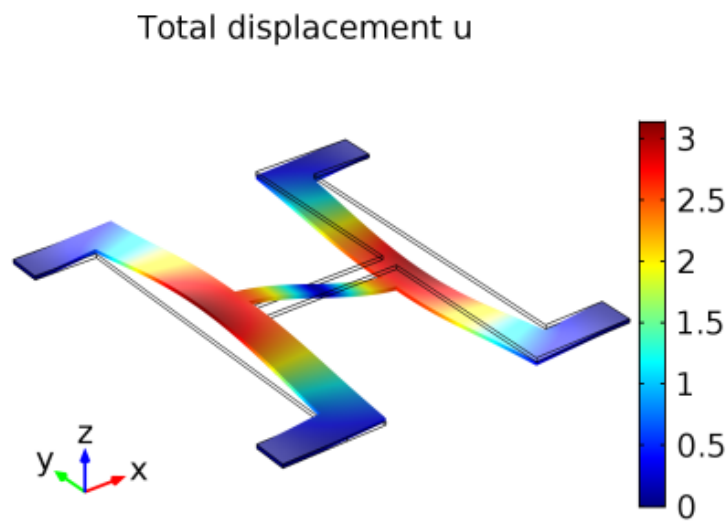


Figure 4.8: Displacements of the 1. as-eigenmode of the basic double-U structure at $T = 223 \text{ K}$. Scale is in arbitrary units.

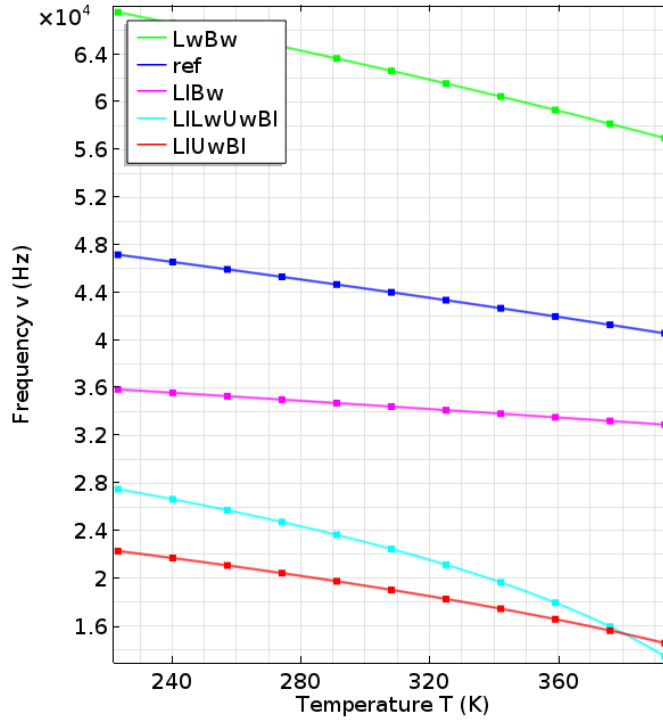


Figure 4.9: Frequency of 1. as-eigenmode versus temperature for reference and extremal combinations: **1.** $\mathbf{LwBw} = (-, Lw, -, -, -, Bw) \rightarrow \max.\Delta\nu_{223K}$, **2.** $\mathbf{ref} = (-, -, -, -, -, -)$, **3.** $\mathbf{LIBw} = (Ll, -, -, -, -, Bw) \rightarrow \max.\Delta k_\nu$, **4.** $\mathbf{LILwUwBl} = (Ll, Lw, -, Uw, Bl, -) \rightarrow \min.\Delta k_\nu$, **5.** $\mathbf{LIUwBl} = (Ll, -, -, Uw, Bl, -) \rightarrow \min.\Delta\nu_{223K}$.

The explanations for the combinations yielding extremal $\Delta\nu_{223K}$ and Δk_ν for the first as-eigenmode is not as easy as for the first ss-eigenmode due to the fact that primarily the U-bottoms are moving instead of the bridge like in the first ss-eigenmode. Thereby, the approximation of the mode with a mode of an Euler-Bernoulli beam is not as good as for the first ss-eigenmode and we need a more detailed discussion which would go beyond the scope of this thesis.

$$\begin{aligned}
 & (Ll, Lw, Ul, Uw, Bl, Bw) \\
 & (Ll, -, -, Uw, Bl, -) \rightarrow \min.\Delta\nu_{223K} = -24.9 \text{ kHz} \\
 & (-, Lw, -, -, -, Bw) \rightarrow \max.\Delta\nu_{223K} = 20.3 \text{ kHz} \\
 & (Ll, Lw, -, Uw, Bl, -) \rightarrow \min.\Delta k_\nu = -88.2 \text{ Hz/K for } T = 359 - 393 \text{ K} \\
 & (Ll, -, -, -, -, Bw) \rightarrow \max.\Delta k_\nu = 21.7 \text{ Hz/K}
 \end{aligned} \tag{4.3}$$

Nevertheless, we will go through each combination with an extremal $\Delta\nu_{223K}$ or Δk_ν and look whether it is derivable by the results for the single parameter changes or not. In this case we will try to give at least a feasible explanation.

The $\Delta\nu_{223K}$ - and Δk_ν -values of the 1. as-mode for each single parameter change are listed in Tab. 4.4.

Table 4.4: $\Delta\nu_{223\text{K}}$ and Δk_ν of the 1. as-eigenmode for all combinations where only one parameter was changed.

	Ll	Lw	Uw	Bl	Bw
$\Delta\nu_{223\text{K}}(\text{kHz})$	-13.4	18.3	-9.6	-6	1.3
$\Delta k_\nu(\text{Hz/K})$	20	-25.8	-14.7	-5.8	4

The max. $\Delta\nu_{223\text{K}}$ caused by the parameter change $(-, Lw, -, -, -, Bw)$ is derivable by the single parameter combinations as only a modification of $Lw \rightarrow (-, Lw, -, -, -, -)$ or $Bw \rightarrow (-, -, -, -, -, Bw)$ entails a positive $\Delta\nu_{223\text{K}}$ (see Tab. 4.4).

The same is true for the min. $\Delta\nu_{223\text{K}}$ with combination $(Ll, -, -, Uw, Bl, -)$ because each of the single parameter combinations $(Ll, -, -, -, -, -)$, $(-, -, -, Uw, -, -)$ and $(-, -, -, -, Bl, -)$ leads to a negative $\Delta\nu_{223\text{K}}$.

One is also able to conclude $(Ll, -, -, -, -, Bw)$ yielding the max. Δk_ν as an enlargement of Ll or Bw leads to positive Δk_ν .

Only the combination $(Ll, Lw, -, Uw, Bl, -)$ yielding min. Δk_ν for the temperature interval 359 – 393 K is not derivable because the parameter Ll is included which leads in single combination $\rightarrow (Ll, -, -, -, -, -)$ to a positive Δk_ν . An answer could be that (like in our discussion for the min. Δk_ν of the first ss-eigenmode) the first as-mode gets modified with the temperature and this modification is the largest for the combination $(Ll, Lw, -, Uw, Bl, -)$ over the interval 359 – 393 K yielding a strong temperature dependence over this interval and hence, to the min. Δk_ν as $k_\nu = -88.2 \text{ Hz/K}$ for the first as-mode of the structure (see Tab. 4.1).

4.4 1. sa-mode

One can see the shape of the first sa-eigenmode in Fig. 4.10 of the basic double-U structure at the temperature 223 K. The mode's shape stays in principle the same for all other parameter combinations and temperatures. The parameter combinations that lead to extremal $\Delta\nu_{223\text{K}}$ and Δk_ν are shown in Eq. (4.4). Additionally, we listed the $\Delta\nu_{223\text{K}}$ - and Δk_ν -values of the mode for all combinations where only one parameter was changed in Tab. 4.5 in order to make the verification easier whether the extremal-value parameter combinations are derivable from the single parameter combinations or not. Furthermore, we

plotted the frequency versus the temperature for the parameter combinations yielding extremal values and the reference combination in Fig. 4.11.

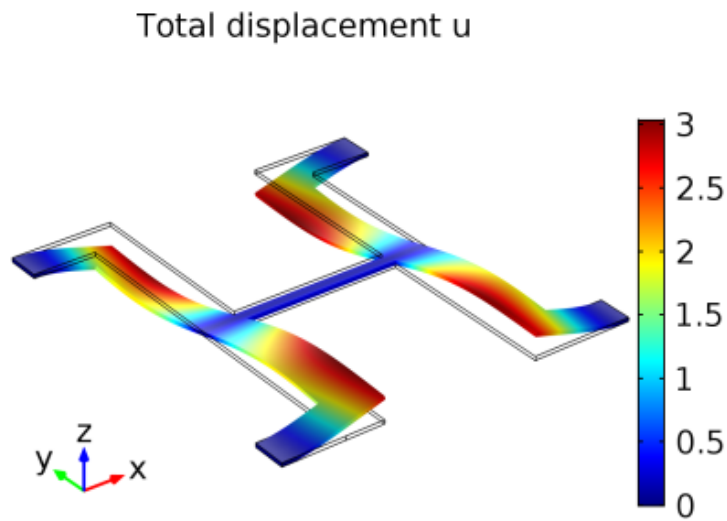


Figure 4.10: Displacements of the 1. sa-eigenmode of the basic double-U structure at $T = 223$ K. Scale is in arbitrary units.

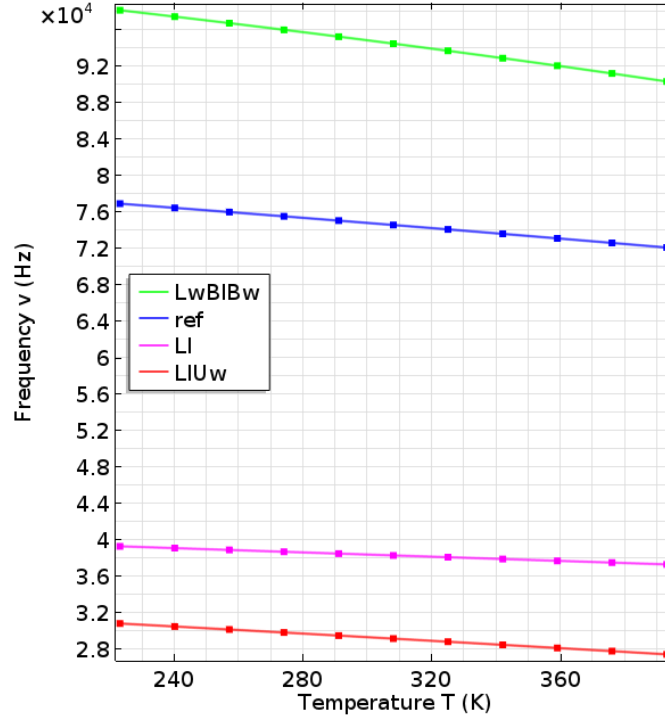


Figure 4.11: Frequency of 1. sa-eigenmode versus temperature for reference and extremal combinations: **1. LwBIBw** = $(-, Lw, -, -, Bl, Bw) \rightarrow \max.\Delta\nu_{223K}$ and $\min.\Delta k_\nu$, **2. ref** = $(-, -, -, -, -, -)$, **3. LI** = $(Ll, -, -, -, -, -) \rightarrow \max.\Delta k_\nu$, **4. LIUw** = $(Ll, -, -, Uw, -, -) \rightarrow \min.\Delta\nu_{223K}$.

Table 4.5: $\Delta\nu_{223K}$ and Δk_ν of the 1. sa-eigenmode for all combinations where only one parameter was changed.

	Ll	Lw	Uw	Bl	Bw
$\Delta\nu_{223K}(\text{kHz})$	-37.6	21	-24	0	0
$\Delta k_\nu(\text{Hz/K})$	16.4	-10	0	-2.3	-2.3

$$(Ll, Lw, Ul, Uw, Bl, Bw)$$

$$(Ll, -, -, Uw, Bl / -, Bw / -) \rightarrow \min.\Delta\nu_{223K} \approx -46 \text{ kHz}$$

$$(-, Lw, -, -, Bl / -, Bw / -) \rightarrow \max.\Delta\nu_{223K} \approx 21.2 \text{ kHz} \quad (4.4)$$

$$(-, Lw, -, -, Bl, Bw) \rightarrow \min.\Delta k_\nu = -17 \text{ Hz/K}$$

$$(Ll, -, -, -, -, -) \rightarrow \max.\Delta k_\nu = 16.4 \text{ Hz/K}$$

Comparing Tab. 4.5 with the combinations leading to extremal values 4.4 one is able to deduce $(Ll, -, -, Uw, Bl / -, Bw / -)$ for the $\min.\Delta\nu_{223K}$,

$(-, Lw, -, -, Bl / -, Bw / -)$ for the max. $\Delta\nu_{223\text{K}}$, $(-, Lw, -, -, Bl, Bw)$ for min. Δk_ν and $(Ll, -, -, -, -, -)$ for max. Δk_ν . In Fig 4.11 we picked out only one combination for each extremal value. In fact one could also assume $(Ll, -, -, Uw, -, -)$ yielding max. Δk_ν and $(-, Lw, -, Uw, Bl, Bw)$ yielding min. Δk_ν because the parameter Uw has no effect on Δk_ν (see Tab. 4.5). However, these assumptions are not right as $(Ll, -, -, Uw, -, -)$ leads to $\Delta k_\nu = 8.8 \text{ Hz/K}$ and $(-, Lw, -, Uw, Bl, Bw)$ to $\Delta k_\nu = -11.7 \text{ Hz/K}$ (see Tab. 4.2). Comparing in Tab. 4.2 parameter combination pairs where Uw is one time unchanged and one time changed we find that a combination with unchanged Uw has always a larger magnitude $|\Delta k_\nu|$ than the same combination with changed (bigger) Uw . Thus, the parameter Uw describing the U-bottoms' width seems to act like a buffer reducing the change of the frequency's slope Δk_ν caused by other parameter modifications. To find the reason for that characteristic more researches are essential regarding this subject which would go beyond the scope of this thesis.

4.5 1. aa-mode

The shape of the first aa-eigenmode is shown in Fig. 4.12 with the basic double-U structure at $T = 223 \text{ K}$ (the mode's shape stays in principle the same for all other parameter combinations and temperatures). One can find the parameter combinations that lead to extremal $\Delta\nu_{223\text{K}}$ and Δk_ν in Eq. (4.5). In Tab. 4.6 we listed the $\Delta\nu_{223\text{K}}$ - and Δk_ν -values of the mode for all combinations where only one parameter was changed. Furthermore, we plotted the frequency in terms of the temperature for the parameter combinations yielding extremal values and the reference combination in Fig. 4.13.

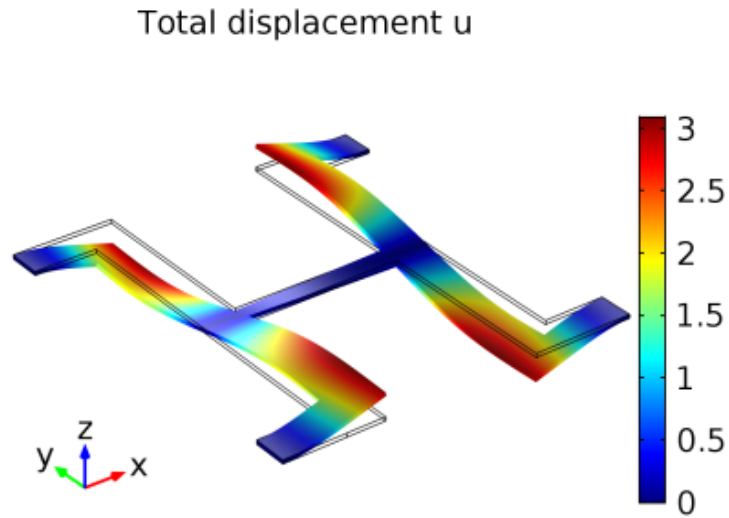


Figure 4.12: Displacements of the 1. aa-eigenmode of the basic double-U structure at $T = 223$ K. Scale is in arbitrary units.

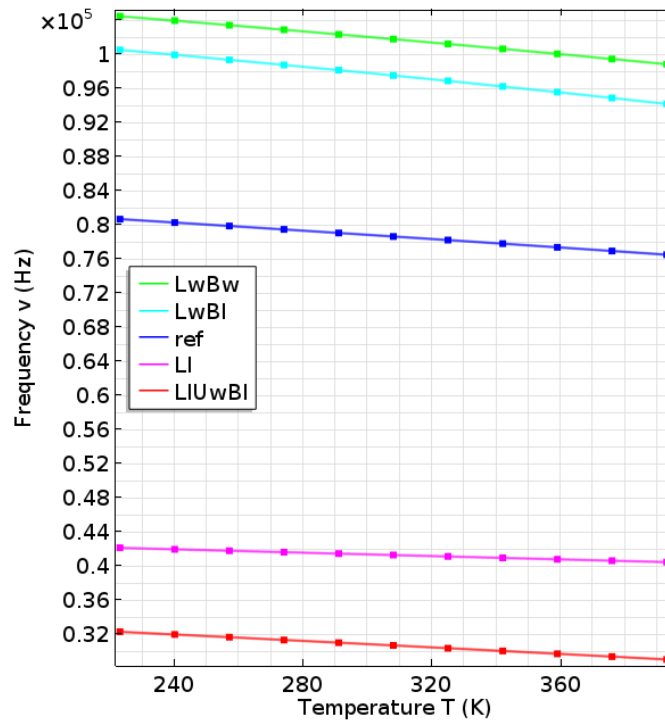


Figure 4.13: Frequency of 1. aa-eigenmode versus temperature for reference and extremal combinations: **1.** $\mathbf{LwBw} = (-, Lw, -, -, -, Bw) \rightarrow \max.\Delta v_{223K}$, **2.** $\mathbf{LwBl} = (-, Lw, -, -, Bl, -) \rightarrow \min.\Delta k_v$, **3.** $\mathbf{ref} = (-, -, -, -, -, -)$, **4.** $\mathbf{LI} = (Ll, -, -, -, -, -) \rightarrow \max.\Delta k_v$, **5.** $\mathbf{LIUwBl} = (Ll, -, -, Uw, Bl, -) \rightarrow \min.\Delta v_{223K}$.

Table 4.6: $\Delta\nu_{223\text{K}}$ and Δk_ν of the 1. aa-eigenmode for all combinations where only one parameter was changed.

	Ll	Lw	Uw	Bl	Bw
$\Delta\nu_{223\text{K}}(\text{kHz})$	-38.5	20.7	-25	-1	3.5
$\Delta k_\nu(\text{Hz/K})$	14.7	-10	0	-2.3	0

$$\begin{aligned}
& (Ll, Lw, Ul, Uw, Bl, Bw) \\
& (Ll, -, -, Uw, Bl, -) \rightarrow \min.\Delta\nu_{223\text{K}} = -48.4 \text{ kHz} \\
& (-, Lw, -, -, -, Bw) \rightarrow \max.\Delta\nu_{223\text{K}} = 23.8 \text{ kHz} \tag{4.5} \\
& (-, Lw, -, -, Bl, Bw/-) \rightarrow \min.\Delta k_\nu \approx -12.5 \text{ Hz/K} \\
& (Ll, -, -, -, -, Bw/-) \rightarrow \max.\Delta k_\nu \approx 15 \text{ Hz/K}
\end{aligned}$$

Looking at Tab. 4.6 and 4.5 all the extremal valued combinations are deducible with the results of the single combinations. But still one might deduce more parameter combinations which are not included in 4.5 namely $(-, Lw, -, Uw, Bl, Bw/-)$ for min. Δk_ν and $(Ll, -, -, Uw, -, Bw/-)$ for max. Δk_ν . Looking at Tab. 4.2 we find that these conclusions are not valid as $(-, Lw, -, Uw, Bl, Bw/-)$ yields $\Delta k_\nu = -10/0 \text{ Hz/K}$ and $(Ll, -, -, Uw, -, Bw/-)$ yields $\Delta k_\nu = 5.8/7.1$. Again, we compare in Tab. 4.2 parameter combination pairs where Uw is one time unchanged and one time changed and conclude that a combination with unchanged Uw has always a larger magnitude $|\Delta k_\nu|$ than the same one with changed (larger) Uw . Thus, we see the same effect like in the first sa-mode making Uw a buffer that reduces alterations (by other parameter changes) of the frequency-slope.

4.6 2. ss-mode

Figure 4.14 depicts the second ss-eigenmode's shape of the basic double-U structure at $T = 223 \text{ K}$. The mode's shape stays in principle the same for all other parameter combinations and temperatures. The parameter combinations yielding extremal $\Delta\nu_{223\text{K}}$ and Δk_ν are given in Eq. (4.6). Table 4.7 lists the $\Delta\nu_{223\text{K}}$ - and Δk_ν -values of the 2. ss-mode for all combinations where only one parameter was changed. Furthermore, we plotted the frequency in terms of the

temperature for the parameter combinations leading to extremal values and the reference combination in Fig. 4.15 (if more combinations lead to the same extremal value we chose only one of them for Fig. 4.15). Additionally, we show in Fig. 4.15 the mode's frequency of the combination $(Ll, -, -, Uw, Bl, Bw)$ because of its interesting characteristic.

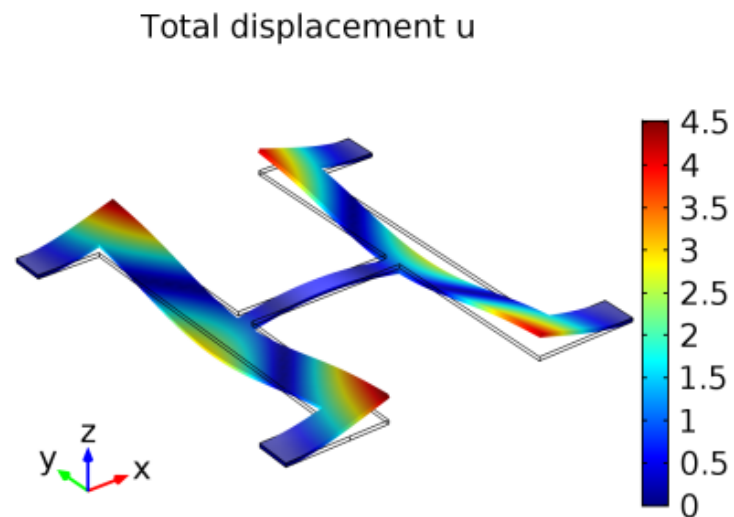


Figure 4.14: Displacements of the 2. *ss*-eigenmode of the basic double-U structure at $T = 223$ K. Scale is in arbitrary units.

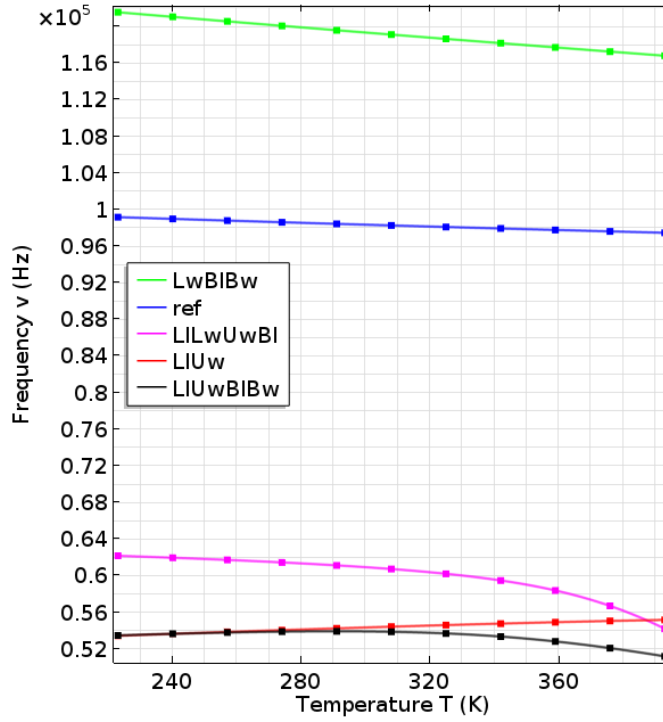


Figure 4.15: Frequency of 2. ss-eigenmode versus temperature for reference and extremal combinations and combination with interesting properties: **1.** **LwBIBw** = $(-, Lw, -, -, Bl, Bw) \rightarrow \max.\Delta v_{223K}$, **2.** **ref** = $(-, -, -, -, -, -)$, **3.** **LILwUwBl** = $(Ll, Lw, -, Uw, Bl, -) \rightarrow \min.\Delta k_v$, **4.** **LIUw** = $(Ll, -, -, Uw, -, -) \rightarrow \min.\Delta v_{223K}$ and $\max.\Delta k_v$, **5.** **LIUwBIBw** = $(Ll, -, -, Uw, Bl, Bw)$ featuring interesting properties.

Table 4.7: Δv_{223K} and Δk_v of the 2. ss-eigenmode for all combinations where only one parameter was changed.

	Ll	Lw	Uw	Bl	Bw
$\Delta v_{223K}(\text{kHz})$	-36	21.2	-33.8	2.3	2.8
$\Delta k_v(\text{Hz/K})$	6.5	-21.2	8	0	0

$$(Ll, Lw, Ul, Uw, Bl, Bw)$$

$$(Ll, -, -, Uw, -, -) \rightarrow \min.\Delta v_{223K} = -45.8 \text{ kHz}$$

$$(-, Lw, -, -, Bl, Bw) \rightarrow \max.\Delta v_{223K} = 22.4 \text{ kHz} \quad (4.6)$$

$$(Ll, Lw, -, Uw, Bl, -) \rightarrow \min.\Delta k_v = -113.5 \text{ Hz/K for } T = 359 - 393 \text{ K}$$

$$(Ll, -, -, Uw, -, -) \rightarrow \max.\Delta k_v = 20.5 \text{ Hz/K}$$

With Tab. 4.7 one is able to deduce the following parameter combinations leading to extremal values: $(-, Lw, -, -, Bl, Bw)$ for max. $\Delta\nu_{223K}$ and $(Ll, -, -, Uw, -, -)$ for min. $\Delta\nu_{223K}$ and max. Δk_ν . However, with Tab. 4.7 the combinations $(Ll, -, -, Uw, Bl, Bw)$, $(Ll, -, -, Uw, -, Bw)$, $(Ll, -, -, Uw, Bl, -)$ for max. Δk_ν and $(-, Lw, -, -, Bl/-, Bw/-)$ for min. Δk_ν are deducible too but not correct.

In case of the combinations $(Ll, -, -, Uw, Bl, Bw)$, $(Ll, -, -, Uw, -, Bw)$ and $(Ll, -, -, Uw, Bl, -)$ we find by looking at Tab. 4.2 that both parameters Bl and Bw seem to cause effects that lead to a decrease of the frequency's slope with the temperature although Bl and Bw have no effects on k_ν if they are changes solely (Tab. 4.7). Especially Bl leads to a big decrease of the slope over the temperature as we get for example considering $(Ll, -, -, Uw, Bl, -)$ a $\Delta k_\nu = 21 \text{ Hz/K}$ for low temperatures and a $\Delta k_\nu = -11.7 \text{ Hz/K}$ for high temperatures (see Tab. 4.2). The effects evoked by Bl and Bw are summable which clearly leads to a very strong decrease of the frequency's slope by the combination $(Ll, -, -, Uw, Bl, Bw)$ where $\Delta k_\nu = 21.4 \text{ Hz/K}$ for low temperatures and a $\Delta k_\nu = -38.8 \text{ Hz/K}$ for high temperatures (shown in Fig. 4.15).

By evaluating the results of $\Delta\nu_{223K}$ and Δk_ν (Tab. 4.2) and the simulated eigemode shapes of some combinations one can figure out that almost all combinations $(Ll/-, Lw/-, -, Uw, Bl, Bw/-)$ yield a strong shape modification with temperature. An exception are only $(-, Lw, -, Uw, Bl, Bw/-)$, where no shape modification is observed. Hence one can say that all combinations where Uw and Bl are changed except of those where additionally Lw is changed and Ll is unchanged entail strong temperature dependent mode modifications. We show this effect in Fig. 4.16 considering the parameter combination $(Ll, -, -, Uw, Bl, -)$. Here we displayed the 2. *ss-mode*'s shape of the structure corresponding to $(Ll, -, -, Uw, Bl, -)$ for different temperatures (223 K and 393 K).

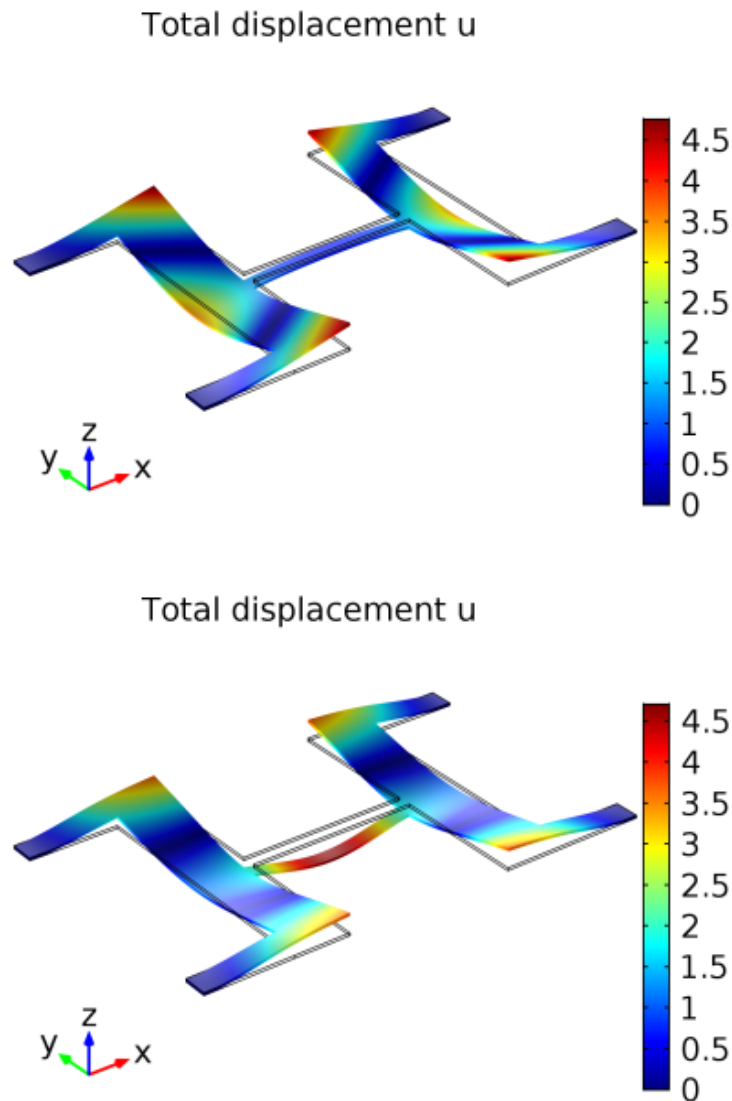


Figure 4.16: Displacements of the 2. ss-eigenmode of the structure corresponding to $(Ll, -, -, Uw, Bl, -)$ at $T = 223$ K (top) and at $T = 393$ K (bottom). Scale is in arbitrary units. The bridge gets a deflection stronger with the temperature where the deflection of the U-corners (the ends where U-bottoms and legs are connected) gets smaller with the temperature.

Looking at the basic shape of the mode (Fig. 4.14 or Fig. 4.16 top) we see that the bridge gets no deflection and primarily the ends of the U-bottoms are moved. With the modification of Uw and Bl (except of the case where additionally Lw is changed and Ll is unchanged) the 2. ss-mode changes the way how the bridge deflects. This effect gets stronger with increasing temperature where the deflection of the U-corners gets smaller with the temperature. The effect causes a modification of the mode's shape with temperature and might be responsible for the huge decrease of the frequency's slope concerning the

combinations $(Ll, -, -, Uw, Bl, -)$ and $(Ll, -, -, Uw, Bl, Bw)$.

However, there is no shape modification observed for the $(Ll, -, -, Uw, -, Bw)$, requiring more detailed investigations.

$(-, Lw, -, -, Bl/-, Bw/-)$ indeed entails a quite negative Δk_v around -20 Hz/K but it is still far away from $\Delta k_v = -113.5 \text{ Hz/K}$ caused by $(Ll, Lw, -, Uw, Bl, -)$ over the interval $359 - 393 \text{ K}$. This effect can also be addressed by the distinct modification of the 2. ss-mode with temperature caused by Uw and Bl .

4.7 2. as-mode

In Fig. 4.17 the 2. as-eigenmode is depicted with the basic double-U structure at the temperature 223 K . Owing to simulations one can say that the mode stays in principle the same for all parameter combinations and temperatures. The parameter combinations which lead to extremal $\Delta v_{223\text{K}}$ and Δk_v are shown in Eq. (4.7). In Tab. 4.8 the $\Delta v_{223\text{K}}$ - and Δk_v -values for all combinations where only one parameter was changed are shown. Furthermore, we plotted the frequency in terms of the temperature for the parameter combinations leading to extremal values and the reference combination in Fig. 4.18 (again if more combinations lead to the same extremal value we chose only one of them for Fig. 4.18).

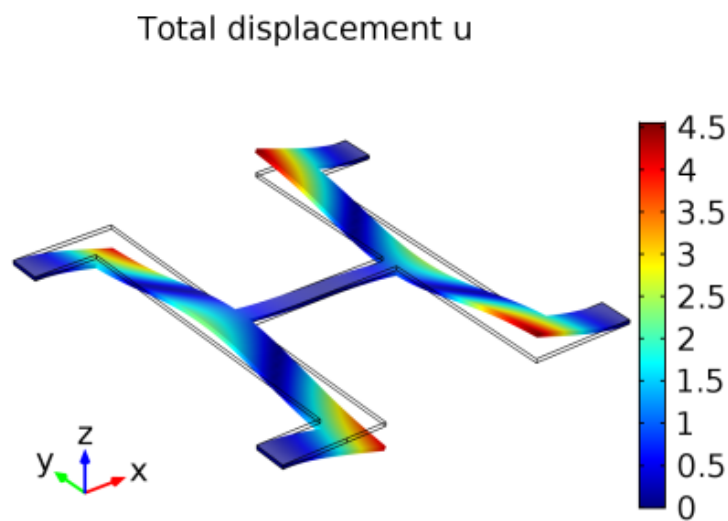


Figure 4.17: Displacements of the 2. as-eigenmode of the basic double-U structure at $T = 223 \text{ K}$. Scale is in arbitrary units.

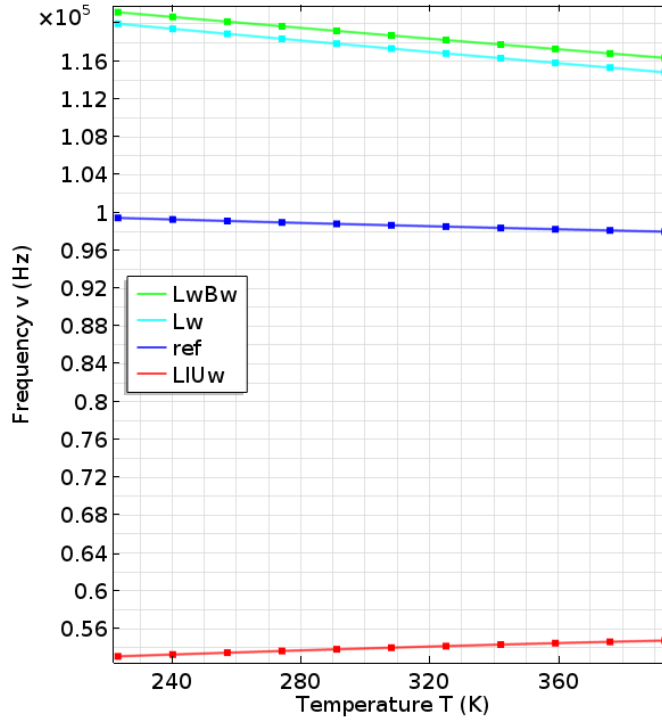


Figure 4.18: Frequency of 2. as-eigenmode versus temperature for reference and extremal combinations: **1.** $\mathbf{LwBw} = (-, Lw, -, -, -, Bw) \rightarrow \max.\Delta v_{223K}$, **2.** $\mathbf{Lw} = (-, Lw, -, -, -, -) \rightarrow \min.\Delta k_v$, **3.** $\mathbf{ref} = (-, -, -, -, -, -)$, **4.** $\mathbf{LIUw} = (Ll, -, -, Uw, -, -) \rightarrow \min.\Delta v_{223K}$ and $\max.\Delta k_v$.

Table 4.8: Δv_{223K} and Δk_v of the 2. as-eigenmode for all combinations where only one parameter was changed.

	Ll	Lw	Uw	Bl	Bw
$\Delta v_{223K}(\text{kHz})$	-36	20.6	-33.2	0	2.3
$\Delta k_v(\text{Hz/K})$	4.4	-22.3	11.1	0	0

$$(Ll, Lw, Ul, Uw, Bl, Bw)$$

$$(Ll, -, -, Uw, Bl / -, -) \rightarrow \min.\Delta v_{223K} \approx -46.4 \text{ kHz}$$

$$(-, Lw, -, -, Bl / -, Bw) \rightarrow \max.\Delta v_{223K} \approx 21.8 \text{ kHz} \quad (4.7)$$

$$(-, Lw, -, -, Bl / -, -) \rightarrow \min.\Delta k_v \approx -22 \text{ Hz/K}$$

$$(Ll, -, -, Uw, Bl / -, Bw / -) \rightarrow \max.\Delta k_v \approx 19 \text{ Hz/K}$$

Looking at Tab. 4.8 and 4.7 we conclude that all the extremal valued combinations of 4.7 are deducible with the results of the single combinations. How-

ever, one might deduce with Tab. 4.8 ($-, Lw, -, -, Bl / -, Bw$) for min. Δk_ν which is not correct. Despite the fact that a change of the parameter Bw has no effect on Δk_ν if all other parameters are not changed it seems to have effects on Δk_ν if other parameters change too. The reason for this is not a special modification of the mode implicated only if Bw and other parameters change as we verified it with our program. Thus, further research is necessary to validate this characteristic.

4.8 Summary of the results

At the end of this chapter we want to summarize our results first for the modes that are symmetric about the S2-axis and second for the modes that are asymmetric about the S2-axis. We separate the results into two groups to facilitate the comparison within symmetric and antisymmetric modes about the S2-axis.

4.8.1 Modes symmetric about the S2-axis

In this subsection we consider the modes that are symmetric about the S2-axis namely the 1. ss-, the 1. sa- and the 2. ss-mode. Table 4.9 lists the $\Delta\nu_{223K}$ -values of the three modes for all combinations where only one parameter was changed, Tab. 4.10 lists the same but for Δk_ν and the parameter combinations leading to extremal values of $\Delta\nu_{223K}$ and Δk_ν for the three modes are given in Tab. 4.11.

Table 4.9: $\Delta\nu_{223K}$ -values (in kHz) of the 1. ss-, the 1. sa- and the 2. ss-mode for all combinations where only one parameter was changed.

	Ll	Lw	Uw	Bl	Bw
1.ss	-12	14.7	-8.2	-2.5	-2
1.sa	-37.6	21	-24	0	0
2.ss	-36	21.2	-33.8	2.3	2.8

Table 4.10: Δk_v -values (in Hz/K) of the 1. ss-, the 1. sa- and the 2. ss-mode for all combinations where only one parameter was changed.

	Ll	Lw	Uw	Bl	Bw
1.ss	15.8	-21.7	-15	-2.9	2.9
1.sa	16.4	-10	0	-2.3	-2.3
2.ss	6.5	-21.2	8	0	0

Table 4.11: Parameter combinations (Ll, Lw, Ul, Uw, Bl, Bw) yielding extremal Δv_{223K} - and Δk_v -values for the 1. ss, the 1. sa and the 2. ss.

	$max\Delta v_{223K}$	$min\Delta v_{223K}$	$max\Delta k_v$	$min\Delta k_v$
1.ss	(-,Lw,-,-,-)	(Ll,-,-,Uw,Bl,Bw)	(Ll,-,-,-,Bw)	(Ll,Lw,-,Uw,Bl,Bw)
1.sa	(-,Lw,-,-,Bl/-,Bw/-)	(Ll,-,-,Uw,Bl/-,Bw/-)	(Ll,-,-,-,-)	(-,Lw,-,-,Bl,Bw)
2.ss	(-,Lw,-,-,Bl,Bw)	(Ll,-,-,Uw,-,-)	(Ll,-,-,Uw,-,-)	(Ll,Lw,-,Uw,Bl,-)

Looking at Tab. 4.9 we find that a single change of the parameters Ll , Lw and Uw has the same (same sign) and considerable effects on Δv_{223K} regarding all the three symmetric modes. The parameters Bl and Bw have not the same effects on Δv_{223K} for the considered modes but their effects are small anyway. Furthermore, considering Tab. 4.11 we see that the extremal combinations regarding Δv_{223K} for all S2-symmetric modes are deducible from the results of the single parameter changes in Tab. 4.9.

Concerning Δk_v we find that the effects caused by a single change of Ll and Lw are strong and the same for all symmetric modes where a change of Bl and Bw entails different and small effects. Thus, regarding these parameters we have the same characteristic as for Δv_{223K} . Only the parameter Uw breaks the ranks as its effects on Δk_v are partly strong and differ between the symmetric modes. Looking at the extremal combinations for Δk_v in Tab. 4.11 we find that the combinations differ between the symmetric modes and are not deducible by the single parameter results except for the parameter Lw . This parameter exhibits the same effect in all extremal combinations which is also deducible by the single results of 4.10.

4.8.2 Modes asymmetric about the S2-axis

With the 1. as-, the 1. aa- and the 2. as-mode we have the modes which are asymmetric about the S2-axis. The $\Delta\nu_{223K}$ - and Δk_ν -values of these three modes for all combinations where only one parameter was changed are shown in Tab. 4.12 and Tab. 4.13. The parameter combinations yielding extremal values of $\Delta\nu_{223K}$ and Δk_ν are listed in Tab. 4.14.

Table 4.12: $\Delta\nu_{223K}$ -values (in kHz) of the 1. as-, the 1. aa- and the 2. as-mode for all combinations where only one parameter was changed.

	Ll	Lw	Uw	Bl	Bw
1.as	-13.4	18.3	-9.6	-6	1.3
1.aa	-38.5	20.7	-25	-1	3.5
2.as	-36	20.6	-33.2	0	2.3

Table 4.13: Δk_ν -values (in Hz/K) of the 1. as-, the 1. aa- and the 2. as-mode for all combinations where only one parameter was changed.

	Ll	Lw	Uw	Bl	Bw
1.as	20	-25.8	-14.7	-5.8	4
1.aa	14.7	-10	0	-2.3	0
2.as	4.4	-22.3	11.1	0	0

Table 4.14: Parameter combinations (Ll, Lw, Ul, Uw, Bl, Bw) yielding extremal $\Delta\nu_{223K}$ - and Δk_ν -values for the 1. as, the 1. aa and the 2. as.

	$max\Delta\nu_{223K}$	$min\Delta\nu_{223K}$	$max\Delta k_\nu$	$min\Delta k_\nu$
1.as	(-,Lw,-,-,Bw)	(Ll,-,-,Uw,Bl,-)	(Ll,-,-,-,Bw)	(Ll,Lw,-,Uw,Bl,-)
1.aa	(-,Lw,-,-,Bw)	(Ll,-,-,Uw,Bl,-)	(Ll,-,-,-,Bw/-)	(-,Lw,-,-,Bl,Bw/-)
2.as	(-,Lw,-,-,Bl/-,Bw)	(Ll,-,-,Uw,Bl/-,-)	(Ll,-,-,Uw,Bl/-,Bw/-)	(-,Lw,-,-,Bl/-,-)

Having a look at Tab. 4.12 we discover that a single change of the parameters Ll , Lw and Uw cause strong and the same (same sign) effects on $\Delta\nu_{223K}$ for all S2-asymmetric modes. The $\Delta\nu_{223K}$ -values caused by Bw are indeed the same for all the considered modes but small. Bl leads to rather small effects which differ between the asymmetric modes. As for the S2-symmetric modes all the extremal combinations concerning $\Delta\nu_{223K}$ in Tab. 4.14 are inducible by the results of the single parameter changes of Tab. 4.12.

Looking at the Δk_ν -values caused by single parameter changes in Tab. 4.13 we find that Ll and Lw have the same (same sign) and Uw , Bl and Bw cause different effects on the S2-asymmetric modes. The Δk_ν -effects of Ll , Lw and Uw are basically strong with exceptions that Δk_ν is small for a change of Ll concerning the 2. as and for a change of Uw concerning the 1. aa. The Δk_ν -values of Bl and Bw are again rather small. Looking at Tab. 4.14 with the extremal values we conclude that the extremal parameter combinations are only deducible from the single results for the parameters Lw and Bl .

Chapter 5

Experimental verification of the simulation

In this chapter we want to verify the simulations by a micromechanically fabricated double-U structure. We consider a double-U structure like in chapter 4 (Fig. 5.1). This design was already available and the structural dimensions are $Ul = 1800 \mu\text{m}$, its legs have a length of $Ll = 575 \mu\text{m}$ and a width of $Lw = 160 \mu\text{m}$. Each U-bottom's (the beam which couples the two legs respectively) width is given by $Uw = 400 \mu\text{m}$.

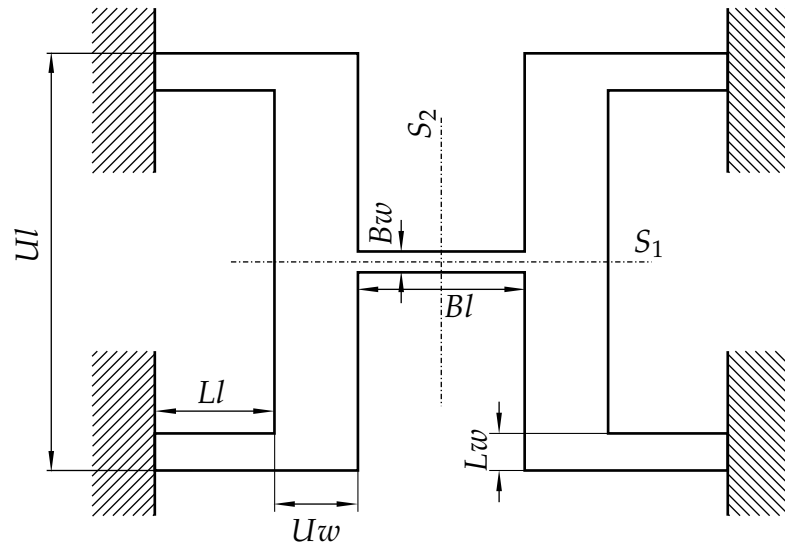


Figure 5.1: Clamped double-U beam structure with $Ll = 575 \mu\text{m}$, $Lw = 160 \mu\text{m}$, $Ul = 1800 \mu\text{m}$, $Uw = 400 \mu\text{m}$, $Bl = 1050 \mu\text{m}$ and $Bw = 120 \mu\text{m}$.

The bridge has a length of $Bl = 1050 \mu\text{m}$ and a width of $Bw = 120 \mu\text{m}$. The thickness of the beam structure $H = 20 \mu\text{m}$ is uniform for the whole structure. Our structure is made of silicon with a mass density of 2329 kg/m^3 . The silicon is assumed to be nonlinear isotropic and its Young's modulus and Poisson's ratio are given by $E = 150 \cdot 10^9 \text{ Pa}$ and $\nu = 0.28$. Its thermal expansion coefficient is $\alpha = 2.6 \cdot 10^{-6} \text{ 1/K}$.

We computed with the FEM software the frequency of the 1. as-mode (shape shown in Fig. 5.2) of this structure in terms of the temperature.

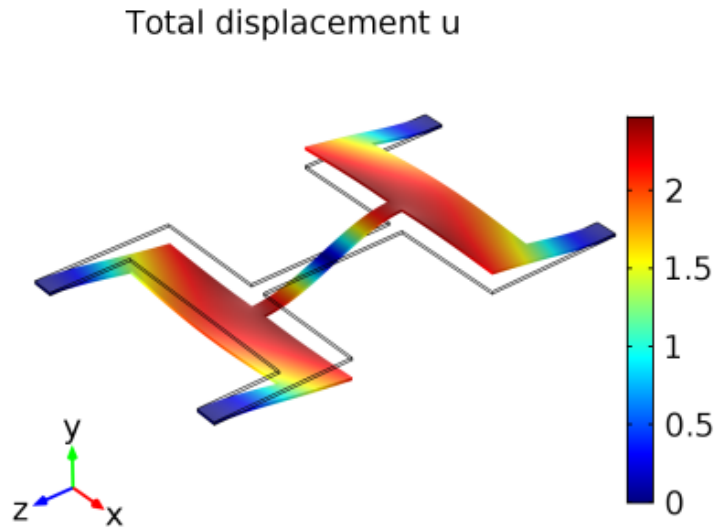


Figure 5.2: Displacements of the 1. as-eigenmode of the double-U structure at $T = 223$ K. Scale is in arbitrary units.

In order to verify our simulations we measured the mode's frequency over the temperature interval of $T = [298 \text{ to } 309]$ K for the same structure. To be precise the measured structure has basically the same geometry and consists of the same material (silicon) like the one we consider in Fig. 5.1. There is only a small difference between them, namely the thin Au-lead on the measured structure. This lead is required to excite the mode by a magnetic field and the alternating current in the lead (Lorentz force). The lead is mounted mirror symmetric about the S1- and S2-axis on the structure and its cross section has a width of $A = 50 \mu\text{m}$ and a height of $H_1 = 100 \text{ nm}$. The measured double-U structure together with the lead is shown in Fig. 5.3 and Fig. 5.4.

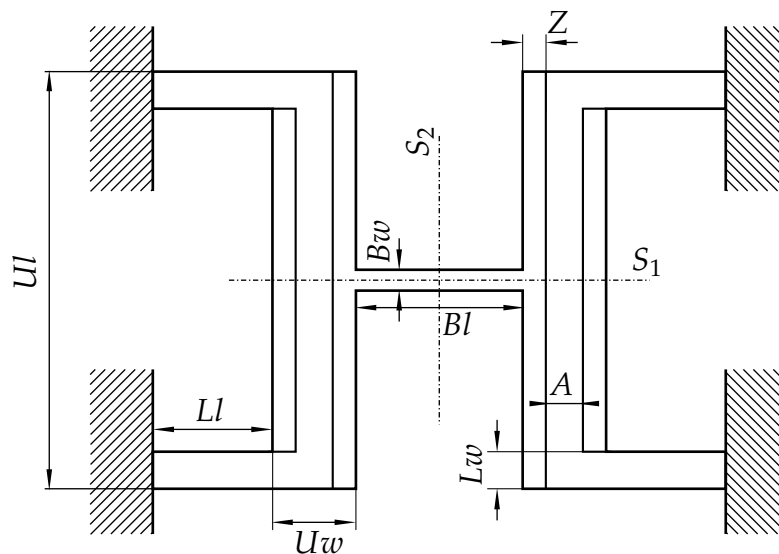


Figure 5.3: Measured double-U beam structure with Au-lead. $L1 = 575 \mu\text{m}$, $Lw = 160 \mu\text{m}$, $U1 = 1800 \mu\text{m}$, $Uw = 400 \mu\text{m}$, $Bl = 1050 \mu\text{m}$ and $Bw = 120 \mu\text{m}$, $A = 160 \mu\text{m}$ and $Z = 120 \mu\text{m}$.

Figure 5.4 depicts a raster electron micrograph of a structure with an analog geometry of the measured double-U structure.

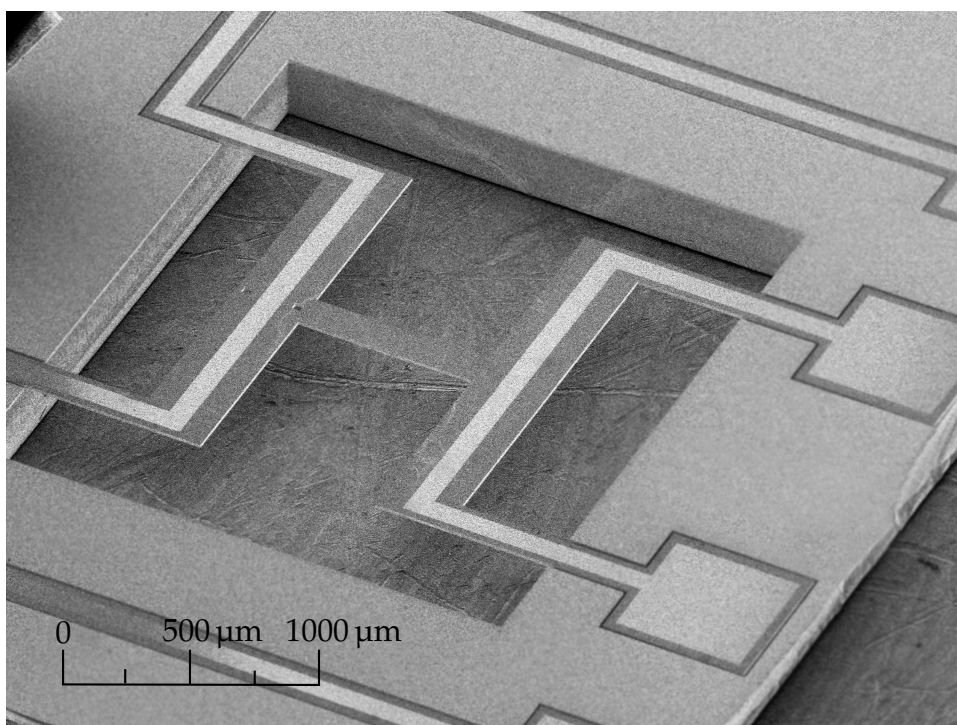


Figure 5.4: Raster electron micrograph of a structure analog to the measured one.

5.1 Fabrication of the structure

The fabrication starts with a wafer consisting of two Si-layers (structure and handle layer) separated by a thin SiO₂-layer utilizing the silicon-on-insulator (SOI) technology. This technology uses the SiO₂-layer as a defined etch stop. The thickness of the structure layer is 20 μm where the one of the handle layer is 350 μm. In the following the main parts of the structure fabrication are demonstrated [22].

1. applying lead (Fig. 5.5): An image reversal photoresist (AZ 5214) is applied uniformly onto the surface of the structure layer. With intense light a photomask of the Au-lead geometry is projected onto the photoresist. Due to light exposure and reversal processes the chemical properties of the resist change the way that the unexposed parts of the photoresist become soluble to the developer (1 % NH₄OH-solution).

After removing the unexposed photoresist with the developer a Ti-layer (60 nm) and a Au-layer (100 nm) are evaporated onto the surface. The titanium acts as a bonding material between wafer and gold.

Afterwards the photoresist with the evaporated layers is removed in an acetone bath and the Au-lead with the desired geometry remains.

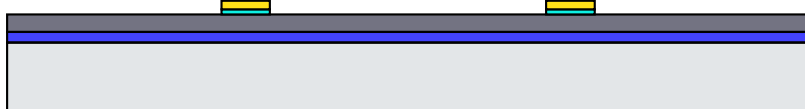
applying photoresist:



evaporating Ti- and Au-layers:



removing photoresist:

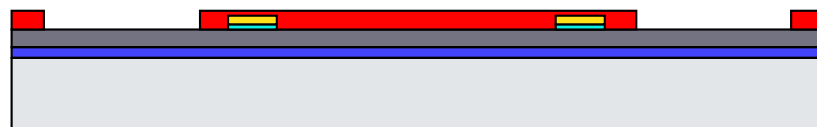


- | | |
|------------------------------------|------------------------|
| □ handle layer (Si) | ■ reversal photoresist |
| ■ silicon dioxide SiO ₂ | ■ gold |
| ■ structure layer (Si) | ■ titanium |

Figure 5.5: Fabrication process of Au-lead on wafer. Vertical section along the S1-axis (see Fig. 5.3).

2. fabricating horizontal structure-geometry (Fig. 5.6): A photomask of the double-U structure is projected onto a positive photoresist (AZ 6624). The light exposed photoresist is removed with the developer (1 % NH_4OH solution). Uncovered silicon is removed via deep reactive ion etching (DRIE). With this process highly anisotropic etching with large aspect ratios (up to 50:1) is possible. The SiO_2 -layer serves as an etch stop. After etching the photoresist is removed with acetone.

applying photoresist:



DRIE etching of uncovered Si:



removing photoresist:



- | | |
|----------------------------------|------------------------|
| □ handle layer (Si) | ■ positive photoresist |
| ■ silicon dioxide SiO_2 | ■ gold |
| ■ structure layer (Si) | ■ titanium |

Figure 5.6: Fabrication process of double-U geometry.

3. fabricating structure thickness (Fig. 5.7): The positive photoresist (AZ 6624) is applied on the surface of the handle layer. After light exposure and development of the resist, DRIE etching is performed to remove the exposed silicon till the SiO_2 -layer. Etching here is quite deep, hence the resist-layer needs to exhibit a sufficient thickness.

As a next step wet etching of the uncovered silicon dioxide is performed. The etching bases on a buffered hydrofluoric acid solution (BHF).

At last the photoresist is removed.

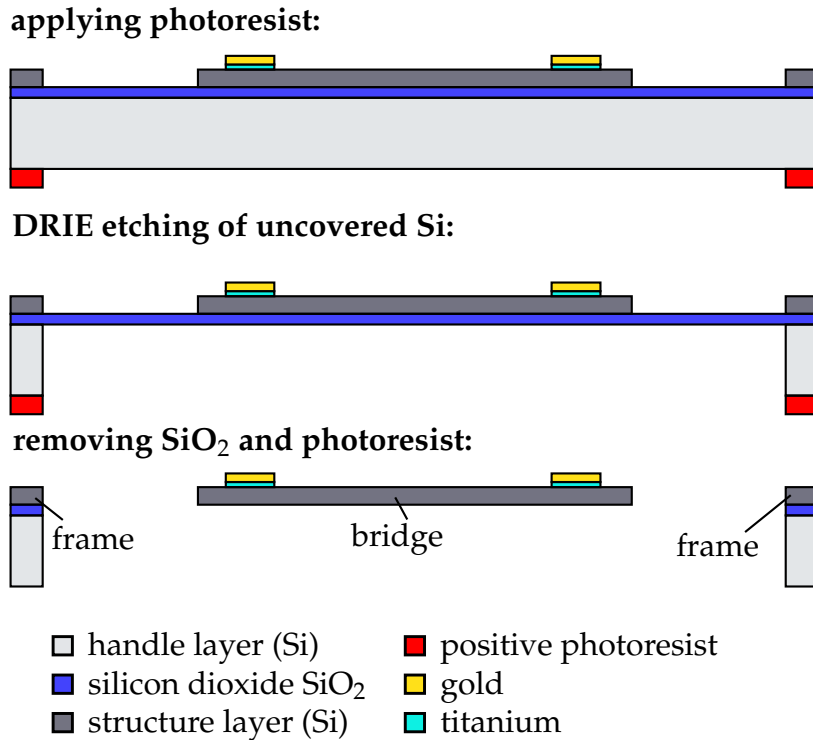


Figure 5.7: Fabrication process of structure thickness.

5.2 Results and discussion

Since the Au-lead is small relative to the whole structure it should have only minor effects on the frequency of the 1. as-mode. Nevertheless, in our simulation we took into account the additional mass due to the Au-lead by a higher effective mass density of $\rho_{\text{eff}} = 2358 \text{ kg/m}^3$ instead of $\rho = 2329 \text{ kg/m}^3$ for pure silicon.

With an experimental setup shown in Fig. 5.8 we heated the double-U structure from 298 K to 309 K and measured the frequency of the mode for each temperature step. Power resistors at each side of the aluminum plate where the measured structure is located are used as heating source (Fig. 5.8). Helmholtz coils generate a constant magnetic field at the site of the measured structure. Simultaneously, an ac current is driven through the Au-lead on the structure. The magnetic field in combination with the ac current cause the Lorentz force which excites vibrations of the structure. The shape of the eigenmode and its frequency are measured with a micro system analyser (MSA). The experimental results for the 1. as-mode are shown in Fig. 5.9 together with the results of the simulation made by the FEM software.

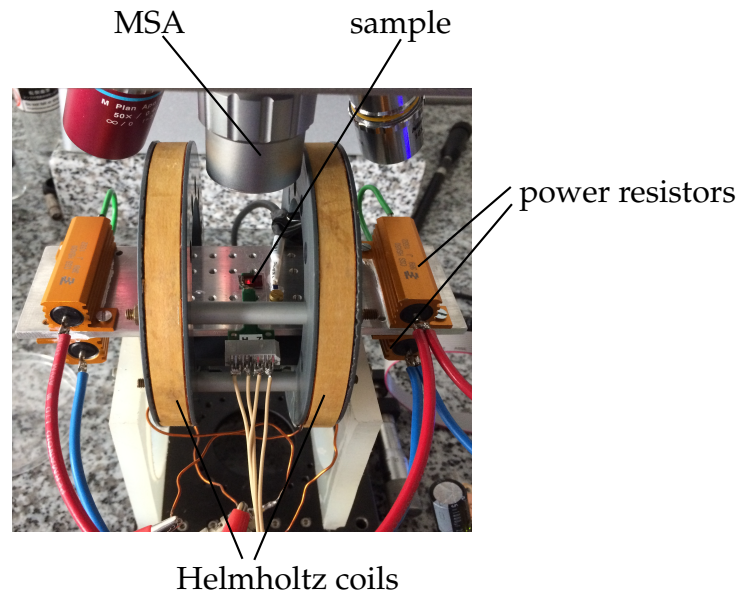


Figure 5.8: Experimental setup to measure the eigenfrequencies depending on the temperature.

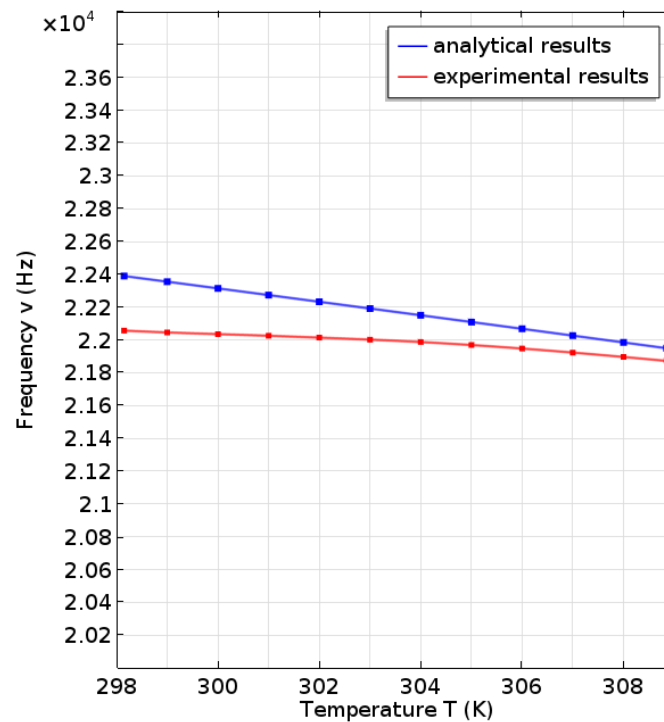


Figure 5.9: Experimental and FEM results for the frequency of the 1. as-eigenmode versus temperature of the double-U structure.

In Fig. 5.9 we see that the experimental results and the FEM-simulation fit well except of relatively small deviations of less than 2%. The simulated resonant frequencies deviate due to simplifications in our simulation. These were necessary to keep the simulation time sufficiently small. In the following

we will describe the main factors for these deviations.

Figure 5.9 reveals that the simulated frequencies (blue) are a little higher than the measured ones (red). The reason for this might be that we didn't take the lead distribution on the structure into account. With the modified density for the structure ρ_{eff} we considered the additional mass but we neglected the real mass-distribution on the structure. Looking at Fig. 5.3 or Fig. 5.4 one can see that there is no gold on the bridge. The gold is actually more focused on the Us of the structure, so they should have a higher effective mass density than ρ_{eff} . The higher effective density at the Us effects the 1. as-mode as here the Us are moved very pronounced (Fig. 5.2) with the consequence that the resonant frequency decreases more than computed.

Furthermore, Fig. 5.9 reveals that the frequency's slope of experiment and FEM for temperatures higher than 307 K are almost equal. However, for temperatures below 307 K the slope of the experiment is significantly smaller than that of the FEM. There are some reasons which might cause this.

The first one is that we assumed in our simulation a constant Young's modulus of $E = 150 \cdot 10^9$ Pa. To be precise this assumption is not perfectly fulfilled as the Young's modulus is actually temperature dependent. It decreases with increasing temperature leading to a decrease of the frequency's slope with higher temperature and hence, to an characteristic that fits better with the one of our experimental result.

Another reason for the deviation is that we assumed in our simulation for the sake of simplicity a uniform temperature T_{st} of the structure and a uniform temperature T_{fr} for the frame. Such a temperature distribution can hardly be achieved in the experiment. There we get a continuous transition of the temperature from T_{st} to T_{fr} around the interface structure-frame. Thus, the simplified temperature distribution is a convenient approximation of the real temperature distribution. This clearly leads to some differences between measurement and FEM.

A third reason is internal stress caused by the different thermal expansion coefficients of the Si-structure ($\alpha_{\text{Si}} = 2.6 \cdot 10^{-6} 1/\text{K}$) and the Au-lead ($\alpha_{\text{Au}} = 14.2 \cdot 10^{-6} 1/\text{K}$).

Chapter 6

Temperature sensor application

The performed study on the resonant frequencies of the double-U structure (chapter 4) showed that k_v (the slope average of the eigenfrequency over the interval $T = [223;393]\text{K}$) is strongly decreased by an increase of parameters Lw and Uw and strongly increased by an increase of Ll (Tab. 4.2). The parameters Bl and Bw have only negligible effects.

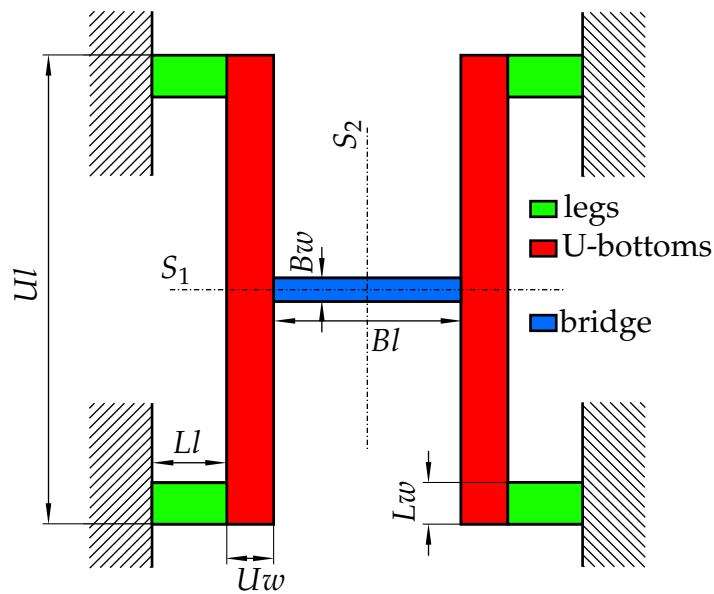


Figure 6.1: Clamped double-U beam structure considered in chapter 4 with $Ll = 319 \mu\text{m}$, $Lw = 177 \mu\text{m}$, $Ul = 2000 \mu\text{m}$, $Uw = 200 \mu\text{m}$, $Bl = 800 \mu\text{m}$ and $Bw = 100 \mu\text{m}$.

To get a beam structure which is suitable as temperature sensor the frequency of a mode (we consider here the first mode) should vary strongly with the temperature (large slope k_v) to get a high sensitivity. The mentioned effects can be utilized to design such a structure. Thus, to get a structure with a very large negative k_v of the 1. ss-eigenmode we start from our basic double-U structure Fig. 6.1 and set $Ll = 0$ or Lw to its maximum value, i. e. the legs of the double-U structure vanish. This yields a beam structure consisting of two cuboids that are connected by a bridge (Fig. 6.2), designated here as barbell

structure. As we started from the double-U structure the barbell structure is symmetric about the S_1 - and S_2 -axis as well. Additionally, with larger Uw k_v of the first ss-eigenmode gets more negative as discussed above. We are also interested in the alteration of k_v with the parameter Ul that has not been examined by means of the double-U structure. After some FEM simulations we find that k_v decreases with larger Ul . Additionally, we investigated k_v of the first ss-mode with respect to the height of the barbell structure and conclude that k_v gets more negative if the ratio between the height of the cuboids H_c and the height of the bridge H_b gets larger.

Let us consider a barbell structure with a bridge length $Bl = 800 \mu\text{m}$, a width $Bw = 100 \mu\text{m}$ and a height $H_b = 10 \mu\text{m}$. Length, width and height of each cuboid are given by $Uw = 2000 \mu\text{m}$, $Ul = 2000 \mu\text{m}$ and $H_c = 200 \mu\text{m}$.

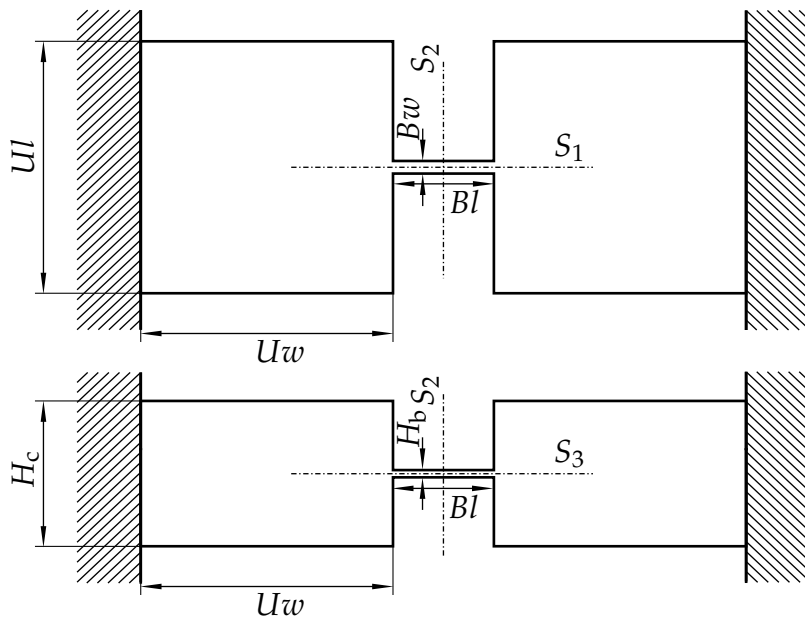


Figure 6.2: Clamped barbell beam structure with $Ul = 2000 \mu\text{m}$, $Uw = 2000 \mu\text{m}$, $H_c = 200 \mu\text{m}$, $Bl = 800 \mu\text{m}$, $Bw = 100 \mu\text{m}$ and $H_b = 10 \mu\text{m}$. Top: horizontal section. Bottom: vertical section.

The barbell structure is as the double-U structure in chapter 4 made of silicon with a mass density of 2329 kg/m^3 . The silicon is assumed to be nonlinear isotropic and its Young's modulus and Poisson's ratio are given by $E = 170 \cdot 10^9 \text{ Pa}$ and $\nu = 0.28$. Its thermal expansion coefficient is $\alpha = 2.6 \cdot 10^{-6} \text{ 1/K}$. We simulated the first ss-eigenmode of our barbell structure and plotted its fre-

quency over the temperature in Fig. 6.3.

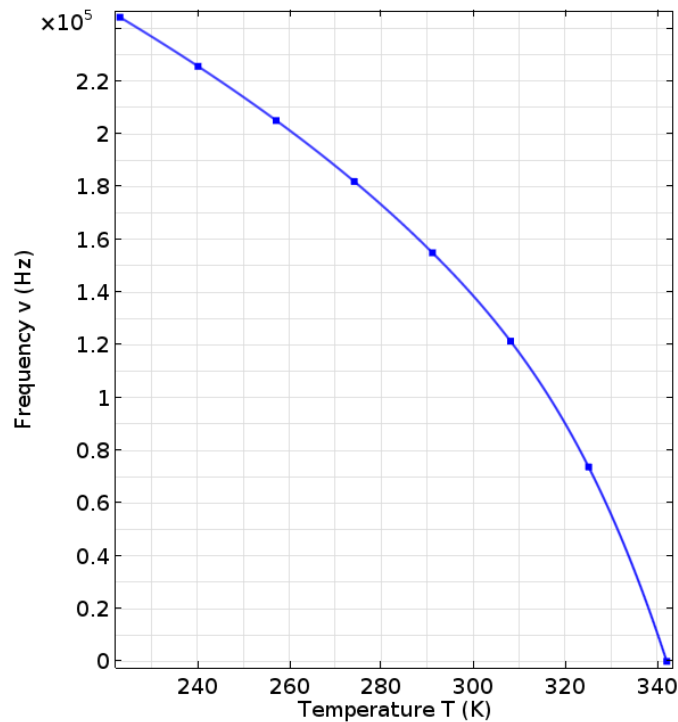


Figure 6.3: Frequency of the 1. ss-eigenmode versus temperature (reference temperature $T_0 = 298$ K) of barbell structure of Fig. 6.2. $k_v = -1\,312$ Hz/K for $T = 223 - 291$ K and $k_v = -3\,039$ Hz/K for $T = 291 - 342$ K.

As the frequency of the mode in Fig. 6.3 depends not linearly on the temperature we split the temperature interval into two intervals ($I_{T1} = [223 \text{ to } 291]$ K and $I_{T2} = [291 \text{ to } 342]$ K) where the frequency varies approximately linearly with the temperature. We determined the slope within these intervals and get $k_v = -1\,312$ Hz/K for $T = 223 - 291$ K and $k_v = -3\,039$ Hz/K for $T = 291 - 342$ K. These frequency slopes are very large especially within the second interval $I_{T2} = [291 \text{ to } 342]$ K. Hence, our considered barbell structure is a suitable beam structure for a temperature sensor as it has a high temperature sensitivity.

Buckling: Structures subjected to high compressive stress get unstable if the stress exceeds a critical point and as a consequence the structure fails by buckling. The resonant frequency of the barbell structure strongly varies with the temperature due to large changes of internal stresses over the bridge. Especially for temperatures beyond T_0 compressive stresses over the bridge increase to considerable amounts. Hence, the bridge is vulnerable to buckling and we

have to find out whether buckling occurs within the desired temperature range. For a beam we can distinguish between four buckling cases, i. e. the Euler buckling cases, depending on the boundary conditions at the ends of the beam (Fig. 6.4) [23].

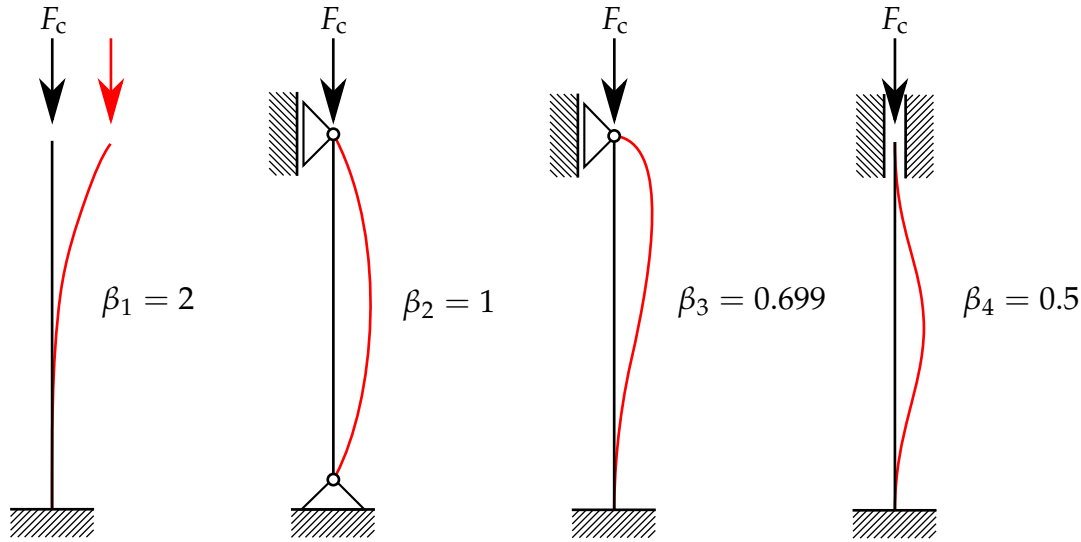


Figure 6.4: Four Euler buckling cases with buckling coefficient β .

The critical force F_c and stress σ_c at which the beam buckles is determined by:

$$F_c = \frac{\pi^2 EI}{\beta^2 l^2} = \frac{\pi^2 E b h^3}{12 \beta^2 l^2},$$

$$\sigma_c = \frac{F_c}{A} = \frac{\pi^2 EI}{b h \beta^2 l^2} = \frac{\pi^2 E h^2}{12 \beta^2 l^2}, \quad (6.1)$$

where β is the buckling coefficient, I the second moment of area, E is the Young's modulus and l is the length of the unstressed beam. The bridge is clamped on both ends (with a cuboid). Thus, it buckles the way depicted in the fourth Euler buckling case with $\beta_4 = 0.5$. This yields the following amount for the σ_c :

$$\sigma_c = \frac{\pi^2 E H_b^2}{12 \beta_4^2 B l^2} = 8.74 \cdot 10^7 \text{ N/mm}^2. \quad (6.2)$$

The simulated stress along the bridge evoked by heating the barbell structure together with σ_c is depicted in Fig. 6.5.

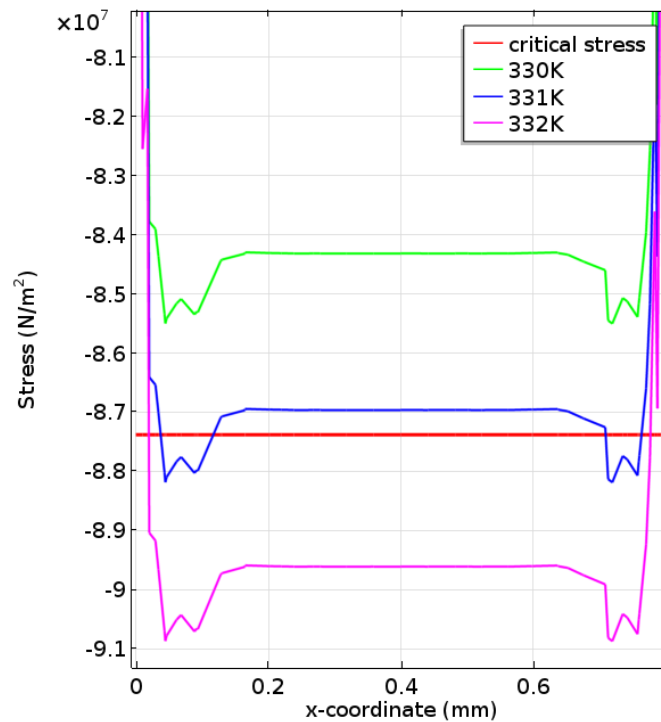


Figure 6.5: Stress σ along the bridge for temperatures $T = 330, 331$ and 332 K and critical stress σ_c .

It reveals that the barbell structure is stable up to 330 K. For temperatures around 331 K and higher the bridge will buckle.

In the simulation of the temperature dependent resonant frequency we did not take the case of buckling into account as it would go beyond the scope of this thesis. However, we draw attention to deviations of the resonant frequency to the one of Fig. 6.3 for temperatures higher than 331 K as a consequence of buckling.

In the following sections we review typical temperature sensors and their sensitivities in order to compare them with our barbell structure.

6.1 Vanadium oxide resonant thermal sensor

N. Inomata et al. [5] present a vanadium oxide resonant thermal sensor. The resonator is a cantilever made of vanadium oxide VO_x shown in Fig. 6.6 where VO_x comprises 55% of VO_2 and 45% of V_2O_5 .

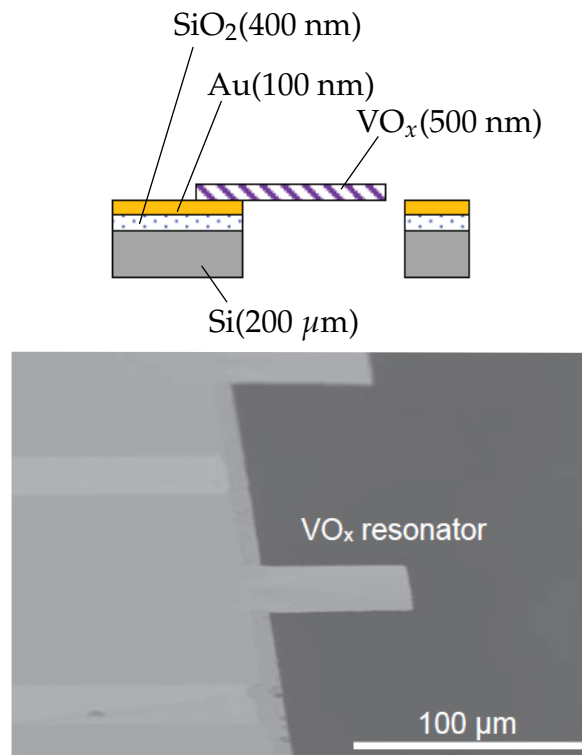


Figure 6.6: Vanadium oxide VO_x resonator [5].

The resonant frequency of the temperature sensor depends linearly on the temperature and its slope is given by $k_v = -67.5 \text{ Hz/K}$ over the temperature range of $T = 293 - 373 \text{ K}$.

6.2 Quartz crystals

Quartz crystals which are highly piezoelectric can be utilized for temperature sensors too. With a suitable cut their resonant frequency changes linearly with the temperature at about 1000 Hz/K over a range of $T = 293 - 373 \text{ K}$ [6].

6.3 String-based temperature sensors

T. Larsen et al. [7] present a temperature sensor based on the temperature dependence of the resonant frequency of an aluminum string (Fig. 6.7). The string is $200 \mu\text{m}$ long, $3 \mu\text{m}$ wide and 30 nm thick.

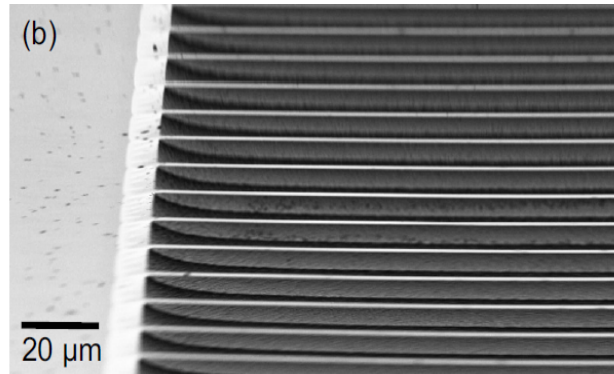


Figure 6.7: Aluminum strings of the resonant temperature sensor. One string is 200 μm long, 3 μm wide and 30 nm thick [7].

The resonant frequency of such an aluminum string exhibits a temperature slope of $k_\nu = -3517 \text{ Hz/K}$ over a temperature range of $T = 293 - 343 \text{ K}$.

6.4 Temperature sensor based on electrical spring softening

W.-T. Hsu et al. [8] describe a resonant temperature sensor based on electrical spring softening. The setup of the device is shown in Fig. 6.8. A beam made of polysilicon is used as the resonator. The resonator is flanked by two electrodes of a material with a large thermal expansion coefficient (Au). Between the resonator beam and each electrode is a gap with the spacing d . The beam can be driven into resonance vibration if a voltage gets applied across the gap, where the voltage comprises an ac signal v_i with the beam's resonant frequency and a dc signal V_p applied across the resonator-electrode gap. The electrical spring stiffness k_e varies inversely with d^3 and proportionally with V_p^2 . With a temperature change the electrodes expand or contract and thus, the spacing of the resonator-electrode gap d gets modified. This causes in turn a strong change of the electrical spring stiffness k_e since it is proportional to $1/d^3$ and as a result the resonant frequency of the beam gets changed proportional to $1/d^3$ too. Thus, it is possible to sense temperature shifts via frequency shifts of the resonator.

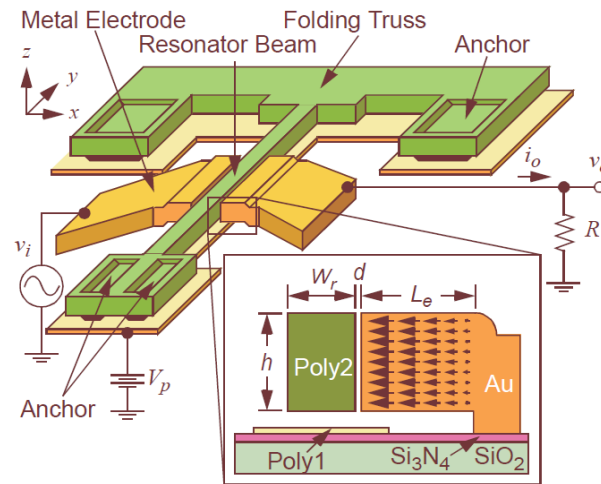


Figure 6.8: Perspective and cross-section views of an electrical spring softening-based resonant temperature sensor [8].

The device exhibits a fairly linear frequency change with the temperature given by -3700 Hz/K over a temperature range of $T = 320 - 380 \text{ K}$.

6.5 Resonant MEMS temperature sensor

T. Kose et al. [9] developed a resonant MEMS temperature sensor (Fig. 6.9), where Si-tines act as resonators. Length, width and thickness of one tine are $1000 \mu\text{m}$, $10 \mu\text{m}$ and $35 \mu\text{m}$ respectively. In Fig. 6.9 are shown two resonators one with long tines and one with short tines. We restrict ourselves onto the resonator with long tines as this one exhibits a higher temperature sensitivity. The tines are electrostatically driven to vibration via electrodes. When the temperature shifts the structure expands or contracts causing a change of the axial load in the tines and in turn a shift of their resonant frequencies. The change of the axial load gets amplified with the strain-amplifying beam. For the amplification similar effects are utilized like our barbell structure.

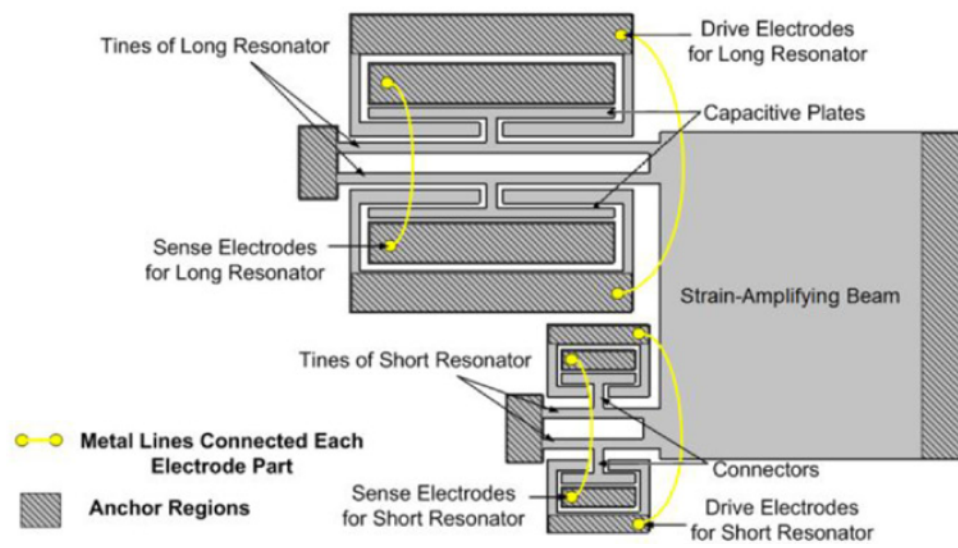


Figure 6.9: Layout of MEMS temperature sensor [9].

The resonant frequency has a temperature coefficient $k_v = 32 \text{ Hz/K}$ over a temperature range of $T = 260 - 320 \text{ K}$.

Chapter 7

Structure with temperature independent resonance

In chapter 6 we looked for a beam structure where the frequency of the 1. ss-mode varies strongly with the temperature in order to utilize it as a temperature sensor. In this chapter we are interested in a structure where the 1. ss-mode's frequency is at most independent of the temperature.

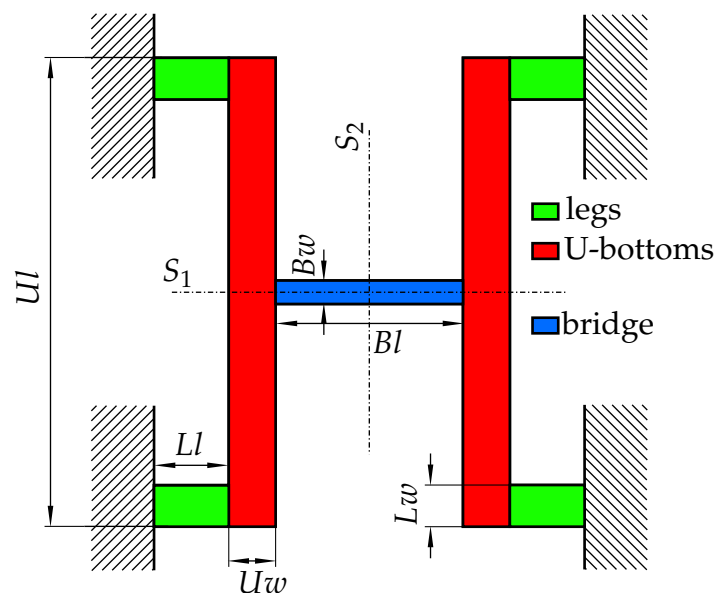


Figure 7.1: Clamped double-U beam structure examined in chapter 4 with $Ll = 319 \mu\text{m}$, $Lw = 177 \mu\text{m}$, $Ul = 2000 \mu\text{m}$, $Uw = 200 \mu\text{m}$, $Bl = 800 \mu\text{m}$ and $Bw = 100 \mu\text{m}$.

In section 4.2 we discussed how the 1. ss-mode's frequency changes with parameter modifications of the basic double-U structure. There we concluded that the slope k_v of the first resonant frequency decreases strongly with an enlargement of Lw and Uw and increases with Ll (Tab. 4.2). The parameters Bl and Bw have also an influence on k_v but it is rather small compared to the influence of the other parameters and hence, it is negligible.

To construct a beam structure with a temperature independent resonant

frequency ($\rightarrow k_\nu = 0 \text{ Hz/K}$) of the first ss-eigenmode we start from the basic double-U structure shown in Fig. 7.1. The frequency of its first ss-mode has a negative slope of $k_\nu = -32.9 \text{ Hz/K}$ [223 to 393] K. Thus, we need parameter modifications which cause positive changes of k_ν . According to our discussion in section 4.2 an increase of the parameter Ll and a decrease of the parameters Lw and Uw should entail positive changes of k_ν .

Starting from the basic double-U structure of Fig. 7.1 we increase Ll from $319 \mu\text{m}$ to $797 \mu\text{m}$, decrease Lw from $177 \mu\text{m}$ to $59 \mu\text{m}$ and decrease Uw from $200 \mu\text{m}$ to $66 \mu\text{m}$ and get a beam structure shown in Fig. 7.2. Let us call the new structure narrow-double-U structure as it has the same shape as the basic double-U structure but with narrower beams. The narrow-double-U is as the basic double-U structure mirror symmetric about the S1- and S2-axis. All other parameters which we did not modify are the same as for the basic double-U structure. That means that $Ul = 2000 \mu\text{m}$, $Bl = 800 \mu\text{m}$, $Bw = 100 \mu\text{m}$ and the height of the narrow-double-U structure is $H = 20 \mu\text{m}$. Furthermore, the structure is as the basic double-U structure made of silicon with a mass density of 2329 kg/m^3 . The silicon is also assumed to be nonlinear isotropic and its Young's modulus and Poisson's ratio are given by $E = 170 \cdot 10^9 \text{ Pa}$ and $\nu = 0.28$. Its thermal expansion coefficient is $\alpha = 2.6 \cdot 10^{-6} \text{ 1/K}$.

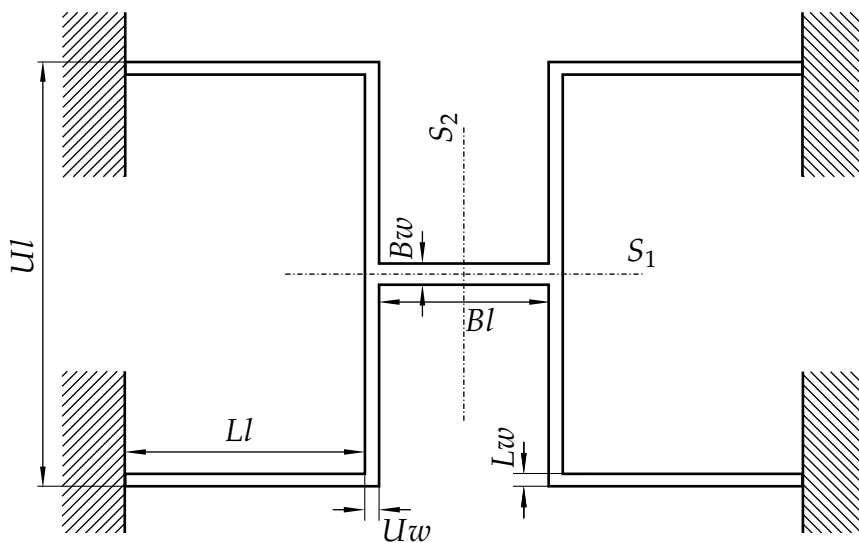


Figure 7.2: Clamped narrow-double-U structure with $Ll = 797 \mu\text{m}$, $Lw = 59 \mu\text{m}$, $Ul = 2000 \mu\text{m}$, $Uw = 66 \mu\text{m}$, $Bl = 800 \mu\text{m}$ and $Bw = 100 \mu\text{m}$.

The simulated resonant frequencies of the 1. ss-eigenmode are plotted in

Fig. 7.3. Additionally, the values of the unchanged structure are depicted for comparison.

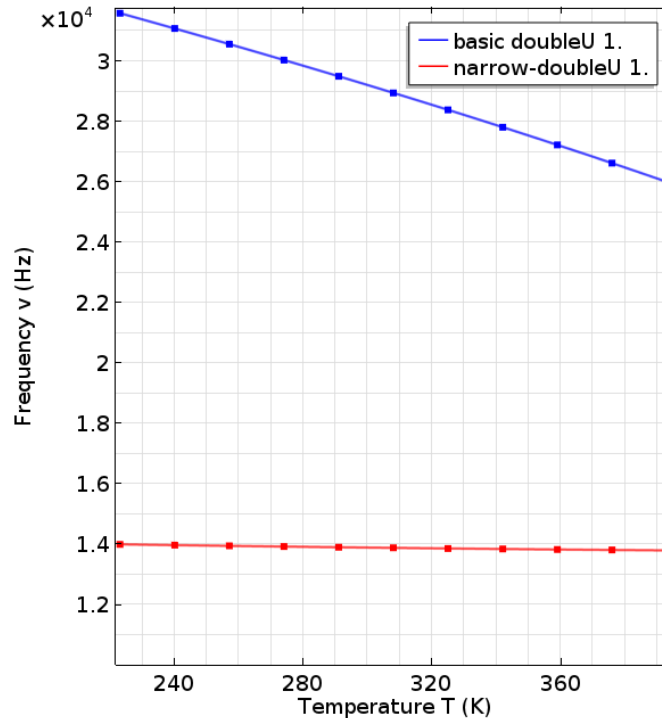


Figure 7.3: Temperature dependence of the 1. ss-eigenmode (reference temperature $T_0 = 298 \text{ K}$) of narrow-double-U structure and basic double-U structure. $k_\nu = -2.35 \text{ Hz/K}$ for the narrow-double-U and $k_\nu = -32.9 \text{ Hz/K}$ for the basic double-U structure.

The slope average of the mode over the interval $T = [223 \text{ to } 393] \text{ K}$ of the basic double-U structure is $k_{\nu\text{bas}} = -32.9 \text{ Hz/K}$. Where the one of the narrow-double-U structure is $k_{\nu\text{nar}} = -2.35 \text{ Hz/K}$. Thus, we conclude that with a modification of the three parameters Ll , Lw and Uw we were able to minimize the temperature dependence of the resonance by a considerable factor of $\eta = k_{\nu\text{bas}}/k_{\nu\text{nar}} = -32.9 / -2.35 = 14$. Hence, we got with the narrow-double-U a structure with a resonant frequency almost independent of the temperature and a structure which is still easy to construct.

Buckling: Considering the narrow-double-U structure, the analytical determination of the critical buckling stress is not trivial as now the whole structure is vulnerable to buckling and a restriction to the bridge is not possible. Therefore we solved the problem numerically with FEM. The results revealed that there exists no critical temperature T_c at which the structure buckles.

Chapter 8

Conclusion and Outlook

Owing to investigations of dynamics of an isotropic Si-structure performed in this thesis, many useful and interesting effects could be revealed.

The reliability of the FEM results is proofed by verifications of the FEM software with analytical computed problems and an experiment. The deviations between FEM and analytical computation are quite small and can be ascribed to simplifications in the analytical calculation. Comparing FEM with experiment the deviations are smaller than 2 % and are a consequence of simplifications in the simulation which were difficult to realize in the experiment.

An important conclusion of the examination is that effects caused by changing parameters can be approximately considered as a sum of effects where only one parameter was changed respectively. There are only few exceptions, for example $(Ll, -, -, Uw, Bl, -)$ regarding the 2. ss-mode of the double-U structure (section 4.6). Most of these exceptions are a consequence of mode modifications with the temperature. This is also true for $(Ll, -, -, Uw, Bl, -)$ where the 2. ss-mode exhibits a modification depicted in Fig. 4.16. It should be noted that especially the 1. ss-, 1. as- and 2. ss-modes are vulnerable to such modifications. Additionally, one finds that they are not observed if only one parameter is changed and that they have strong effects on the temperature dependence of the frequency. Hence, further research for understanding these modifications would be useful for preventing but also utilizing them.

With the effects of parameter changes on the resonant frequencies one has been able to construct MEMS structures exhibiting a resonant frequency with strong temperature dependence (chapter 6) as well as temperature independence (chapter 7). Despite these features both structures can be fabricated easily. Furthermore, it should be stressed that still the potential of these structures has not been fully exploited. Thus, further development for optimizing their features could be done.

Beside the developed structures the thesis still provides effects that can be

utilized for structures with other features. One could develop a structure where the temperature coefficient of the resonant frequency varies with the temperature. In particular the 1. ss-, 1. as- and 2. ss-modes are suitable for such an application as they exhibit for some parameter combinations a temperature dependent temperature coefficient (see Tab. 4.2).

Furthermore, temperature dependent mode modifications could be utilized for devices that control processes with temperature. For this the 2. ss-mode would be suitable as it has considerable mode modifications for some parameter sets. The thesis also provides effects that shift the frequency of modes. One can use these to get a mode with a desired frequency or to enlarge the frequency range between modes so that they don't interfere with each other. For example, one is able to increase the frequency difference of the 1. ss and 1. as by an enlargement of the two parameters Lw and Bw .

With the great amount of revealed effects this thesis serves as a basis for further investigations (regarding different materials or anisotropies etc.) and developments (regarding new features) of MEMS structures.

Bibliography

- [1] P. Gummert K.-A. Reckling, *Mechanik*, Vol. 3, 8.1 Grundgleichungen
- [2] P. Gummert K.-A. Reckling, *Mechanik*, Vol. 3, 6.3 Zug/Druck
- [3] P. Gummert K.-A. Reckling, *Mechanik*, Vol. 3, 6.2 Materialgleichungen
- [4] P. Gummert K.-A. Reckling, *Mechanik*, Vol. 3, 6.4 Biegung (elementare Balkentheorie)
- [5] N. Inomata, Microfabricated vanadium oxide resonant thermal sensor with a high temperature coefficient of resonant frequency, *IEEE*, 1042-1045, 2016
- [6] W. Göpel J. Hesse J. N. Zemel, *Sensors Thermal Sensors*, Vol. 4, 2.6.2.5 Quartz Crystals
- [7] T. Larsen, Ultrasensitive string-based temperature sensors, *Appl. Phys. Lett.*, Vol. 98, 121901, 2011
- [8] W.-T. Hsu, A resonant temperature sensor based on electrical spring softening, *Digest of Technical Papers*, 1484-1487, 2001
- [9] T. Kose, Design and fabrication of a high performance resonant MEMS temperature sensor, *IOP Science*, Vol. 26, 045012, 2016
- [10] P. Hauptmann, *Sensoren Prinzipien und Anwendungen*, 4.4 Temperatursensoren
- [11] K. W. Bonfig, *Sensorik Temperatursensoren Prinzipien und Anwendungen*, Vol. 6, 2.1 Ausdehnungsthermometer
- [12] https://en.wikipedia.org/wiki/Bimetal#/media/File:Bimetallic_stripe.svg
- [13] K. W. Bonfig, *Sensorik Temperatursensoren Prinzipien und Anwendungen*, Vol. 6, 2.2 Widerstandsthermometer

-
- [14] K. W. Bonfig, Sensorik Temperatursensoren Prinzipien und Anwendungen, Vol. 6, 2.3 Thermoelemente
- [15] F. Keplinger, Sensorik, 2.8 Optische Dehnungsmessstreifen
- [16] K. W. Bonfig, Sensorik Temperatursensoren Prinzipien und Anwendungen, Vol. 6, 2.6 Pyrometer
- [17] <http://www.accurate.kiwi/temperature/pyrometers.htm>
- [18] St. Beeby G. Ensell M. Kraft N. White, MEMS Mechanical Sensor, chapter 1 Introduction
- [19] <http://www.inocal.com>
- [20] A. Talić, FEM and Measurement Analysis for Flow Sensor Featuring Three Different Operating Modes, Procedia Engineering, Vol. 5, 746-749, 2010
- [21] A. Talić, MEMS Flow Sensors Based on Self-Heated aGe-Thermistors in a Wheatstone Bridge, Sensors, Vol. 15, 10004-10025, 2015
- [22] M. Stifter, Lorentz Force Actuated Resonant MEMS Magnetometer with Capacitive Read-out, 4.1 Device Fabrication
- [23] P. Gummert K.-A. Reckling, Mechanik, Vol. 3, 6.13.4 Konsequenzen für die Anwendungen in der Ingenieurpraxis